



**NAVAL
POSTGRADUATE
SCHOOL**

MONTEREY, CALIFORNIA

THESIS

**REDUCTION EXPANSION SYNTHESIS OF CHROMIUM
AND NICKEL METAL COATINGS**

by

Christopher J. Pelar

June 2017

Thesis Advisor:
Second Reader:

Jonathan Phillips
Claudia C. Luhrs

Approved for public release. Distribution is unlimited.

THIS PAGE INTENTIONALLY LEFT BLANK

REPORT DOCUMENTATION PAGE			<i>Form Approved OMB No. 0704-0188</i>	
Public reporting burden for this collection of information is estimated to average 1 hour per response, including the time for reviewing instruction, searching existing data sources, gathering and maintaining the data needed, and completing and reviewing the collection of information. Send comments regarding this burden estimate or any other aspect of this collection of information, including suggestions for reducing this burden, to Washington headquarters Services, Directorate for Information Operations and Reports, 1215 Jefferson Davis Highway, Suite 1204, Arlington, VA 22202-4302, and to the Office of Management and Budget, Paperwork Reduction Project (0704-0188) Washington, DC 20503.				
1. AGENCY USE ONLY (Leave blank)	2. REPORT DATE June 2017	3. REPORT TYPE AND DATES COVERED Master's thesis		
4. TITLE AND SUBTITLE REDUCTION EXPANSION SYNTHESIS OF CHROMIUM AND NICKEL METAL COATINGS			5. FUNDING NUMBERS	
6. AUTHOR(S) Christopher J. Pelar				
7. PERFORMING ORGANIZATION NAME(S) AND ADDRESS(ES) Naval Postgraduate School Monterey, CA 93943-5000			8. PERFORMING ORGANIZATION REPORT NUMBER	
9. SPONSORING /MONITORING AGENCY NAME(S) AND ADDRESS(ES) N/A			10. SPONSORING / MONITORING AGENCY REPORT NUMBER	
11. SUPPLEMENTARY NOTES The views expressed in this thesis are those of the author and do not reflect the official policy or position of the Department of Defense or the U.S. Government. IRB number ____N/A____.				
12a. DISTRIBUTION / AVAILABILITY STATEMENT Approved for public release. Distribution is unlimited.			12b. DISTRIBUTION CODE	
13. ABSTRACT (maximum 200 words) This thesis represents a step forward in a program to provide the Department of Defense (DOD) alternative approaches to the production of anti-corrosion metal coatings. Specifically, a method was developed to make micron thick but irregular nickel coatings on iron, based on Reduction Expansion Synthesis (RES) chemistry. Previous success using RES processes to make sub-micron nickel, iron, and alloy particles provided a general direction to the program and led to the successful protocol. Physical mixtures of nickel (II) oxide particles and urea were used to create a paste. The paste was coated on an iron foil, which was briefly heated at 1100°C in an inert atmosphere. Also described are partially successful attempts to develop a RES protocol to chrome coat iron. This is motivated by the need to eliminate the carcinogenic intermediate in the current electrolytic technology, hexavalent chromium.				
14. SUBJECT TERMS Reduction Expansion Synthesis (RES), metal coating, chrome coating, nickel coating			15. NUMBER OF PAGES 121	
			16. PRICE CODE	
17. SECURITY CLASSIFICATION OF REPORT Unclassified	18. SECURITY CLASSIFICATION OF THIS PAGE Unclassified	19. SECURITY CLASSIFICATION OF ABSTRACT Unclassified	20. LIMITATION OF ABSTRACT UU	

NSN 7540-01-280-5500

Standard Form 298 (Rev. 2-89)
Prescribed by ANSI Std. Z39-18

THIS PAGE INTENTIONALLY LEFT BLANK

Approved for public release. Distribution is unlimited.

**REDUCTION EXPANSION SYNTHESIS OF CHROMIUM AND NICKEL
METAL COATINGS**

Christopher J. Pelar
Lieutenant, United States Coast Guard
B.S., United States Coast Guard Academy, 2006

Submitted in partial fulfillment of the
requirements for the degree of

MASTER OF SCIENCE IN MECHANICAL ENGINEERING

from the

**NAVAL POSTGRADUATE SCHOOL
June 2017**

Approved by: Jonathan Phillips
Thesis Advisor

Claudia C. Luhrs
Second Reader

Garth V. Hobson
Chair, Department of Mechanical and Aerospace Engineering

THIS PAGE INTENTIONALLY LEFT BLANK

ABSTRACT

This thesis represents a step forward in a program to provide the Department of Defense (DOD) alternative approaches to the production of anti-corrosion metal coatings. Specifically, a method was developed to make micron thick but irregular nickel coatings on iron, based on Reduction Expansion Synthesis (RES) chemistry. Previous success using RES processes to make sub-micron nickel, iron, and alloy particles provided a general direction to the program and led to the successful protocol. Physical mixtures of nickel (II) oxide particles and urea were used to create a paste. The paste was coated on an iron foil, which was briefly heated at 1100°C in an inert atmosphere. Also described are partially successful attempts to develop a RES protocol to chrome coat iron. This is motivated by the need to eliminate the carcinogenic intermediate in the current electrolytic technology, hexavalent chromium.

THIS PAGE INTENTIONALLY LEFT BLANK

TABLE OF CONTENTS

I.	INTRODUCTION.....	1
A.	COMMON MANUFACTURING METHODS USED FOR METAL COATINGS.....	1
1.	Electroplating	1
2.	Electroless Plating.....	2
3.	Sputtering	4
4.	Cold Spray	5
5.	Thermal Spray	6
6.	Thermal Evaporation	7
B.	HEALTH AND ENVIRONMENTAL HAZARDS.....	8
C.	REDUCTION EXPANSION SYNTHESIS (RES).....	9
D.	MOTIVATION AND GOALS.....	9
II.	EXPERIMENTAL METHODS	11
A.	SURFACE TREATMENT OF METAL SUBSTRATES.....	11
B.	CHROMIUM BASED RES PROTOCOLS	11
1.	RES Coating Protocol I.....	12
2.	RES Chromium (III) Oxide Precursor Protocol.....	15
3.	RES Coating Protocol II.....	17
4.	Chromium Powder RES Experiments	20
C.	NICKEL POWDER RES PROTOCOLS.....	24
1.	Nickel Powder RES Experiments	24
2.	Nickel Coating RES Protocol.....	26
D.	CHARACTERIZATION	29
1.	Sample Preparation	29
2.	Optical Microscopy	33
3.	Scanning Electron Microscopy (SEM) – Energy Dispersive Spectroscopy	33
4.	X-ray Diffraction (XRD)	34
5.	Focused Ion Beam (FIB).....	35
III.	RESULTS AND ANALYSIS	37
A.	CONTROL STUDIES SURFACE TREATMENT OF IRON SUBSTRATES	38
B.	RESULTS OF CHROMIUM BASED RES PROTOCOLS.....	44
1.	Chromium Coating Protocol I.....	45
2.	Chromium Precursor Protocol	48

3.	Chromium Coating Protocol II.....	52
4.	Chromium Powder Protocol	69
C.	RESULTS OF NICKEL BASED RES PROTOCOLS.....	76
1.	Nickel Powder Protocol	77
2.	Nickel Coating Protocol.....	84
IV.	DISCUSSION	89
A.	SURFACE PREPARATION	89
B.	DURATION OF COATING METHOD.....	89
C.	TEMPERATURE DURING COATING	90
D.	PRECURSORS USED FOR COATING	90
E.	GEOMETRY OF SUBSTRATE	90
V.	CONCLUSIONS	93
	LIST OF REFERENCES	97
	INITIAL DISTRIBUTION LIST	101

LIST OF FIGURES

Figure 1.	Diagram of Hexavalent Electroplating Process. Source: [10].	2
Figure 2.	Schematic of Electroless Metal Plating. Source: [19].	3
Figure 3.	Comparison Between Electroless and Electroplating Deposition Uniformity. Source: [20].	4
Figure 4.	Physical Vapor Deposition Using Sputtering Method. Source: [22].	5
Figure 5.	Cold Spraying Diagram. Source: [24].	6
Figure 6.	Thermal Spray Coating Diagram. Source [29].	7
Figure 7.	Thermal Evaporation Diagram. Source: [30].	7
Figure 8.	Crushed Urea Powder	12
Figure 9.	Urea and Chromium (III) Nitrate Nonahydrate Paste	13
Figure 10.	RES Protocol I Sample Drying	14
Figure 11.	Chromium Nitrate Nonahydrate Decomposition at 800°C	16
Figure 12.	Chromium Based Precursor Added to Urea Powder	17
Figure 13.	Combined Urea and Chromium Precursor Powder	18
Figure 14.	Urea and Chromium Precursor Paste	18
Figure 15.	Coated Iron Wire Drying That Formed Precipitates	19
Figure 16.	Coated Iron Wire When Cooled to Room Temperature	20
Figure 17.	Post Cleaning of Coated Iron Wire	20
Figure 18.	Lignite and Potassium Carbonate Mixture and Perforated Graphite Foil	22
Figure 19.	Chromium Precursor Loaded on Top of Graphite Foil for RES Protocol	23
Figure 20.	Urea and Nickel (II) Oxide Powders Combined and Mixed	25
Figure 21.	Reduced Nickel Powder Cooling to Room Temperature	26

Figure 22.	Prepared Iron Foil	27
Figure 23.	Nickel Based Paste Coated Iron Foil	28
Figure 24.	Nickel Coated Iron Foil Cooling to Room Temperature	28
Figure 25.	Struers Secotom-10 Saw	30
Figure 26.	Buehler Simplimet 2 Mounting Press	31
Figure 27.	Buehler Grinding Table	32
Figure 28.	Buehler Polishing Wheel	33
Figure 29.	Zeiss Neon 40 Scanning Electron Microscope	34
Figure 30.	Rigaku MiniFlex 600 X-Ray Diffractometer.....	35
Figure 31.	SEM Backscattered Image of Uncoated Sample 1	39
Figure 32.	EDS Analysis of an Uncoated Sample 1.....	39
Figure 33.	SEM Backscattered Diffraction of Uncoated Sample 2	40
Figure 34.	EDS Analysis of Uncoated Sample 2	41
Figure 35.	SEM Backscattered Diffraction of Uncoated Sample 3	41
Figure 36.	EDS Analysis of Uncoated Sample 3	42
Figure 37.	SEM Backscattered Diffraction of Uncoated Sample 4	42
Figure 38.	EDS Analysis of Uncoated Sample 4	43
Figure 39.	SEM Backscattered Diffraction of Uncoated Sample 5	43
Figure 40.	EDS Analysis of Uncoated Sample 5	44
Figure 41.	EDS Analysis of Coated Sample 6	46
Figure 42.	EDS Analysis of Coated Sample 7	47
Figure 43.	EDS Analysis of Coated Sample 8	47
Figure 44.	Sample 9 SEM Micrographs.....	49
Figure 45.	Sample 10 SEM Micrographs.....	49
Figure 46.	EDS Analysis of Sample 10.....	50

Figure 47.	X-Ray Diffraction Spectrum from Sample 9 Precursor.....	51
Figure 48.	X-Ray Diffraction Spectrum from Sample 10 Precursor.....	51
Figure 49.	Visual Inspection of Sample 19	53
Figure 50.	EDS Analysis of Coated Sample 11	54
Figure 51.	EDS Analysis of Coated Sample 12	54
Figure 52.	Optical Microscopy of Sample 13	55
Figure 53.	EDS Analysis of Sample 13 Cross-Sectional Substrate	57
Figure 54.	EDS Analysis of Sample 13 Cross-Sectional Surface Layer.....	57
Figure 55.	EDS Analysis of Sample 13 Cross-Sectional Conductive Material	58
Figure 56.	Inlens SEM Microscopy of Sample 14 Surface Layer.....	59
Figure 57.	FIB Milled Surface of Sample 13	60
Figure 58.	FIB Milled Trench at Area “A” on Sample 13	61
Figure 59.	EDS Surface Analysis of Area “A” on Sample 13	61
Figure 60.	EDS Surface Analysis of FIB Trench at Area “A” on Sample 13.....	62
Figure 61.	FIB Milled EDS Analysis of Chromium Rich Particle on the Surface of Sample 13	63
Figure 62.	FIB Milled EDS Analysis of Iron Surface of Sample 13.....	63
Figure 63.	SEM Backscattered Image of Coated Sample 18 Surface Layer.....	64
Figure 64.	EDS Analysis of Sample 18 Surface Particles.....	65
Figure 65.	EDS Analysis of Sample 18 Substrate.....	66
Figure 66.	X-Ray Diffraction Spectrum of Sample 18	67
Figure 67.	X-Ray Diffraction Spectrum of Sample 18 (Chromium (III) Oxide).....	67
Figure 68.	X-Ray Diffraction Spectrum of Sample 18 (Chromium)	68
Figure 69.	X-Ray Diffraction Spectrum of Sample 21	70
Figure 70.	X-Ray Diffraction Spectrum of Sample 22	71

Figure 71.	X-Ray Diffraction Spectrum of Sample 23	72
Figure 72.	X-Ray Diffraction Spectrum of Sample 24	72
Figure 73.	X-Ray Diffraction Spectrum of Sample 25	74
Figure 74.	X-Ray Diffraction Spectrum of Sample 26	74
Figure 75.	X-Ray Diffraction Spectrum of Sample 27	75
Figure 76.	X-Ray Diffraction Spectrum of Sample 28	75
Figure 77.	X-Ray Diffraction Spectrum of Sample 29	78
Figure 78.	X-Ray Diffraction Spectrum of Sample 30	79
Figure 79.	X-Ray Diffraction Spectrum of Sample 31	80
Figure 80.	X-Ray Diffraction Spectrum of Sample 32	81
Figure 81.	X-Ray Diffraction Spectrum of Sample 33	82
Figure 82.	X-Ray Diffraction Spectrum of Sample 34	83
Figure 83.	Optical Microscopy of Sample 35	84
Figure 84.	SEM Microscopy of Sample 35	85
Figure 85.	EDS Analysis of Surface on Sample 35	85
Figure 86.	EDS Analysis of Agglomerated Particle on Sample 35.....	86
Figure 87.	SEM Microscopy of Sample 35	87
Figure 88.	EDS Point Analysis of Reduced Particles on Sample 35	87
Figure 89.	EDS Analysis of Iron Substrate on Sample 35	88

LIST OF TABLES

Table 1.	Hexavalent Chromium Compared to Other Well-Known Carcinogens. Adapted from [10].....	8
Table 2.	Surface Treatments of Iron Wire Substrate	38
Table 3.	Iron EDS Peak Identification by Series. Adapted from [45].	40
Table 4.	Protocol I Variation in Experimental Procedures	45
Table 5.	Chromium Precursor Samples	48
Table 6.	Chromium EDS Peak Identification by Series. Adapted from [45].....	50
Table 7.	RES Coating Protocol II Samples.....	52
Table 8.	Protocol II Coating Measurements from Mounted Samples.....	56
Table 9.	Chromium Oxide Powder Experimental Parameters	69
Table 10.	Quantitative Results of Chromium Based Powder Composition.....	76
Table 11.	Nickel Oxide Powder Experimental Parameters.....	77
Table 12.	Quantitative Results of Nickel Based Powder Composition	83

THIS PAGE INTENTIONALLY LEFT BLANK

LIST OF ACRONYMS AND ABBREVIATIONS

μm	micrometer
DOD	Department of Defense
EDS	Energy Dispersive Spectroscopy
EPA	Environmental Protection Agency
FIB	Focused Ion Beam
nm	nanometer
OSHA	Occupational Safety and Health Administration
RES	Reduction Expansion Synthesis
SCCM	standard cubic centimeters per minute
SEM	Scanning Electron Microscope/Microscopy
XRD	X-Ray Diffraction

THIS PAGE INTENTIONALLY LEFT BLANK

ACKNOWLEDGMENTS

First, I would like to thank my wife and family for their support and especially for the sacrifices made to family time while in pursuit of my master's degree. Without their constant encouragement, this professional achievement would not have been possible.

I also wish to thank my thesis advisor, Jonathan Phillips, for his guidance in exploring thin metal coatings. His knowledge and perseverance were influential in the completion of this study. In addition, I wish to extend my gratitude to the following members of the Mechanical Engineering Material Science staff: Sarath Menon, William Wu, Chanman Park, Claudia Luhrs and Hugo Zea for their incredible assistance with preparation and equipment training for various characterization techniques used in this study.

THIS PAGE INTENTIONALLY LEFT BLANK

I. INTRODUCTION

It is well known that electroplated chrome coatings has been used by many industries for its corrosion and wear resistance as well as decorative applications [1]–[2]. However, medical research has found a correlation with the use of hexavalent chromium used in electroplating chrome with cancer [3]–[6]. The Department of Defense has mandated the use of hexavalent chromium used in protective coatings to be minimized [7]. This has led to research to develop safer alternative processes. This thesis study is an effort to find a safe alternative to electroplating chrome, by using a novel approach to apply coatings using the Reduction Expansion Synthesis (RES) method. In sum in this thesis, it is shown the RES method can be used to create unique nickel coating on an iron foil. However, a means to create a high quality chrome coating remains elusive.

This chapter discusses: (i) methods currently used to manufacture metal coatings in industry, (ii) the associated health and environmental risks with the use of hexavalent chromium, (iii) the RES method studied and further developed in this thesis, and (iv) the motivation and goals for this thesis.

A. COMMON MANUFACTURING METHODS USED FOR METAL COATINGS

There are several different methods to apply metal coatings on substrates, generally metal, on different scales ranging from machinery components to small electrical circuits. This section briefly describes six common methods that can be used to manufacture metal coatings.

1. Electroplating

The electroplating process has four components: (i) an electrolyte solution that contains coating material, (ii) the component desired to be coated (cathode), (iii) a permanent inert anode, and (iv) an external power source to apply an electric current, as described in [8]–[9]. Specifically, for chromium electroplating a hexavalent electrolyte solution is used containing chromium (VI) trioxide (CrO_3) sulfuric acid (H_2SO_4) [10], as

shown in Figure 1. Once an electric current is applied, the chromium ions in the solution are attracted to the positively charged cathode and begin to coat the substrate.

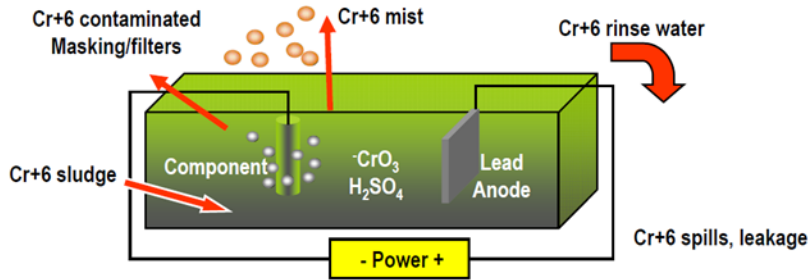


Figure 1. Diagram of Hexavalent Electroplating Process. Source: [10].

Technically, electrolytic coating of metal substrates with chrome is a mature, effective technology. However, safety issues makes it nearly unacceptable. The electroplating process creates a hexavalent chromium aerosol mist that poses a hazard both to the personnel who work in the coating industry and the environment [2]. To mitigate the exposure to personnel and the environment proper engineering controls have been implemented, such as respirators and filtered ventilations systems. Also, other harmful byproducts of this process include the sludge that settles to the bottom of the coating tank and the waste water created when rinsing the coated parts and cleaning the coating tank [2], [10]–[11]. To mitigate hexavalent chromium exposure in manufacturing processes, coating manufacturers must comply with Occupational Safety and Health Administration (OSHA) and Environmental Protection Agency (EPA) regulations [12]–[14]. Ongoing research is being conducted, in pursuit of DOD’s goal to improve electrolytic solutions for electroplating with the use of the non-toxic trivalent form of chromium [7], [15]–[18].

2. Electroless Plating

As Schlesinger [19] explains, electroless plating is another form of metal plating, particularly used for nickel coatings, which undergoes an autocatalytic process between a chemical reducing agent found in a solution to reduce metallic ions to their pure metallic state. This process differs from electroplating, as the electroless plating does not require

an external power source [19]. This process is similar to electroplating as the metal salts are placed into the solution and the metal substrate is the cathode. Schlesinger also explained that one unique aspect of this method is it requires the substrate to have a catalyst placed on the surface in order for the nucleation of a coating to occur.

Schlesinger [19] explains, there are two methods to apply coatings using electroless plating, as shown in Figure 2. Schlesinger outlines the initial steps of cleaning and surface etching that are necessary for either method used. The first method uses chemical solutions to sensitize and catalyze the substrate to be coated [19]. The second method uses a catalyzing chemical solution that is mixed with colloids and a chemical solution to activate or accelerate the reaction [19]. The metal substrate is rinsed with water between each successive step [19].

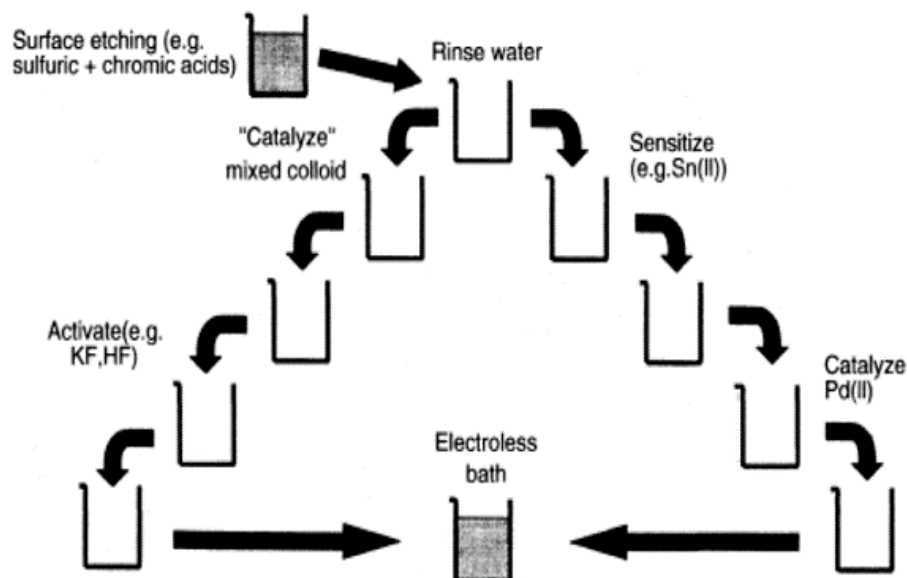


Figure 2. Schematic of Electroless Metal Plating. Source: [19].

One advantages of using electroless plating is that the surface coating will be less porous and may increase the corrosion resistance for the component [19]. As Parkinson [20] describes, another advantage of electroless plating is the resultant coating will be more uniform than any coating achieved via electroplating (Figure 3). This method of plating offers less porous coatings that have better corrosion resistance [19]. As Benaben

[21] described, the use of electroless plating on steel requires a thin film of copper to be deposited on the steel prior chromium plating, as an intermediary step to prevent the contamination of the plating bath.

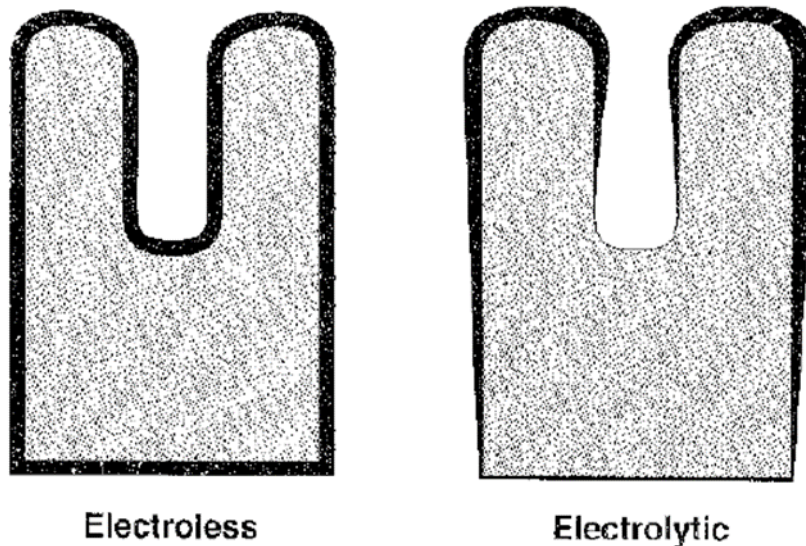


Figure 3. Comparison Between Electroless and Electroplating Deposition Uniformity. Source: [20].

3. Sputtering

Sputtering is classified as a physical vapor deposition that is generally used for creating thin films. In a PVD process, no chemical reactions take place. The metal is added by mechanical means only. In the sputtering process, an inert gas (e.g., argon) is supplied to a vacuum chamber with a target material and a substrate [22]. Positively charged argon ions created by electric breakdown, accelerate and bombard the target material [22]. The interaction between these argon ions and the target material causes atoms from the target material to vaporize upon hitting the substrate at high kinetic energy and then deposit on the substrate [22], as shown in Figure 4.

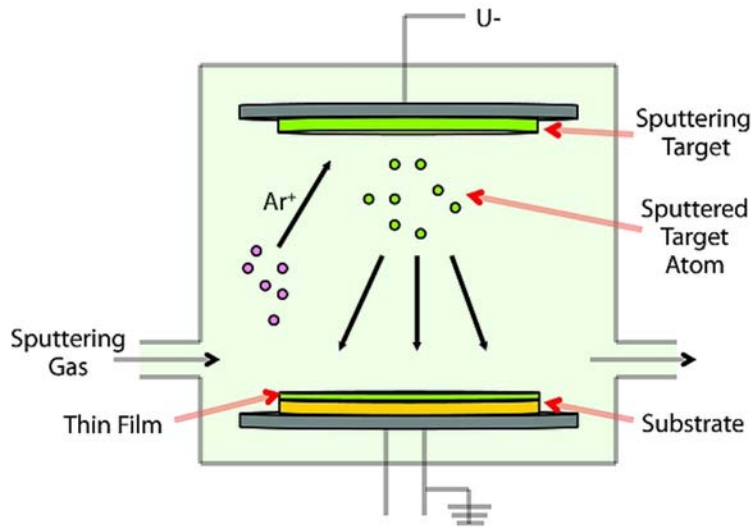


Figure 4. Physical Vapor Deposition Using Sputtering Method. Source: [22].

This process can be used to create thin films that are several nm or microns thick [22]. There are a few issues with this method of coating. First, the desired component that needs the coating has to be small enough to place into a vacuum chamber. Second, the for complex component geometries have to be rotated and tilted during coating deposition in order to provide a uniform coating to the surface [1]. This also can place constraints on the geometry of the component that requires a coating. However, sputtering is ideal and widely used to create thin films used for a variety of different applications (e.g., biomedical applications, optical or electrical components, conductive coatings) [22]–[23]. There are limits to sputtering technology, particularly chrome coatings are not currently deployed commercially [1].

4. Cold Spray

Cold spraying is another physical technique that uses metal powder and compressed gas to feed the powder to a converging-diverging nozzle [24], as shown in Figure 5. The converging-diverging nozzle has no moving parts and the pressures and temperature increase until the mixture reaches the throat at which point the gas accelerates to a supersonic speed [24]–[25]. To prevent undesired combustion, an inert gas is required for because the gas temperature increases to 100–500°C in the converging

section on the nozzle [24]. The powder is accelerated to minimum velocity of 500–800 m/s before it impacts the target substrate to ensure the particles fuse to the surface of the substrate [24].

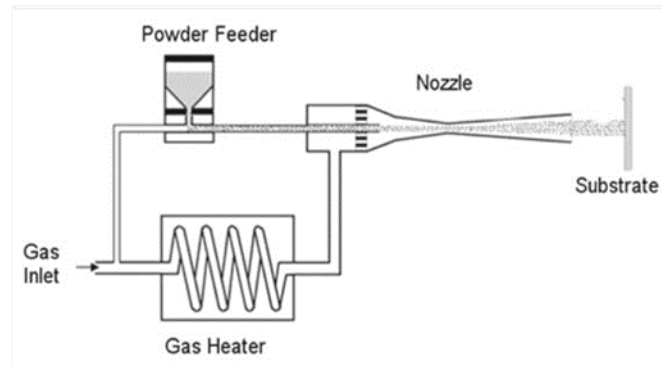


Figure 5. Cold Spraying Diagram. Source: [24].

5. Thermal Spray

The preparation of the substrate is crucial for another physical method, thermal spraying. The surface needs to be cleaned and slightly roughened to promote a strong bond between the substrate and the metal coating [26]. Thermal spraying uses wires that are fed into the arc-gun which instantaneously liquefies the metal, as a compressed gas forces the molten metal droplets to strike and deposit on the substrate, as shown in Figure 6 [27]–[28]. The most commonly applied coatings for iron substrates are zinc and aluminum and thicknesses can range from 76–304 μm depending on the intended use of the component [27]. In addition, a nickel-chrome alloy is used when the component's operating temperature is approximately 980°C [27]. One limitation of this method is that the metal spray is limited to a line of sight, therefore it would not be beneficial to use on a substrate with an intricate design [26].

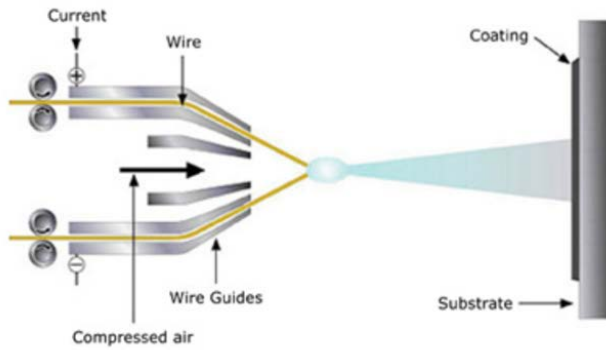


Figure 6. Thermal Spray Coating Diagram. Source [29].

6. Thermal Evaporation

In the thermal evaporation process, first, a crucible is filled with an evaporant that contain the material for film generation [30]. Second, the crucible is heated to a temperature that will make the source material, which will then condense on the substrate and absorbed into the surface, as shown in Figure 7 [30]. Chen [30] further explains, that the deposition rate for this method is a function of the source temperature and vapor pressure of the evaporant. This method is ideal for generating thin films on small substrates, as the substrate needs to be placed into a vacuum chamber.

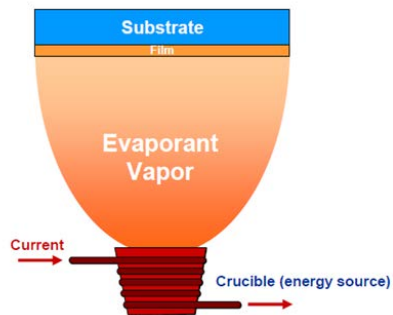


Figure 7. Thermal Evaporation Diagram. Source: [30].

B. HEALTH AND ENVIRONMENTAL HAZARDS

It is well known that the electroplating process produces toxic and harmful vapors that effect both the environment and the health of those who work in that industry. Chromium primarily occurs in the form of either trivalent or hexavalent chromium [31]. The highest rate of exposure to hexavalent chromium is the inhalation of the aerosol mist during the electroplating process and the addition of chromic acid to the coating tank [2]. As a result, OSHA has mandated that a respiratory protection shall be used, when operations will exceed the permissible exposure limit for hexavalent chromium [12]. Other sources of exposure to hexavalent chromium include ingestion (e.g., water and soil) and skin contact, which have proven to be less harmful [32]. In contrast, according to the EPA [33]–[34], trivalent chromium does not pose a carcinogenic threat to humans.

Several studies conducted report that exposure to hexavalent chromium may result in lung cancer, skin lesions, and also birth defects when drinking, water is contaminated [3]–[6]. In 2006, OSHA updated the permissible exposure limit of hexavalent chromium lowering from $52 \mu\text{g}/\text{m}^3$ to $5 \mu\text{g}/\text{m}^3$ to reduce exposure to those in the electroplating industry [3], [12]. When compared to six other well-known carcinogens hexavalent chromium exposure results in a highest risk of cancer as shown in Table 1.

Table 1. Hexavalent Chromium Compared to Other Well-Known Carcinogens. Adapted from [10].

Material	Cancer Risk (per 1000)	OSHA Ruling
Asbestos	6.7	June 1986
Benzene	10	September 1987
Formaldehyde	0.0056 – 2.64	December 1987
Cadmium	3-15	September 1992
1,3 – Butadiene	1.3 – 8.1	November 1996
Methylene Chloride	3.6	January 1997
Chromium VI	10-45	February 2006

C. REDUCTION EXPANSION SYNTHESIS (RES)

The RES method, focus of this thesis, is a relatively simple process that generates metallic particles from metal precursor species, salts such as NiO, Fe₂O₃ and Fe(NO₃)₂. Zea et al. [35] describes this reductive process as two steps. First, metal precursors are combined with a reducing agent (urea) [35]–[36]. Second, this mixture is placed into a furnace to increase the temperature (approximately 700°C), to the point where the reducing agent decomposes [35]. When the reducing agent decomposes, a gaseous reducing species is released to reduce the metal oxide to its pure metallic form [35], [37].

This RES process is the guiding framework for the proposed work. To create a thin film of reduced metal, a metallic paste is created by adding deionized water to the mixture containing the metal precursor and reducing agent. This paste is applied to a metal substrate, then using the RES method, a thin metal coating will be deposited on the surface of the metal substrate.

D. MOTIVATION AND GOALS

In recent years, the implementation of government regulations on the use of hexavalent chromium coatings have increased due to the serious health and environmental risks associated with the current manufacturing methods [2], [7], [11]–[13], [32], [38]–[39]. As a result of these regulations, the life cycle maintenance costs of many DOD assets have increased, suggesting that a safe alternative to the use of hexavalent chromium coatings needs to be developed. To find a suitable replacement for the current methods widely used in industry, other research is being pursued for chrome coating applications. This research includes the following methods high-velocity oxygen fuel, sputtering, plasma nitride PVD, trivalent chromium electrodeposition, and arc PVD [11], [15]–[18], [40]–[42]. The focus of this study is to build on the research completed by Greenaway [40], with use of the RES process to find a suitable replacement for the hexavalent chromium coating processes by using trivalent chromium as the metal precursor.

The first goal of this study is to determine whether the RES method can be used to create metal coatings. The findings from this study show that the RES method was

successful at creating a unique nickel coating on an iron foil. To validate the use of a trivalent form of chromium, the second goal is to determine if chromium (III) oxide can be used to create a chrome coating on an iron substrate. However, the results of all the chromium-based experiments did not fully reduce to create a chrome coating on the surface of iron wires.

II. EXPERIMENTAL METHODS

This chapter describes the experimental procedures used to reduce the metal oxides and nitrides to their pure elemental form for use in coating applications. Throughout this study, iron was used as the metal substrate for the coating process. Initially iron was chosen because generally, when iron is alloyed with other materials, it is the most widely used metal engineering material. Moreover, coating iron is a common practice, as a means to reduce and mitigate the effects of corrosion. For these experiments, two different geometric substrates were used: initially an iron wire (Sigma Aldrich, 99.99%) with a 1 mm diameter, then a thin foil (Alfa Aesar, 99.99%) with a nominal thickness of 0.25 mm. The iron wire substrates were cut to an average length of 3.8 cm (1.5 inches), then coated using one of the coating protocols. Once the substrate was coated, it was placed into a tube furnace (Lindberg Blue M) to permit the temperature control required for the RES method of metal film formation.

A. SURFACE TREATMENT OF METAL SUBSTRATES

Prior to the coating application process outlined in the protocols, the iron substrate was first polished using Pol Metal Polish (Reckit Benckiser). In this process, the iron substrate was coated with the metal polish. Then using a lint-free wipe (Sigma Aldrich), the polish was rubbed on the surface of the iron to remove any contaminants and oxides (rust). This polishing process was only conducted prior to the first coating application. Subsequent coating applications were rinsed with ethanol (Sigma-Aldrich) and then cleaned with the lint-free wipe (Sigma-Aldrich) to remove any unreduced reactants or chemical byproducts. A brief set of experiments were conducted to characterize the surface of the iron wire to obtain a baseline composition of the material.

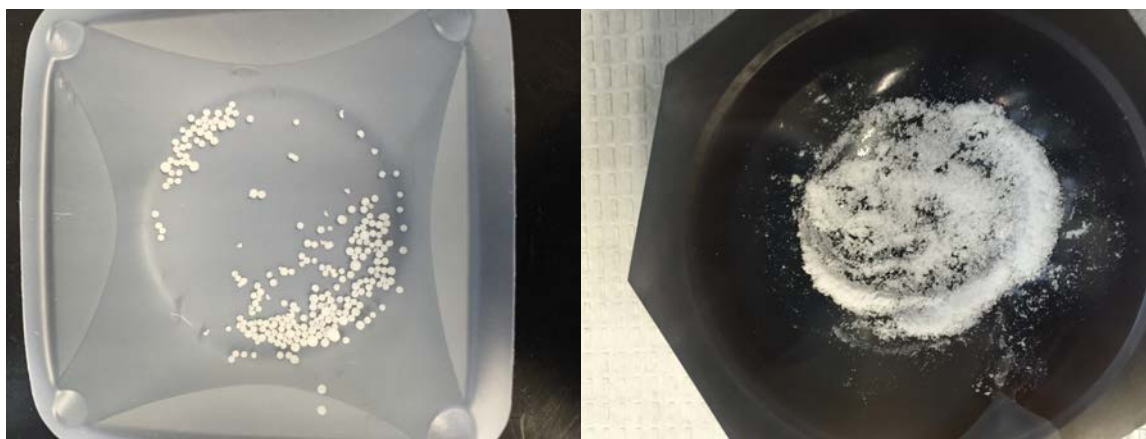
B. CHROMIUM BASED RES PROTOCOLS

Three chromium-based protocols were developed during the course of this study. The first and second protocols were used to coat iron wires to be characterized to determine if the coating contained a fully reduced chromium. The third protocol was

developed to determine if the precursor used in RES Coating Protocol II could be reduced alone when mixed with a reducing agent in an inert atmosphere.

1. RES Coating Protocol I

Initially, this study used two reactants: chromium (III) nitrate nonahydrate (Sigma-Aldrich, 99%) and urea (Sigma-Aldrich, 99.5%). First, to obtain the desired weight ratio of urea to chromium (III) nitrate nonahydrate, the mass of these two chemicals were carefully measured. After initial SEM analysis, it was noted that the samples created using a 1:1 weight ratio contained an excessive amount of oxygen. Thus, in an attempt to reduce the amount of oxygen present, the weight ratio of urea to chromium (III) nitrate nonahydrate was increased to 2:1. Using a mortar and pestle, the urea pellets were crushed into a fine powder, as shown in Figure 8. The chromium (III) nitrate nonahydrate was then added to the urea, further crushed, and mixed using the mortar and pestle. During the process of mixing the two reactants, the powder mixture converts to a dark colored paste, as shown in Figure 9. This paste was then placed into a clean vial and sealed to prevent water intrusion, using parafilm (Sigma-Aldrich). The vial was placed into an ultrasonic cleaner for 10 minutes to create a uniform solution.



The image on the left shows the urea pellets as purchased from the manufacturer. The image on the right shows the urea pellets after being crushed into a fine powder.

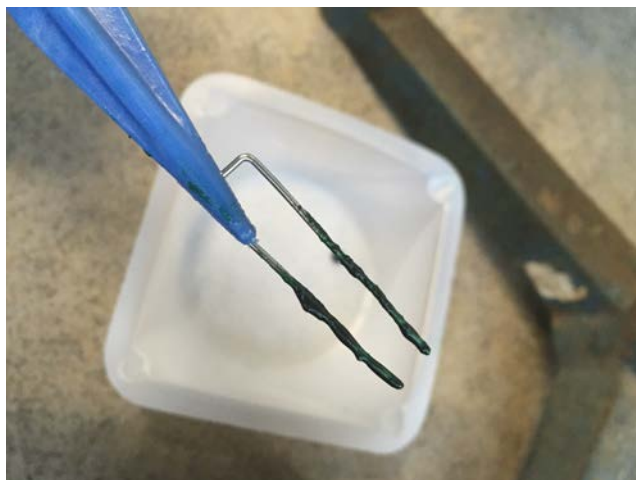
Figure 8. Crushed Urea Powder



By mixing the urea with the chromium (III) nitrate nonahydrate, it began to form a paste that was then further processed prior to applying to an iron wire sample.

Figure 9. Urea and Chromium (III) Nitrate Nonahydrate Paste

The iron wire was then prepared, by initially cutting the wire to a length of 3.8 cm. Subsequent preparations included increasing the length of the iron wire to approximately 8.25 cm then bending the wire into a “U” shape in order to coat two samples at once. First, the sample wire was then polished using the Pol metal polish and wiped clean with a lint-free wipe. Second, the sample wire was rinsed clean with ethanol and dried with a lint-free wipe. Next, the sample wire was placed into the uniform solution of urea and chromium (III) nitrate nonahydrate and allowed to soak for one minute. Then sample wire was removed from the solution and air-dried with an electric fan. During the process of drying, it was noted that the coating would “sag” toward the ground as the sample was orientated in the vertical direction and allowed to slowly dry. Thus, the coating at the bottom end of the wire was invariably slightly thicker, as shown in Figure 10. The iron wire was placed into a pair of clamps and placed over a fan to allow the solution to air-dry on the wire.



The chromium (III) nitrate nonahydrate coating would “sag” due to gravity, as the sample was orientated in a vertical position during the drying process.

Figure 10. RES Protocol I Sample Drying

Once the solution had dried, the iron wire was placed into an alumina crucible, and placed into a 20 mm diameter quartz tube, in preparation for the reductive process. The reductive process is best described as a five-step process. Step 1, the quartz tube was attached to a gas control system, and then a leak check was conducted using the exhaust tube and a beaker of water. The tube was placed into the furnace with the sample outside of the heated area and cooled with electric fans. Step 2, the furnace was energized and thermostat set to the desired temperature for the experiment. Step 3, once the tube was purged with nitrogen gas (Praxair, 5.0 Ultra High Purity), the flow rate was reduced to the desired flowrate for the experiment. Step 4, approximately 14 minutes after heating initiated, the furnace temperature reached the correct temperature for the experiment and the quartz tube was positioned such that the sample was in the center of the furnace for 10 minutes. Notably, during this process of sliding the quartz tube into the furnace (step 4), the temperature would decrease approximately 250°C from the set point. During the 10 minute reductive process, the temperature would steadily rise, reaching the set point prior to the end of the 10 minute process. Step 5, once the reductive heating process was complete, the quartz tube was quickly removed from the furnace and placed on a cooling rack to allow the sample to cool to room temperature. The cooling was assisted by using

an electric fan on the exterior of the quartz tube. During the cooling process, the nitrogen flowrate was increased to 100 SCCM from the desired experimental flowrate.

During the reductive process, after approximately 45 seconds, a white gas became visible in the quartz tube, leaving the heated portion of the furnace. Once the sample was at room temperature, visual observations were made and the sample was rinsed with ethanol and dried using a lint-free wipe. The sample was then placed into a clean vial and cataloged for future analysis. Some of these samples were coated multiple times in an effort to increase the coating thickness, using the coating method previously mentioned.

2. RES Chromium (III) Oxide Precursor Protocol

The following procedures were used to synthesize chromium (III) oxide (Cr_2O_3) from chromium nitrate nonahydrate. The mass of the chromium nitrate nonahydrate was measured to obtain its initial mass. Next, the chromium nitrate nonahydrate was placed into an alumina crucible in preparation for the heat treatment. Then, the crucible was placed into a 20 mm diameter quartz tube. The ends of the quartz tube were sealed with fittings in order to contain any potential hazardous gasses from the decomposition of the chromium nitrate nonahydrate. For this protocol, the quartz tube was not purged to remove any excess oxygen prior to heating. The sealed quartz tube was then placed into a furnace at 800°C for 10 minutes. During the decomposition process, it was noted that after approximately 45 seconds of heating, a white gas was observed leaving the heated section of the quartz tube. After 60 seconds, a dark orange gas was observed leaving the heated portion of the quartz tube, as shown in Figure 11.



Decomposing chromium nitrate nonahydrate to form the precursor material at 800°C.

Figure 11. Chromium Nitrate Nonahydrate Decomposition at 800°C

Following the reductive process, the powder was cooled to room temperature. Once the powder had reached room temperature, the quartz tube was purged with nitrogen at 100 SCCM for 5 minutes, to remove any hazardous gasses from the tube via the ventilation hood. When the byproducts reached room temperature, it was observed to be a green-colored chromium-based precursor powder. The mass of the synthesized precursor was then measured and recorded. This precursor powder was then analyzed using a Rigaku MiniFlex 600 X-ray Diffractometer (XRD) to determine the crystal.

It was noted from this procedure, much of the chromium present in the precursor mixture was “lost” during the process. In one case, after placing 0.529 grams of chromium nitrate nonahydrate into the furnace, only 0.0960 grams of material (later revealed as chromium (III) oxide) was recovered. Approximately 18% of the initial weight remained after the heated synthesis. In order to increase the amount of precursor synthesized various experiments were conducted by increasing the amount of chromium nitrate nonahydrate to 3.3690 grams to increase amount of material synthesized for subsequent coating applications. By increasing the amount of chromium nitrate nonahydrate, the efficiency gained was purely the weight of the material produced, but did not improve the percent of weight of the initial mass used in the experiment.

3. RES Coating Protocol II

This method used the urea and chromium (III) oxide precursor generated by using the “RES Chromium (III) Oxide Precursor Protocol” to coat iron wire samples. Several compositions were attempted based on changing the urea and precursor ratio. Initially this coating protocol started with a lower weight ratio of urea to chromium (III) oxide, which resulted in a dark coating. Further experiments were conducted with an increased urea to chromium (III) oxide weight ratio in order to increase the amount of carbon in the reaction. First, the chromium (III) oxide precursor and urea masses were measured and recorded. Then, the urea pellets were crushed into a fine powder using a mortar and pestle. Next, the chromium (III) oxide was added to the urea powder, as depicted in Figure 12. Once the mixed powder obtained a uniform color, as shown in Figure 13, it was placed into a plastic mixing boat. The total mass of the mixture was recorded. To create a paste with the urea and chromium (III) oxide powder, deionized water (Weber Scientific) was incrementally added using a dropper, until the powder formed a paste, as shown in Figure 14. The mass of the paste was then measured and recorded along with the number of drops used to make the paste.



This image shows the chromium based precursor being added to the urea powder for further processing.

Figure 12. Chromium Based Precursor Added to Urea Powder



The urea and chromium precursor powders were mixed using the mortar and pestle to create a uniform powder.

Figure 13. Combined Urea and Chromium Precursor Powder



Deionized water was added to the mixed urea and chromium precursor powder to create a paste applied to the iron substrate.

Figure 14. Urea and Chromium Precursor Paste

Next, the iron wire was prepared for coating. The sample was cut to the requisite length then polished using the POL metal polish. Then, the wire was placed into the paste for 2 minutes. After the two minutes, the wire was allowed to air dry using an electric fan. As some of the water evaporated from the paste, a white powder began to form on

the exterior of the coating, illustrated in Figure 15. In order to assess the effect of coating thickness on the outcome, in some cases the “coat/dry” process was repeated multiple times before using the reductive heating process.



When the coated iron wire paste began to dry, white precipitates began to form on the exterior of the coating.

Figure 15. Coated Iron Wire Drying That Formed Precipitates

The coated wire was placed into the furnace using the standard reductive process as previously outlined. Once the sample had cooled to room temperature, it was removed from the quartz tube. The heat treatment of the coated wire resulted in a brittle powder on the exterior of the wire, as shown in Figure 16. In order to remove this prior to subsequent coatings or analysis, the sample was cleaned by rinsing with ethanol and wiping clean with a lint-free wipe, as shown in Figure 17. The sample was then placed in a clean vial and cataloged for future analysis.



After removing the sample from the quartz tube, it was observed to have a dark green brittle coating.

Figure 16. Coated Iron Wire When Cooled to Room Temperature



After rinsing and cleaning the coated sample was observed to be very shiny, which led a hypothesis that a thin chromium layer formed on the iron substrate.

Figure 17. Post Cleaning of Coated Iron Wire

4. Chromium Powder RES Experiments

Due to the lack of success achieved with the previous chromium experiments (see 'Results' section), a brief study was attempted to reduce the chromium (III) oxide powder to the pure metallic form by changing the weight ratio, furnace temperature, and nitrogen

flowrate. The protocol was essentially identical to the coating experiments described in the prior sections, but without coating any object. In this series of experiments, the mass of urea was measured and recorded based on the appropriate weight ratio. The urea pellets were then crushed using a mortar and pestle to create a fine powder. Next, the mass of chromium (III) oxide was measured and recorded. The oxide powder was added to the urea powder and mixed until it created a uniform powder. The mass of the mixture was measured, recorded, and placed into an alumina crucible. This crucible was placed into the standard 20 mm diameter quartz tube and processed using the standard reductive process, with a few exceptions. The purge duration was reduced from 30 minutes to 10 minutes at an increased nitrogen flowrate of 150 SCCM. Following the reductive process, the sample was removed from the tube and the mass of the product was measured. These samples were analyzed using the XRD to determine the chemical composition of the powder.

a. Urea, Iron, and Chromium (III) Oxide

Using the same procedure outlined for Chromium Powder RES Protocol, an experiment was conducted by adding iron powder (Alfa Aesar, 98+%) to the urea and chromium (III) oxide. The guiding hypothesis was that the iron would preferentially oxidize and remove the oxygen atoms from the chromium oxide. This powder was created by using a weight ratio of approximately 2.4:1.1:1 of urea to iron to chromium (III) oxide. First the urea mass was measured, then the urea pellets were placed into the mortar and crushed to create a fine powder. Next, the chromium (III) oxide powder was measured and added to the urea and mixed in the mortar. Finally, the iron powder was measured and added to the mixture of urea and chromium, in order to have enough iron to accept the oxygen atoms from the chromium (III) oxide.

This powder was processed using the same technique and parameters for the temperature and nitrogen flow rate as previously outlined. Upon cooling the powder to room temperature it was noted that the byproduct of the reaction had a very similar green color when compared to the chromium (III) oxide.

b. Potassium Carbonate, Lignite and Chromium (III) Oxide

Another experiment was conducted to attempt to reduce the chromium (III) oxide to the pure metallic form. In this experiment, 0.0499 grams of lignite (Phillips) was mixed with 1.7287 grams of potassium carbonate (Sigma-Aldrich, 99.995%). This mixture was placed into the bottom of the alumina crucible. Next, a thin piece of graphite foil (Fralock) was cut into a rectangle approximately 3 cm by 7.5 cm. A metal tack was then used to place holes into the graphite foil, as depicted in Figure 18. Then, 0.3164 grams of chromium (III) oxide was placed on top of the graphite foil to allow gasses from the lignite and potassium carbonate to perforate through the foil to reduce the chromium (III) oxide, as shown in Figure 19. Upon cooling the sample to room temperature, it was noted that the chromium (III) oxide powder retained the same color and appeared the same as prior to conducting this experiment. Then, the sample was placed in to a clean vial to await further analysis using the XRD.



Lignite and potassium carbonate mixture were placed in the crucible with a perforated piece of graphite foil.

Figure 18. Lignite and Potassium Carbonate Mixture and Perforated Graphite Foil



The chromium precursor was placed on top of the graphite foil, which was placed over the lignite and potassium carbonate mixture.

Figure 19. Chromium Precursor Loaded on Top of Graphite Foil for RES Protocol

c. Carbon and Chromium (III) Oxide Powders

Similar to the previous chromium-based powder experiments, an additional experiment was conducted using a carbon powder (Cabot Vulcan XC72). A weight ratio was selected for this experiment and the two powders were measured. The chromium (III) oxide and carbon powders were mixed together using a mortar and pestle. Once the powders were mixed, they were placed into an alumina crucible and placed into the furnace using the standard 5-step reductive process previously described. This sample was then prepared for XRD analysis.

d. Carbon, Potassium Carbonate, and Chromium (III) Oxide Powders

Another powder-based experiment was conducted using potassium carbonate, carbon, and the chromium (III) oxide powders. A preselected weight ratio was used to portion the powders properly and mixed together using a mortar and pestle. Once these powders were mixed, they were placed into an alumina crucible and processed using the 5-step reductive heating process. This sample was prepared for XRD analysis.

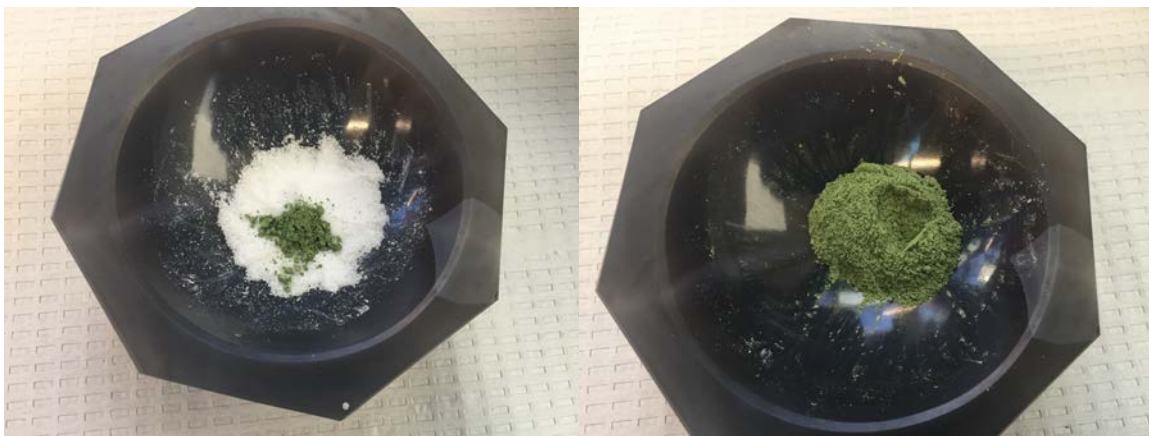
C. NICKEL POWDER RES PROTOCOLS

Two nickel based protocols were used during this portion of the study. The first protocol used was strictly to determine the parameters needed to reduce the nickel precursor to a nickel powder. The second protocol used was similar to the RES Coating Protocol II, although an iron foil was chosen as the substrate.

1. Nickel Powder RES Experiments

In order to demonstrate the potential applications of the RES method, experiments were conducted using a metal oxide that could be easily reduced, as demonstrated in [37], [40]. Specifically powder-based experiments were conducted with urea and Nickel (II) Oxide (Sigma-Aldrich, 99%) to determine the correct weight ratio and other parameters to increase the probability of reducing the oxide to its pure metallic form. The Gibbs Free Energy (ΔG) of formation of chromium (III) oxide is -249, whereas the ΔG of formation of nickel (II) oxide is -52, therefore the latter is more easily reduced [43].

The protocol employed was nearly identical to that used in the chromium powder and urea protocol, except nickel (II) oxide was substituted in place of the chromium precursor. First, the mass of urea was measured based on the proper weight ratio and recorded. Then the mass of nickel (II) oxide was measured and recorded for the appropriate experimental ratio. Then, using a mortar and pestle, the urea pellets were crushed into a powder. The nickel (II) oxide was then added to the urea powder and mixed together to create a uniform powder, as shown in Figure 20. This mixture was placed in to an alumina crucible and placed into a 20 mm diameter quartz tube. The ends of the quartz tube were sealed with fittings and the nitrogen flowrate was initially set to 5 SCCM to conduct a leak check with a beaker filled with water. After a successful leak check, the nitrogen flowrate was increased to 150 SCCM for 10 minutes to purge the quartz tube of any oxygen. Once the purge was completed, the nitrogen flowrate and furnace thermostat temperatures were adjusted to the desired flowrate for the experiment.



The image on the left shows the crushed urea powder and the nickel (II) oxide powder added. The image on the right shows the two powders mixed to form a uniform powder.

Figure 20. Urea and Nickel (II) Oxide Powders Combined and Mixed

Once the furnace reached the desired temperature, the quartz tube was placed into the furnace, with the powder outside of the heated zone and cooled with electric fans. Once the furnace temperature reached the desired set point, the quartz tube was repositioned, exposing the sample to the heat for 10 minutes. After the 10 minutes elapsed, the quartz tube was removed from the furnace, the nitrogen flowrate was increased to 100 SCCM and allowed the sample to cool to room temperature using the cooling fans on the quartz tube, as shown in Figure 21. Once the powder cooled, the mass of the product was measured and recorded. These samples were labeled and later analyzed in the XRD to determine the chemical composition of the samples.



The reduced nickel powder cooling to room temperature.

Figure 21. Reduced Nickel Powder Cooling to Room Temperature

2. Nickel Coating RES Protocol

For this proof of concept experiment, an 8:1 weight ratio of urea to nickel (II) oxide was used, as previous experiments discovered that it fully reduced to pure metallic nickel, according to [37]. First, the iron foil was cut into a rectangular sample of 1 cm by 0.75 cm, as shown in Figure 22. The mass of the iron foil was measured and determined to be 0.1944 grams. The surface of the iron foil was then polished, using the POL metal polish, for approximately two minutes to remove any surface contaminants that may have been present from the packaging. The metal polish was removed using a lint-free wipe and then rinsed with ethanol. The mass of the iron foil was again measured at 0.1938 grams and noted a decrease in mass of 0.0006 grams.

First, the urea and nickel (II) oxide were measured and mixed. Second, the urea was measured and placed into the mortar. Using the mortar and pestle, the urea pellets were crushed into a fine powder. Next, the nickel (II) oxide was measured and added to the crushed urea in the mortar. The urea and nickel (II) oxide were then mixed together to create a uniform powder. The mass of the combined powder was measured. Some of the material was difficult to remove from the mortar after mixing, which resulted in a loss of material. Then deionized water was added using a dropper until the powder created a

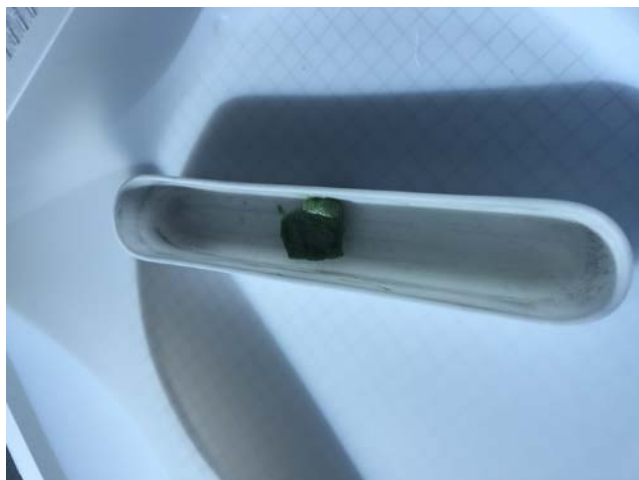
uniform paste. It was noted that the nickel (II) oxide was not very soluble in the deionized water, similar to the chromium (III) oxide.



Iron foil sample after being polished with POL metal polish.

Figure 22. Prepared Iron Foil

Paste was applied to the iron foil, using a spatula in an attempt to obtain a uniform thickness. The mass of the iron sample with paste was measured to determine the mass of the paste applied to the foil, as shown in Figure 23. The standard RES reductive heating process with some modifications was employed with the following exceptions: the leak check was conducted at 5 SCCM, the gas purge flowrate was increased to 150 SCCM for 10 minutes, furnace temperature was increased to 1100°C, and the gas flowrate during the experiment was decreased to 8 SCCM. When positioning the tube at the furnace center, it was noted that the temperature decreased to approximately 760°C and steadily increased throughout the 10 minutes the sample was in the furnace. The furnace finally achieved 1100°C after the sample had been in the furnace for approximately nine minutes.



The paste was applied to the sample using a spatula, and placed into the alumina crucible for the reductive heat treatment.

Figure 23. Nickel Based Paste Coated Iron Foil

After approximately 25 minutes, the sample had cooled to room temperature, as shown in Figure 24. Next, the sample was removed from the quartz tube and displayed the same characteristics as the reduced nickel powder from previous experiments. The surface was coated with a dull-gray colored nickel based powder. The mass of the iron foil was measured again following the heated synthesis to determine the mass of the reduced nickel coating applied.



Nickel coated foil sample cooling to room temperature.

Figure 24. Nickel Coated Iron Foil Cooling to Room Temperature

D. CHARACTERIZATION

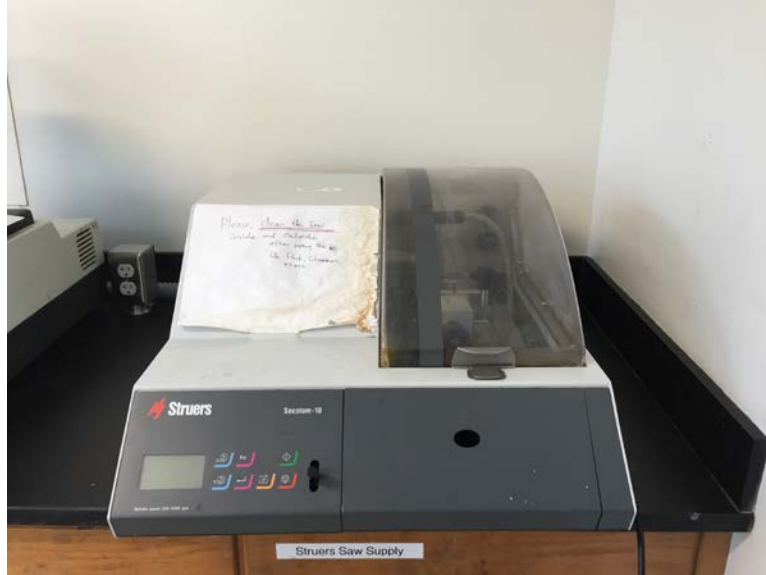
Characterization of the samples was conducted to determine first if the precursor had reduced to the metallic form of either chromium or nickel. Also during characterization, the surface morphology was examined to determine whether the coating applied was uniform. The following characterizations methods were used: optical microscopy, scanning electron microscopy (SEM) with energy dispersive spectroscopy (EDS), x-ray diffraction (XRD), and focused ion beam (FIB) in the SEM.

1. Sample Preparation

The following processes were used to prepare each sample for subsequent analysis. The process employed, evolved as required to yield more accurate information about the coatings, which formed during the film synthesis on wire and foils.

a. Cutting

After the sample had been coated, the iron wire was cut using a Struers Secotom-10 high-speed saw with a rotational speed of 300 RPM and a feed rate of 0.5 mm per minute, as shown in Figure 25. Cutting the sample exposed the cross-sectional area that would be mounted and further analyzed to characterize the coating. It was decided to use a saw to cut the sample, in order to reduce the effects of mechanically cutting the sample with pliers to reduce grinding and polishing as encountered in [40]. This resulted in very little deformation compared to that of the pliers and decreased the amount of grinding required to achieve a uniform cross-section for observation.



The Struers Sectom-10 saw was used to cut the wire samples prior to mounting for future characterization of the coatings.

Figure 25. Struers Sectom-10 Saw

b. Mounting

Mounting the sample for future characterization was accomplished using a Buehler Simplimet 2 hot mounting press, as seen in Figure 26. Once the iron wire was cut to a length of less than 2 cm, it was placed vertically into a spring specimen holder. The sample was placed in the press and KonductoMet (Buehler) conductive mounting material was added on top of the dye. Following the standard operating procedure, the hot mounting press formed a puck around the coated sample. Once the mounted sample had cooled to room temperature, it was engraved for identification purposes.



This mounting press was used to mount samples to characterize the cross sections and measure the nominal thickness of the applied coatings.

Figure 26. Buehler Simplimet 2 Mounting Press

c. Grinding

In order to prepare a very smooth surface appropriate for cross sectional analysis in the SEM, mounted samples were subjected to a grinding process using a Buehler grinding table as shown in Figure 27. This grinding process uses a course silicon carbide sand paper and then incrementally changed to finer grinding papers throughout the process. First, the sample was manually ground using a 240-grit silicon carbide sand paper for 2 minutes, while rotating the sample every 30 seconds. This was followed by a 320-grit silicon carbide sand paper for 5 minutes while rotating the sample every 30 seconds. Then, the mounted sample was ground using a 400-grit silicon carbide sand paper for 10 minutes, while rotating the sample every 30 seconds. Finally, the sample was ground using a 600-grit silicon carbide sand paper for 10 minutes, while rotating the sample every 30 seconds. Upon completion, the sample was visually inspected to ensure there were no visible scratches on the surface of the mounting material and sample wire.

It was noted during this process, that some of the samples were not perfectly mounted perpendicular to the dye, because of the sample shifting in the specimen holder during the mounting process.



Buehler grinding table used to grind the mounted samples prior to polishing.

Figure 27. Buehler Grinding Table

d. Polishing

To complete the process of producing a cross-section optimized for SEM analysis, a final polishing step was performed using a Buehler polishing wheel for 30 minutes as shown in Figure 28. During this process deionized water and a 0.05 μm alumina powder solution were used to polish and keep the sample cool. The alumina solution was applied every two minutes while the sample was being polished and water was applied approximately every 60 seconds. While polishing, the sample was rotated approximately every 30 seconds to ensure the surface of the cross section would be as flat as possible to better view the sample with the SEM.



Buehler polishing wheel used to polish sample for 30 minutes.

Figure 28. Buehler Polishing Wheel

2. Optical Microscopy

A Nikon Epiphot 200, computer operated optical microscope was used initially to view the surface of the coated samples prior to analyzing with a high resolution SEM. In addition, a Dino-Lite Digital Microscope was used for visual observations on the coated samples and RES powders prior to further analysis. When using the optical microscope only a small portion of the iron wire was clearly visible, while the rest of the sample was out of focus. This method was more useful to observe the cross-sections of the mounted samples, as the entire area was within focus.

3. Scanning Electron Microscopy (SEM) – Energy Dispersive Spectroscopy

The Zeiss Neon 40 scanning electron microscope was used to complete most of the analysis on the samples, as seen in Figure 29. The SEM was used to obtain microscopic images of the surface of the material and the areas that had been coated

using secondary electrons to view the topography of the sample [44]. The SEM also had the Energy Dispersive Spectroscopy (EDS) feature, which was used to determine the chemical composition of the material and the applied coating. The SEM's backscatter diffractometer was used to visualize the contrast in atomic composition, as higher atomic numbers will appear brighter [44]. During the characterization of the samples, the instrument was used the following settings: voltage of 20 kV, an aperture of 60 μm , and a working distance of 5–6 mm to obtain the best results.



The Zeiss Neon 40 scanning electron microscope was used to characterize the coated samples and powders by using energy dispersive spectroscopy.

Figure 29. Zeiss Neon 40 Scanning Electron Microscope

4. X-ray Diffraction (XRD)

Figure 30 shows the Rigaku MiniFlex 600 XRD used to analyze and obtain diffraction spectrums from the chromium-based precursor, chromium, and nickel RES protocol experiments. During analysis, the instruments parameters were set to a voltage

of 40 kV and an amperage of 15 mA. The instrument recorded the x-rays that were diffracted by the loaded sample. This spectrum of peaks was loaded into the PDXL2 software and further processed to characterize the samples and generate the intensity versus 2θ (degrees) spectrums, in order to identify the material composition each sample.



The Rigaku MiniFlex 600 was used to characterize the powders to identify the material composition.

Figure 30. Rigaku MiniFlex 600 X-Ray Diffractometer

5. Focused Ion Beam (FIB)

The Zeiss Neon 40 SEM was used to mill the surface of one sample with a Focused Ion Beam in an effort to obtain a coating thickness measurement. This was conducted by milling two separate trenches on the surface of the sample. Then, this area was characterized using EDS to determine if the interface of the coating and substrate could be located. This method was also used to mill the surface, in order to reduce the amount of carbon detected during an EDS analysis.

THIS PAGE INTENTIONALLY LEFT BLANK

III. RESULTS AND ANALYSIS

This chapter discusses the results of the analysis of three categories of iron samples: (i) uncoated, (ii) chromium coated, and (iii) nickel coated. The goal of the first study was to establish a baseline composition of the substrate after cleaning and polishing. The goal of the second set of studies was to determine the phase, morphology, and thickness of “chrome coatings” as a function of the protocol employed. The goal of the third set of studies was to determine the phase, morphology, and thickness of the nickel film that formed.

The results of the first study of the uncoated samples demonstrated that polishing the sample reduced the initial amount of carbon present on the sample. This study did not find a correlation of the reduction in carbon content as a function of the duration of polish. It confirmed that simply using a wipe to remove the polishing compound removed any chemical trace that could be detected using the EDS. In addition, this study determined that the use of ethanol to rinse the sample resulted in no chemical traces of hydrocarbons and removed contaminants from the cutting process.

The results of the second study indicated that the chromium (III) nitrate nonahydrate and the chromium (III) oxide precursor used in the experiments never fully reduced to a metallic chromium state. These experiments resulted in samples that were partially coated, primarily with partially reduced chromium oxide particles that did not reduce to form the target morphology of a uniform chromium metal surface. Several powder-based experiments were conducted to further explore the effects of different weight ratios, temperatures, and chemicals that could be employed to reduce the chromium (III) oxide. The results of the powder-based experiments illustrated that the chromium (III) oxide cannot be fully reduced with the parameters and chemicals employed in the RES protocols.

The results of the third study illustrated that nickel (II) oxide can be reduced to form nickel particles, when using the correct parameters. With the success of reducing a nickel based powder, a RES coating protocol was developed and employed to create a

coated sample. This sample was characterized and determined to have a surface layer with a reduced nickel layer. This demonstrated that the RES process for creating a metal layer on a metal substrate is possible. It also suggests a path forward for making other metal layers other than nickel, including chromium.

A. CONTROL STUDIES SURFACE TREATMENT OF IRON SUBSTRATES

During the coating application of the chromium oxide precursor paste, it became apparent that the paste would not adhere to the surface of the wire. A spatula was used to manually apply the paste to the sample wire. In order to determine if the polishing compound created a thin chemical film that would prevent the adhesion of the coating or in any fashion impact the results, a few experiments were conducted on the iron wire substrate, in which no chemical coating process was performed (Table 2).

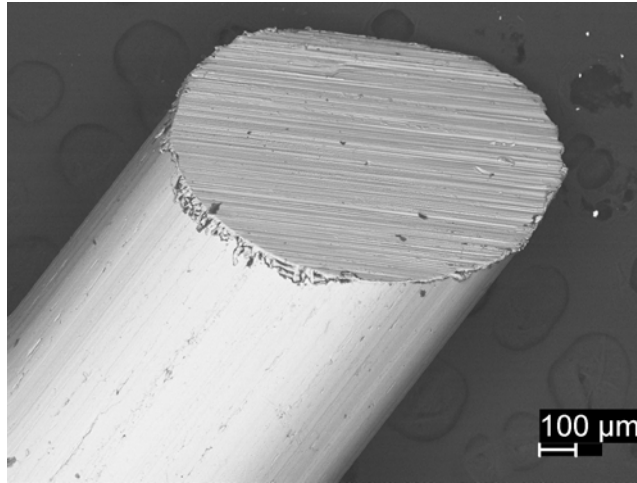
Table 2. Surface Treatments of Iron Wire Substrate

Sample No.	Polishing	Ethanol Rinse
1 - Control	None	None
2	30 seconds	None
3	30 seconds	Yes
4	120 seconds	None
5	120 seconds	Yes

This table outlines the substrate preparation used for Sample 1–5. The characterization of these samples will determine the best approach to preparing the samples prior to coating application.

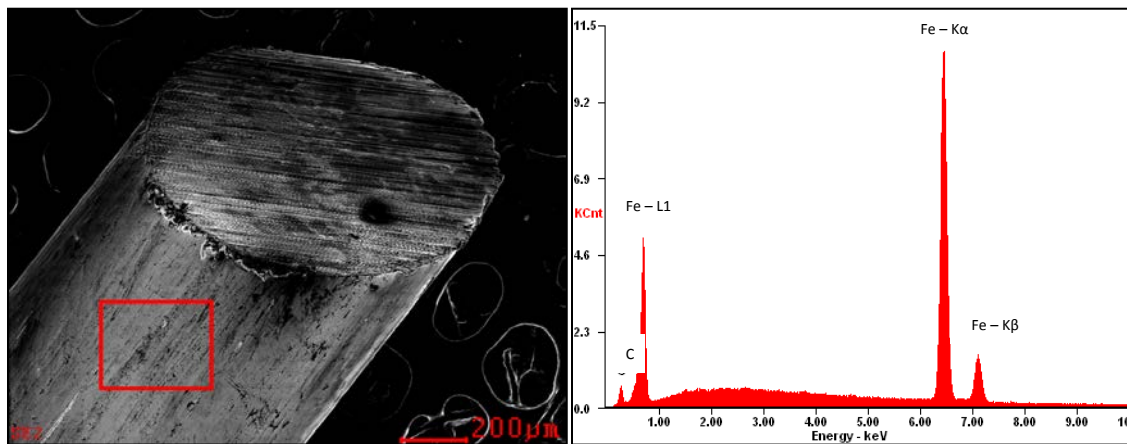
First, Sample 1 was analyzed. This sample was not subjected to polishing or an ethanol rinse, so it represents the base material received from the supplier. The SEM’s backscatter diffractometer was used to capture an image of the substrate, as shown in Figure 31. This SEM backscatter image shows large particles that do not have the same atomic composition as the iron substrate. Then using EDS, Sample 1 was qualitatively characterized and confirmed to contain mostly iron with some traces of carbon, as shown in Figure 32. For ease of viewing in Figure 32, each iron peak has been identified by the atomic shell from which the energy is being released. The energy from these characteristic peaks for iron are outlined in Table 3. Subsequent EDS analysis will omit

the identification of the $K\beta$ peak, as it will be implied to be the Fe- $K\beta$ peak. It is uncertain how the carbon was deposited on the surface of the sample. One hypothesis is that the carbon was imbedded during processing the wire.



Backscattered diffraction of Sample 1 (control), shows that the large particles that are do not have the same atomic composition as the iron substrate.

Figure 31. SEM Backscattered Image of Uncoated Sample 1



EDS analysis of the iron wire sample 1 that was not polished or rinsed with ethanol shows minor traces of carbon on the surface of the wire.

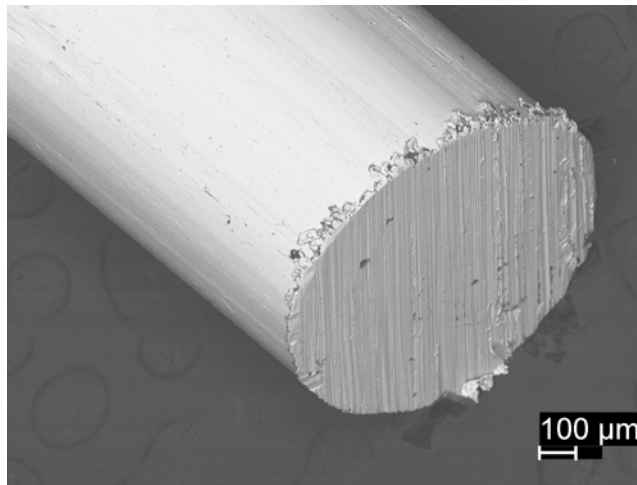
Figure 32. EDS Analysis of an Uncoated Sample 1

Table 3. Iron EDS Peak Identification by Series. Adapted from [45].

Element	K α [keV]	K β [keV]	L1 [keV]
Fe	6.398	7.056	0.615
Relative Intensity	100%	10-20%	-

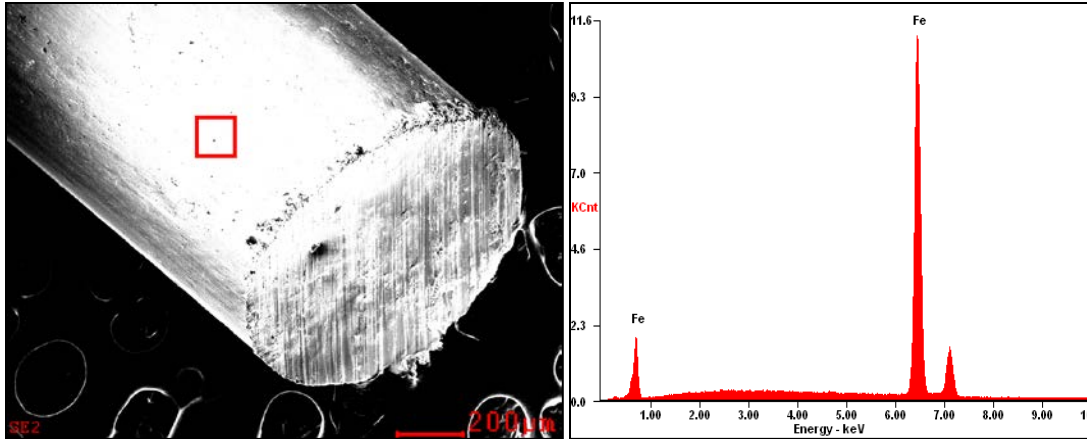
This table shows the EDS peaks for iron and their associated energy. Also, the relative intensity of the K series peaks are shown so that the K β peak will always be approximately 10–20% of the K α peak.

Next, Sample 2 was characterized using the SEM's backscatter diffractometer, as shown in Figure 33. This figure shows a nearly uniform surface with some heterogeneity of small particles on the surface that were produced by the cutting process. Then, Sample 2 was analyzed using the EDS. Notably, the amount of carbon on this sample had decreased compared to Sample 1, as shown in Figure 34.



The backscattered diffraction of Sample 2 shows that the sample has a uniform atomic composition, with the exception of a few particles thought to be contaminants from the cutting process.

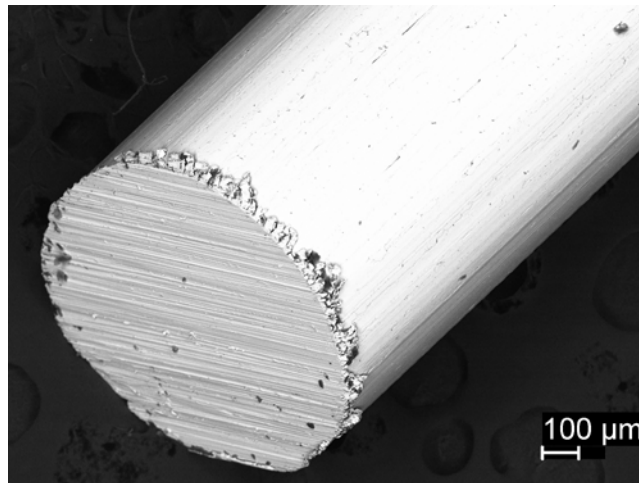
Figure 33. SEM Backscattered Diffraction of Uncoated Sample 2



The EDS analysis of Sample 2 indicates a pure iron composition with no traces of any other chemical elements.

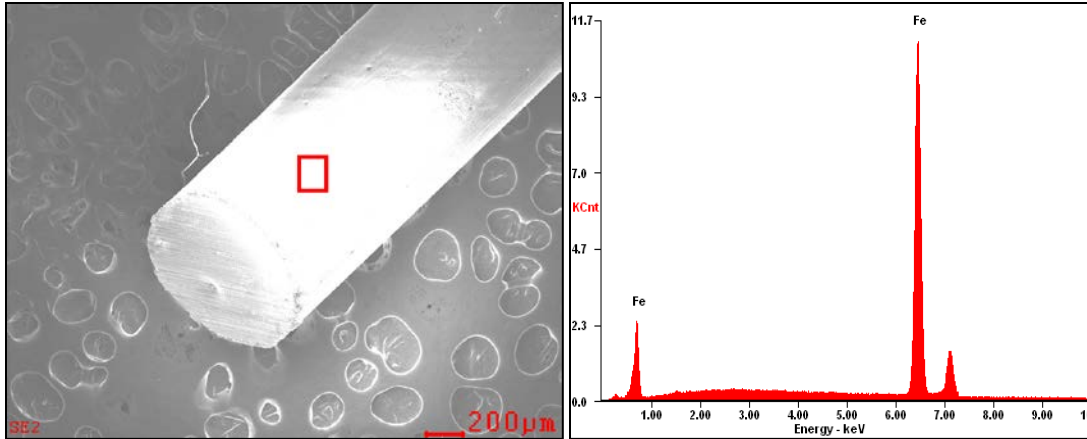
Figure 34. EDS Analysis of Uncoated Sample 2

Iron wire Sample 3, was analyzed using the same techniques. First, the backscattered diffraction shows the sample appears to have a uniform atomic composition, as shown in Figure 35. Then EDS analysis was conducted indicated a pure iron surface, as shown in Figure 36. Notably, the amount of carbon had also decreased from the amount that was present in Sample 1.



The backscattered diffraction of Sample 3 shows that the sample has a uniform atomic composition, with the exception of a few particles thought to be contaminants from the cutting process.

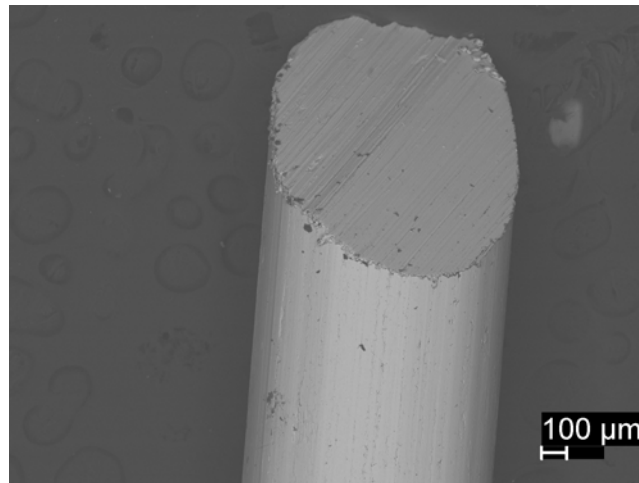
Figure 35. SEM Backscattered Diffraction of Uncoated Sample 3



EDS analysis of the Sample 3 indicates a pure iron composition with no traces of any other chemical elements.

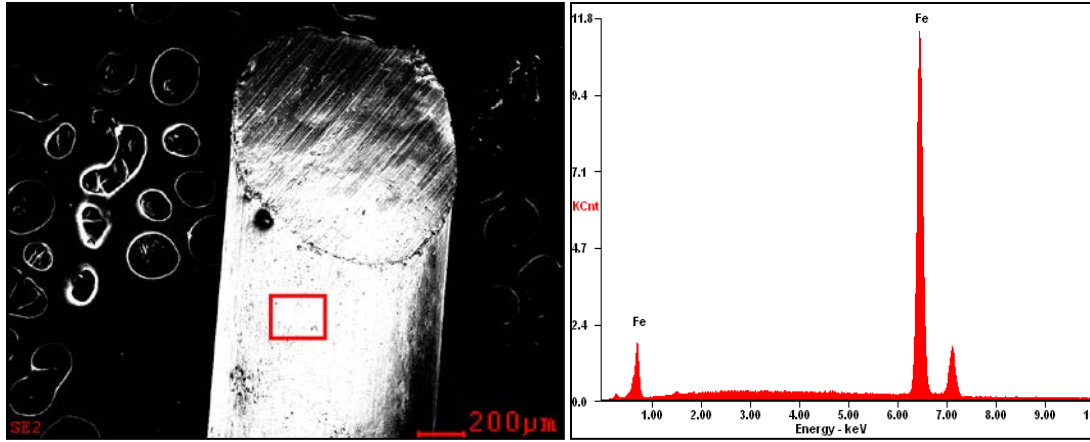
Figure 36. EDS Analysis of Uncoated Sample 3

Iron wire Sample 4 analysis shows the wire has a remarkably uniform atomic composition with some contaminants as shown by backscattered diffraction (Figure 37). These contaminants are assumed to be from the cutting process. EDS analysis of Sample 4 indicates a pure iron substrate, even in the region in which a contaminant was visually seen in the backscattered image, as shown in Figure 38.



The backscattered diffraction of Sample 4 shows that the material has a uniform atomic composition, with the exception of a few particles that are thought to be contaminants from the cutting process.

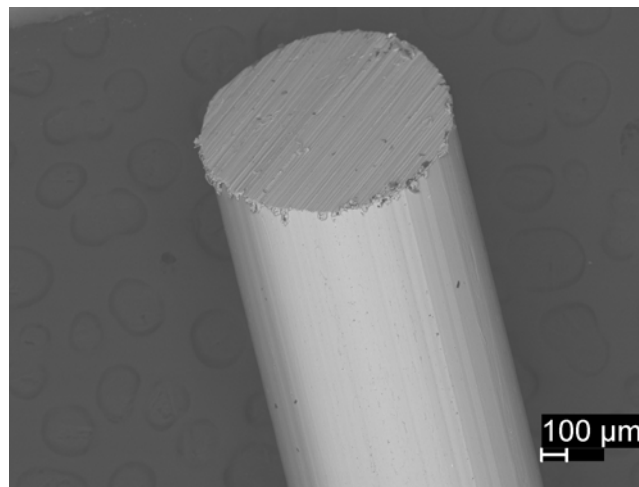
Figure 37. SEM Backscattered Diffraction of Uncoated Sample 4



EDS analysis of Sample 4 shows a uniform surface composition with no traces of any other chemical elements.

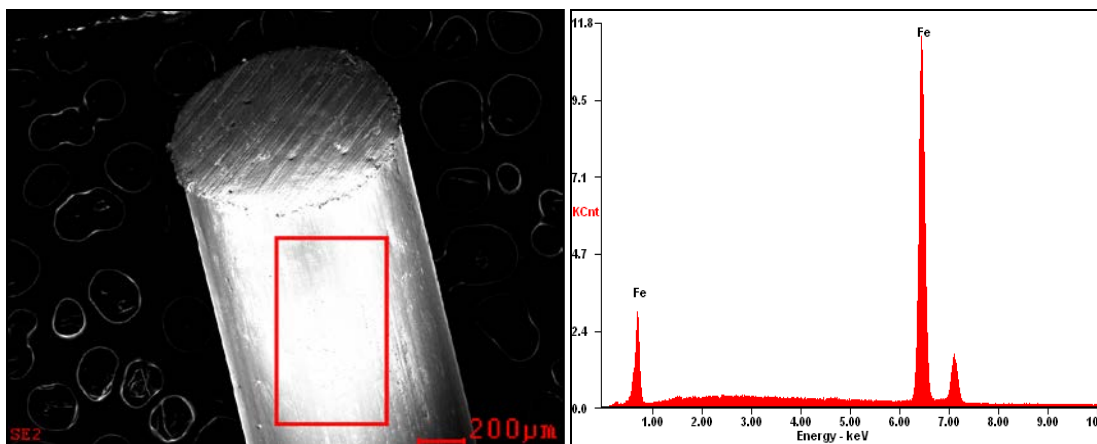
Figure 38. EDS Analysis of Uncoated Sample 4

Sample 5 was also analyzed using the same techniques. First, the backscattered diffraction indicated a uniform atomic composition (Figure 39). Next, EDS analysis of Sample 5 confirmed that there are no detectable trace elements on the surface (Figure 40).



The backscattered diffraction of the Sample 5 shows that the material has a uniform atomic composition, with the exception of a few particles that are thought to be contaminants from the cutting process.

Figure 39. SEM Backscattered Diffraction of Uncoated Sample 5



EDS analysis of the Sample 5 shows a uniform surface composition with no traces of any other chemical elements.

Figure 40. EDS Analysis of Uncoated Sample 5

In sum, the analysis of these “uncoated” samples revealed a nearly pure iron surface or the only measureable contaminant is carbon. Moreover, even a short polish removed most of the carbon, as the duration of polishing was determined to have no impact on the chemical analysis. In addition, there was no chemical impact to the sample whether or not it was rinsed with ethanol following the polishing process. Therefore, future samples were polished using the POL metal polish followed by a rinse with ethanol prior to the coating application.

B. RESULTS OF CHROMIUM BASED RES PROTOCOLS

This section presents and discusses the results of the various chromium-based coating protocols. Initially, “RES Protocol I” was used and resulted in a large amount of carbon and oxygen on the surface of the coated sample. In order to reduce the carbon, “RES Protocol II” was developed and implemented. This method used a chromium-based precursor that was mixed with urea to form a powder. This powder was mixed with deionized water to create a paste for application to the sample. The “RES Protocol II” method was used, but resulted in coatings that contained chromium oxide. To further explore methods to reduce chromium (III) oxide, several powder-based experiments were conducted and resulted in mainly chrome oxide powder.

1. Chromium Coating Protocol I

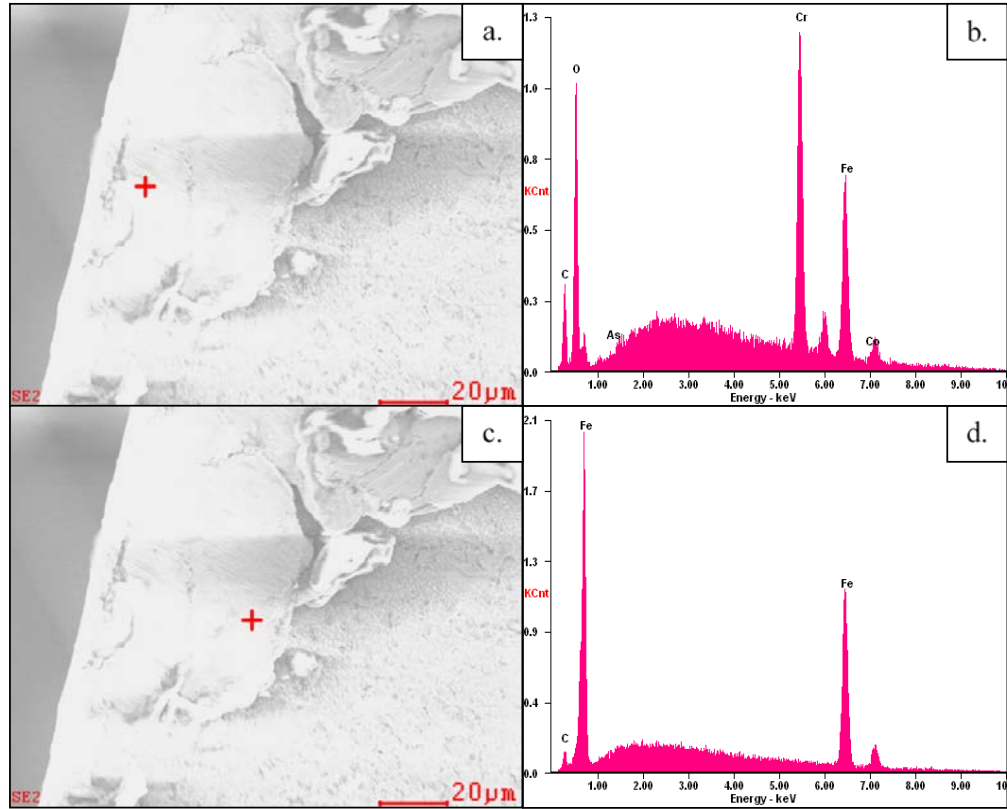
Some of the samples created using the “RES Protocol I” were analyzed, as outlined in Table 4. These samples were mounted directly to the specimen holder using carbon tape. Only an EDS analysis was conducted on the surface of these samples in order to characterize the coating.

Table 4. Protocol I Variation in Experimental Procedures

Sample No.	Weight Ratio	Number of Coatings	Sequence	Furnace Temperature	Nitrogen Flowrate
6	1:1	10	5C,F,5C,F	700°C	25 SCCM
7	1:1	15	5C,F,5C,F,5C,F	700°C	25 SCCM
8	2:1	5	5C,F	700°C	25 SCCM

During the first protocol experiments, the number of coatings and weight ratio of urea to chromium (III) nitrate nonahydrate were varied in an attempt to increase the film thickness of the applied coating. The sequence of the coatings also in order varied to achieve the total number of coatings applied to the wire. The number preceding ‘C’ indicates how many coatings were applied to the wire, while ‘F’ indicates the sample was placed into the furnace.

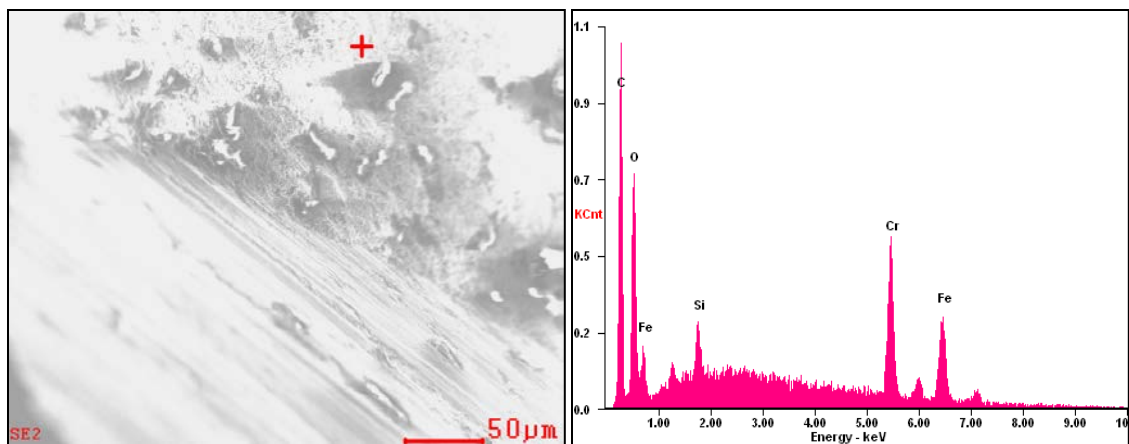
Sample 6 was characterized using the EDS as shown in Figure 41. This sample was prepared by coating the wire 5 times and then placing in the furnace. This process was repeated once again to achieve 10 coatings in order to create a thick chromium layer. Two EDS point scans were taken of Sample 6. The first indicated a region rich in chromium, but also contained oxygen and carbon. The second EDS point scan of Sample 6 was taken approximately 30 μm from the initial location and indicated a region of iron and traces of carbon. From these EDS analyses, it indicates that the coating is not homogeneous. Moreover, when the chromium signal is strong, the oxygen signal is as well.



EDS analysis of Sample 6: (a.) Point scan of wire surface. (b.) EDS spectrum of region chosen which is rich in carbon, oxygen, and chromium. (c.) Point scan of wire surface. (d.) EDS spectrum of region chosen, which shows traces of carbon and mainly iron.

Figure 41. EDS Analysis of Coated Sample 6

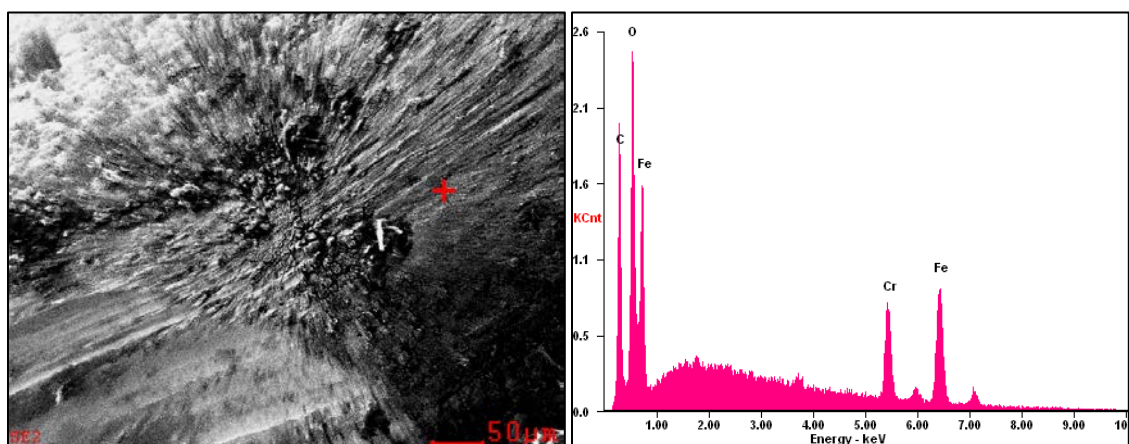
Sample 7 was prepared by repeating the coating and heating process. The sample was coated five times, then heat treated. This process was completed three times in order to achieve 15 coatings. From the EDS analysis, it appears the total amount of carbon present dramatically increased compared to Sample 6 (Figure 42). The oxygen and chromium ratio also increased, which indicates that potential for other oxides to be present (e.g., silicon oxide). Therefore, silicon contamination most likely occurred during the grinding process.



EDS analysis of Sample 7 shows an increase in both carbon and oxygen, as well as a silicon contamination on the sample's surface.

Figure 42. EDS Analysis of Coated Sample 7

In an effort to decrease the amount of carbon and oxygen, Sample 8 was prepared using an increased weight ratio of urea to the chromium nitrate nonahydrate, as shown in Table 4. This sample was coated five times and placed into the furnace. EDS analysis of Sample 8 still indicates a high level of oxygen and carbon on the surface of the coated sample (Figure 43). By increasing the amount of urea, the hypothesis was that it would reduce the oxygen content on the surface, leaving a fully reduced chromium coating on the surface.



EDS analysis of Sample 8 indicated that with the increased weight ratio of urea to chromium (III) nitrate nonahydrate, the amount of oxygen still remained high.

Figure 43. EDS Analysis of Coated Sample 8

Given the finding that “RES Coating Protocol I” produced a chromium coating rich in oxygen and carbon, a new method, RES Coating Protocol II, was devised. This protocol was a different approach in that chromium (III) oxide particles were used in an effort to achieve a fully reduced chromium coating. A new analysis method of preparation was also introduced to measure the thickness of the applied coating. The samples were mounted in a conductive material, followed by a grinding and polishing process, and resulted in a flat cross-sectional area, rather than the curved surface of the 1 mm diameter wire.

2. Chromium Precursor Protocol

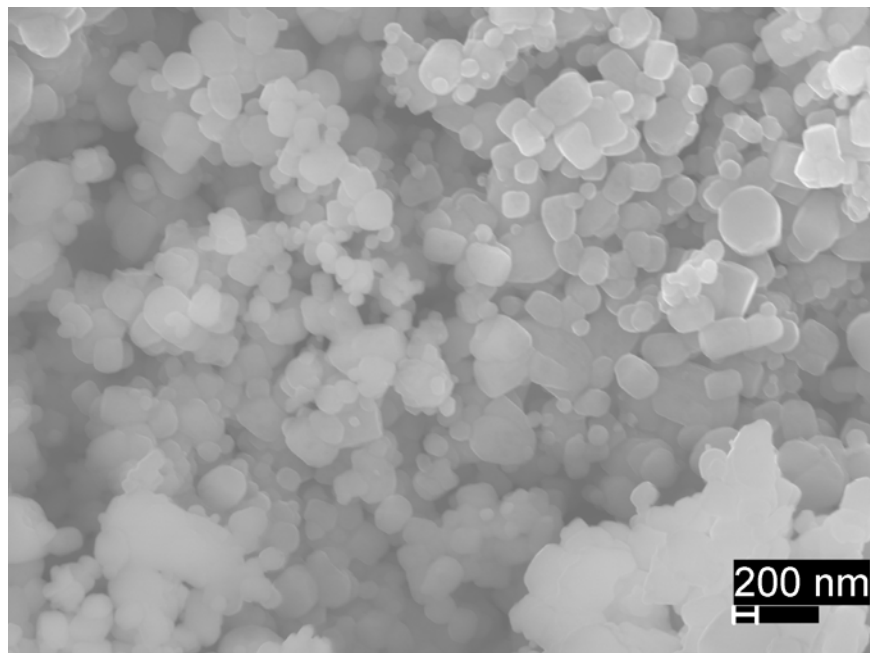
In order to test the impact of the scale of chromium (III) oxide particle production, two samples were prepared and analyzed (Table 5). A high-resolution image of Sample 9 shows submicron particles that have agglomerated, as seen in Figure 44. Similarly, Sample 10 exhibited the same visual characteristics (Figure 45). EDS analysis of Sample 10 shows the relative intensities between the oxygen and chromium energy peaks (Figure 46). Similar to the EDS analysis on Sample 1, it shows two identified chromium peaks as outlined in Table 6. However, the Chromium L1 peak is not observed, because the oxygen peak is very dominant at the same energy level.

Table 5. Chromium Precursor Samples

Sample No.	Chromium (III) Nitrate Nonahydrate	Reduced Material
9	3.3690 grams	0.6274 grams
10	0.5589 grams	0.1020 grams

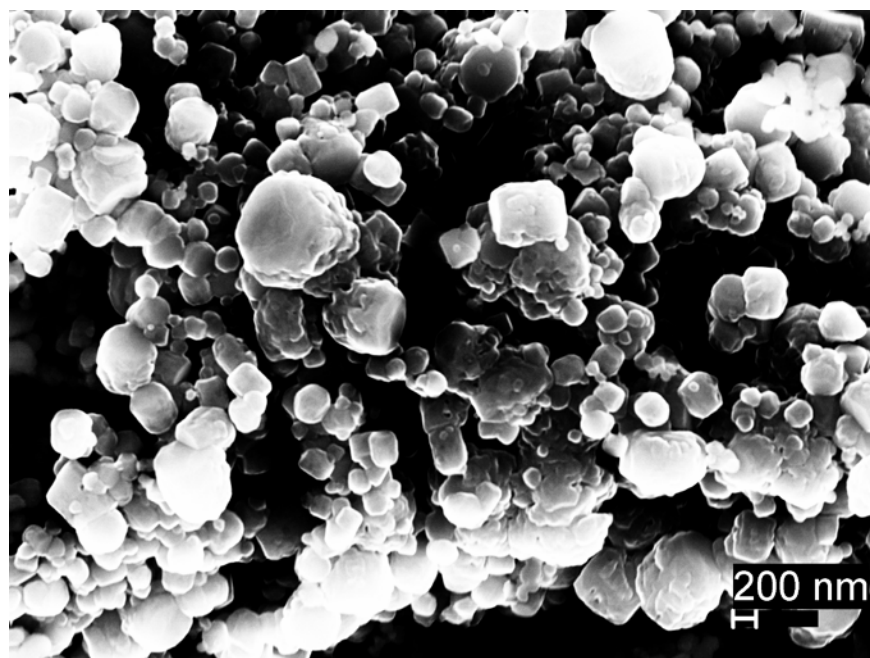
Samples 9 and 10 were prepared using the “RES Chromium (III) Oxide Precursor Protocol.” The amount of chromium (III) nitrate nonahydrate was varied to determine if the crystal structure of the precursor was the same.

After making observations in the SEM, the samples were characterized using XRD in order to determine the crystal structure of the powder. XRD analysis of Samples 9 and 10 confirmed both samples were of the eskolaite phase of chromium (III) oxide (Figure 47 and Figure 48). The analysis conducted on these two samples indicated the particle size is nearly identical and the crystal structure is the same.



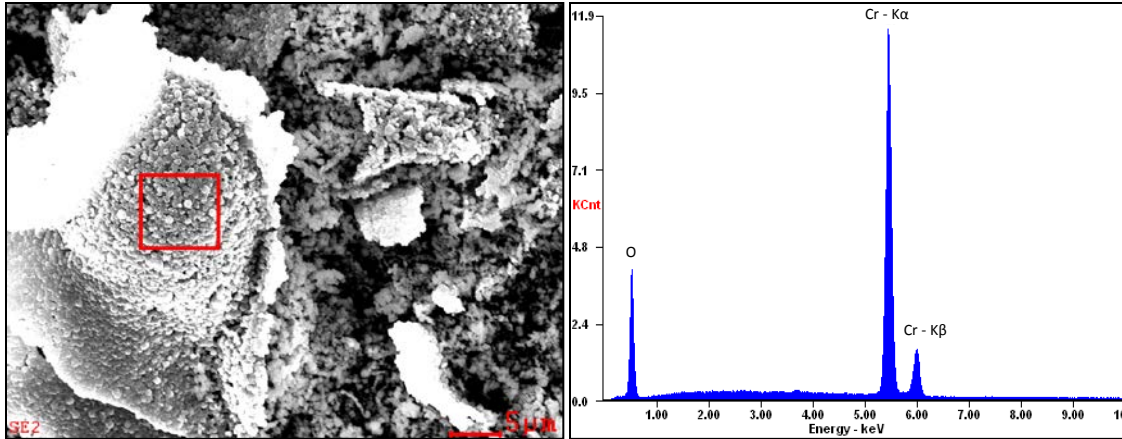
Sample 9, when viewed at a high magnification, illustrates submicron particles that have agglomerated.

Figure 44. Sample 9 SEM Micrographs



Sample 10 also shows submicron particles that have agglomerated when viewed at a high magnification.

Figure 45. Sample 10 SEM Micrographs



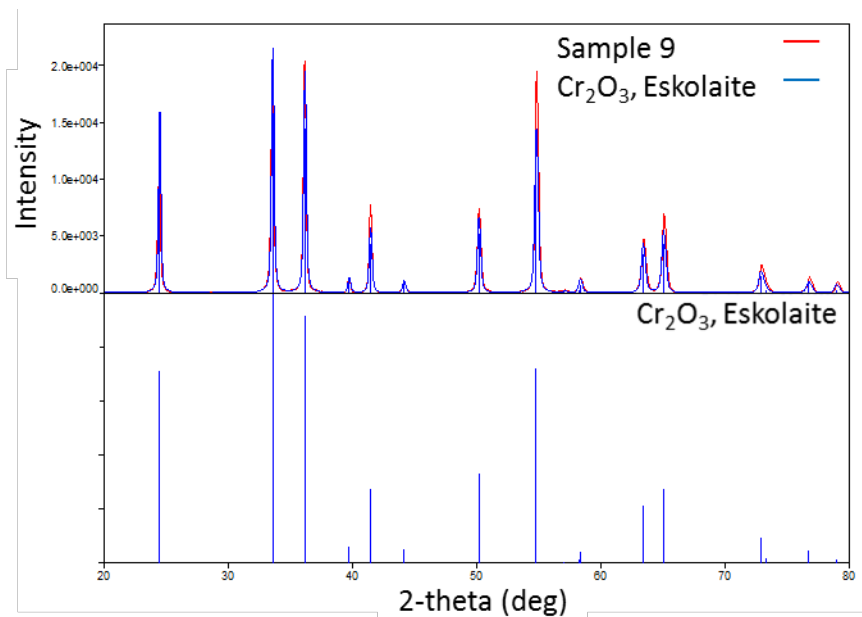
EDS analysis of Sample 10 shows two chromium peaks ($K\alpha$ and $K\beta$) and an oxygen peak. This EDS analysis was conducted to show relative intensity of the chromium peaks to the oxygen peak.

Figure 46. EDS Analysis of Sample 10

Table 6. Chromium EDS Peak Identification by Series. Adapted from [45].

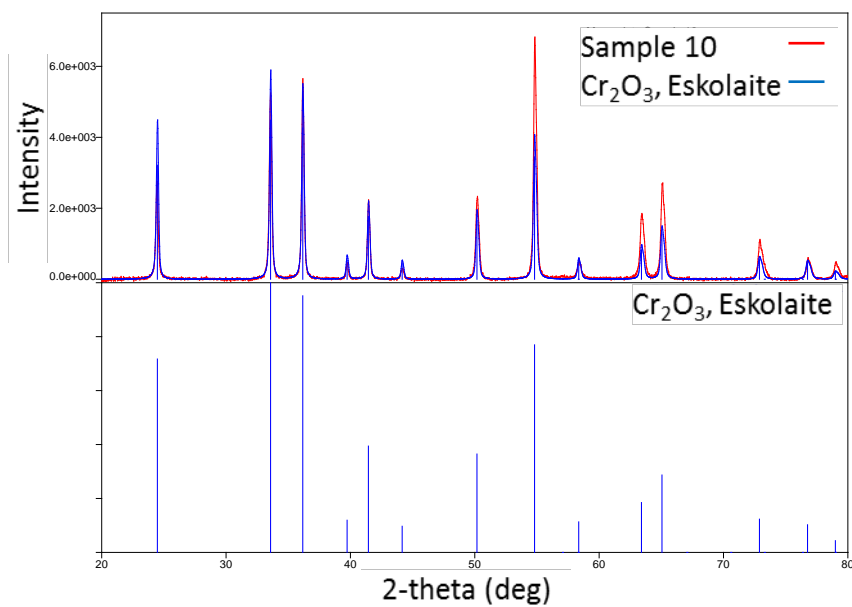
Element	$K\alpha$ [keV]	$K\beta$ [keV]	L1 [keV]
Cr	5.410	5.945	0.5
Relative Intensity	100%	10-20%	-

This table shows the EDS peaks for iron and their associated energy. Also, the relative intensity of the K series peaks are shown so that the $K\beta$ peak will always be approximately 10–20% of the $K\alpha$ peak.



Small-scale Synthesized precursor was confirmed to be Chromium (III) Oxide, Eskolaite phase.

Figure 47. X-Ray Diffraction Spectrum from Sample 9 Precursor



Bulk synthesized precursor was confirmed to be Chromium (III) Oxide, Eskolaite phase.

Figure 48. X-Ray Diffraction Spectrum from Sample 10 Precursor

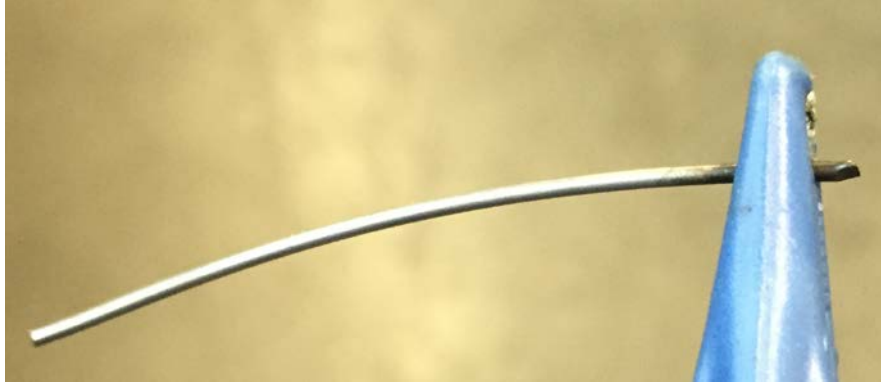
3. Chromium Coating Protocol II

Multiple experiments were conducted using the “RES Coating Protocol II” method, as outlined in Table 7. These coatings were hypothesized to be a reduced chromium layer. Indeed, visual inspections suggested a metallic coating was produced because all samples, unlike those produced using Protocol I, were very shiny and silver in color (Figure 49). The sequence of coating applications were varied in order to determine the most efficient process of creating a reduced chromium coating.

Table 7. RES Coating Protocol II Samples

Sample No.	Weight Ratio	Coatings	Sequence	Furnace Temperature	Nitrogen Flow Rate
11	2.1:1	3	3C,F	700°C	25 SCCM
12	2.1:1	6	3C,F,3C,F	700°C	25 SCCM
13	2.4:1	3	3C,F	800°C	25 SCCM
14	2.4:1	3	3C,F	800°C	25 SCCM
15	2.4:1	5	5C,F	800°C	25 SCCM
16	2.4:1	3	3C,F	800°C	25 SCCM
17	2.4:1	1	C,F	800°C	25 SCCM
18	2.4:1	1	C,F	800°C	25 SCCM
19	2.4:1	5	C,F,C,F,C,F,C,F,C,F	800°C	25 SCCM
20	2.4:1	5	5C,F	800°C	25 SCCM

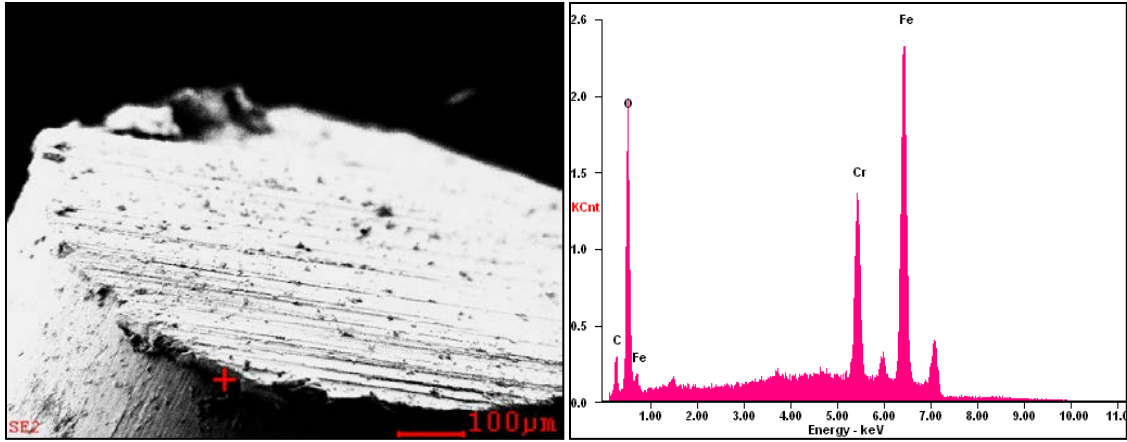
During the RES coating protocol experiments, the number of coatings and weight ratio of urea to the chromium precursor were slightly increased in an attempt to increase the film thickness of the applied coating. The sequence of the coatings also varied to achieve the total number of coatings applied to the wire. The number preceding ‘C’ indicates how many coatings were applied to the wire, while ‘F’ indicates the sample was placed into the furnace.



Visual inspection of Sample 19, after the four applications of coatings shows the coated sample to be shiny and a silver color.

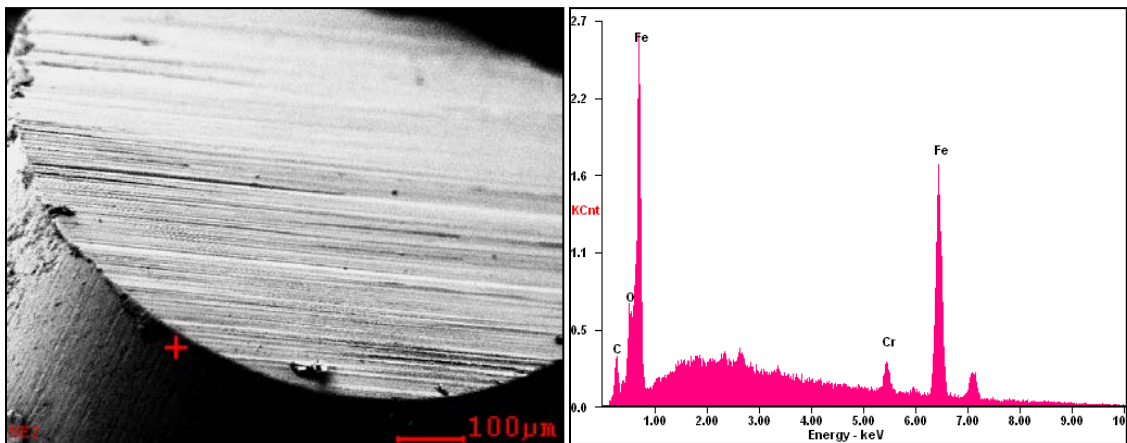
Figure 49. Visual Inspection of Sample 19

EDS analysis was conducted on an unmounted specimen, as shown in Figure 50. From this analysis of the surface coating, it contains chromium, oxygen and carbon, while iron is also present. Due to the interaction volume of the electron beam, it is reasonable to have an iron peak present when analyzing a thin coating on an iron substrate. In addition, the relative intensity of the oxygen peak increase may indicate the formation of iron oxide. Similarly, Sample 12 was analyzed using the EDS, as shown in Figure 51. This analysis of Sample 12, which was designed to have twice the coating thickness of Sample 11, shows a noted decrease in the chromium and oxygen peaks when compared to Sample 11. However, the relative intensity of the oxygen peak was still greater than that of the chromium peak, but the iron L1 peak is much greater and almost makes the oxygen peak indistinguishable from the iron L1 peak. During this process, when the sample was rinsed with ethanol prior to cutting, the surface became less contaminated with debris (Figure 51). This may have also caused the relative intensities of the oxygen and chromium peaks to decrease from those observed on Sample 11.



Surface analysis of sample 11 shows a large amount of chromium, oxygen, and carbon on the surface of the iron wire.

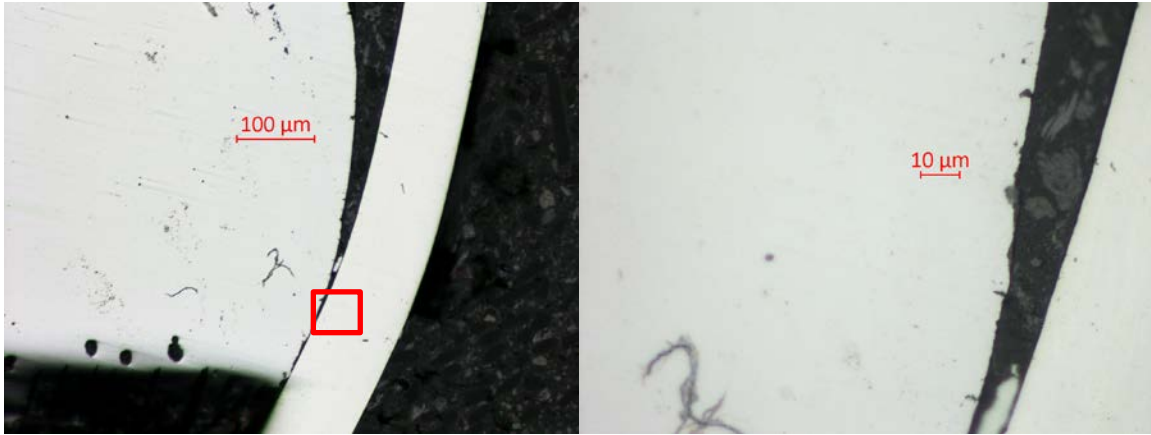
Figure 50. EDS Analysis of Coated Sample 11



Surface analysis of sample 12 shows a notable decrease in the chromium and oxygen peaks, but the relative amount of carbon remained constant.

Figure 51. EDS Analysis of Coated Sample 12

The next sample analyzed was designed to test the impact of furnace temperature and ratio of urea to chromium precursor. Sample 13 was prepared at 800°C and an increased weight ratio of urea to chromium precursor. This sample was characterized using several methods in order to measure the thickness of the coating. First, Sample 13 was observed in the optical microscope following the mounting, grinding and polishing process, as shown in Figure 52. The optical microscopy failed to clearly indicate the presence of a surface coating.



The image on the left was taken at 100 times magnification, as a reference to the second image. The image on the right was taken at 500x magnification and does not indicate the presence of a surface coating.

Figure 52. Optical Microscopy of Sample 13

The samples that were mounted in the conductive material were placed in the SEM to analyze and measure the coating thickness (Table 8). Measurements were taken at four locations on each sample, spaced approximately 90° apart. Some of the samples shifted during the mounting process, which obscured one edge of the sample. Therefore, only three data points were recorded for those respective samples. With only four data points to analyze, the mean thickness calculated is not fully representative of the entire coated surface on any of the samples. Hence, the coefficient of variation is being presented with the data to show relative variability of these measurements, with respect to the mean thickness. This indicates how large the standard deviation is, compared to that of the sample's mean thickness. In this case, a lower the coefficient of variation indicates that the mean thickness is less variable, based upon the four measurements. From these measurements, the sample with the largest mean thickness was only coated once. This indicates that the number of coatings applied did not incrementally increase the thickness of the coatings, as initially suspected. This led to the hypothesis, that the imperfections noted during the drying process would affect the thickness of the coating. Ultimately, the recorded measurements did not accurately reflect the intentions of the experiment, but identified that applying the coating imperfectly will affect the results.

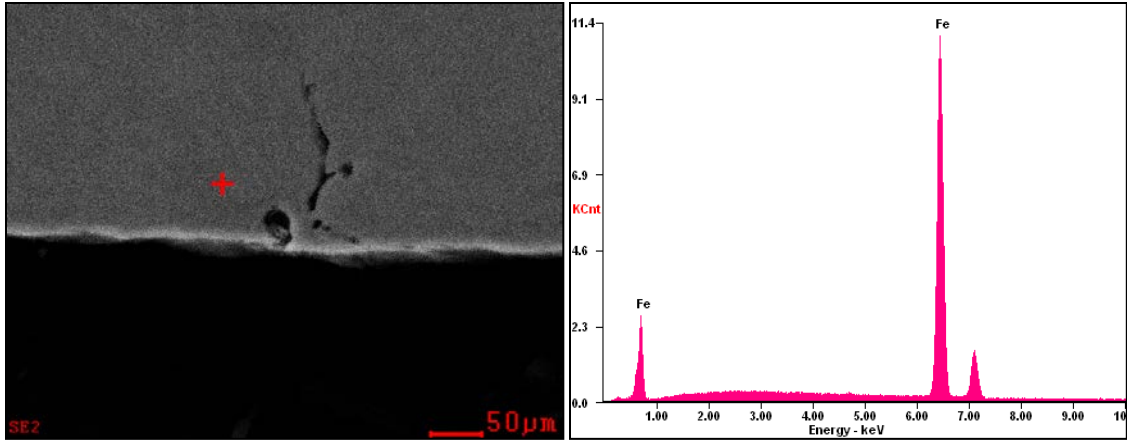
Table 8. Protocol II Coating Measurements from Mounted Samples

Sample No.	# of Measurements	Mean Thickness [nm]	Standard Deviation [nm]	Coefficient of Variation [%]*
13	3	1224.4	917.6	74.9
14	4	1393.6	804.9	57.8
15	3	1616	770.2	47.7
16	4	1652.3	597.9	36.2
17	3	9453.1	11131.6	117.8
18	4	823.5	684.3	83.1
19	4	1096.7	1047.5	95.5
20	4	639.3	494.1	77.3

* Coefficient of Variation was computed by dividing the sample's standard deviation by the sample mean, then multiplying the value by 100 [46]. This table presents the mean thickness measurements of each sample, with its respective standard deviation and coefficient of variation.

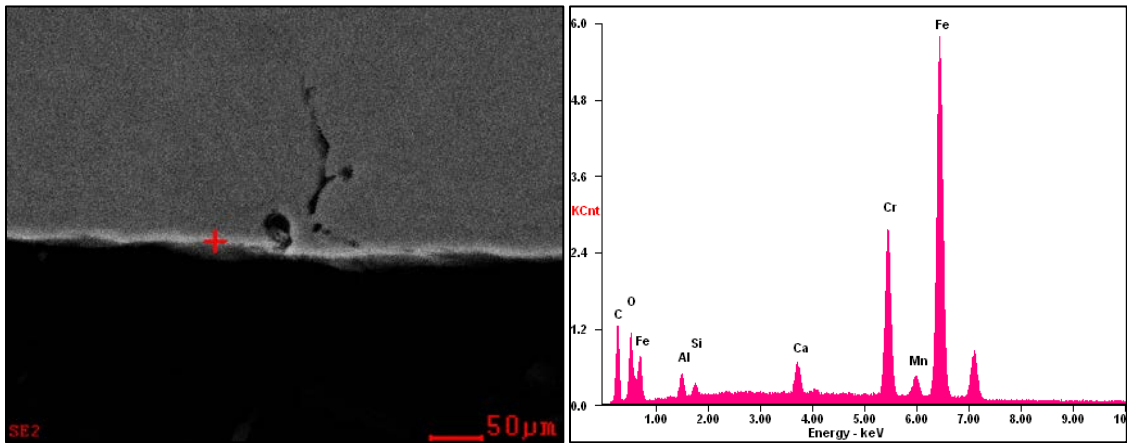
EDS analysis was conducted on Sample 13. During this analysis, a point scan was conducted on the base material and only iron was detected (Figure 53). Then, another point scan was conducted on the surface layer, and indicated although chromium is the strongest signal, there were also many contaminants such as carbon, oxygen, aluminum, silicon, calcium and manganese (Figure 54). This led to the hypothesis that during the grinding and polishing process, the coated region was susceptible to contamination from the silicon carbide grinding paper and the alumina oxide particles used in the polishing process. However, the relative intensities of chromium and oxygen peaks in Figure 54 are much higher than those of the chromium (III) oxide, which indicates that there may be reduced chromium in the coating, and the contaminants may be in the form of oxides.

Next, an EDS analysis was performed on the conductive material to determine the composition, as shown in Figure 55. This analysis of the mounting material also shows many elements, with the exception of chromium and manganese. The presence of manganese cannot be accounted for during the preparation of the sample, and therefore is hypothesized to be a contaminant from the cutting process.



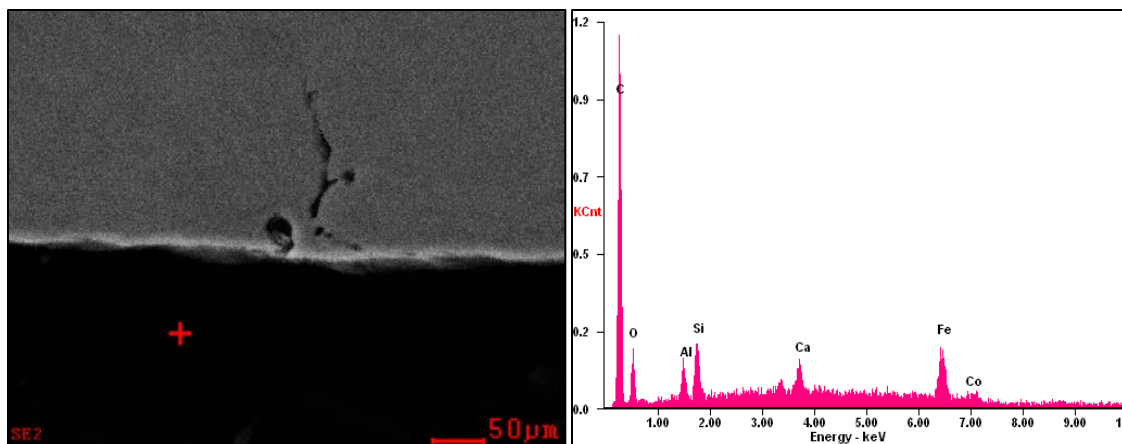
This EDS point scan identifies the substrate material as only iron.

Figure 53. EDS Analysis of Sample 13 Cross-Sectional Substrate



This EDS analysis of the surface layer indicates the presence of various contaminants.

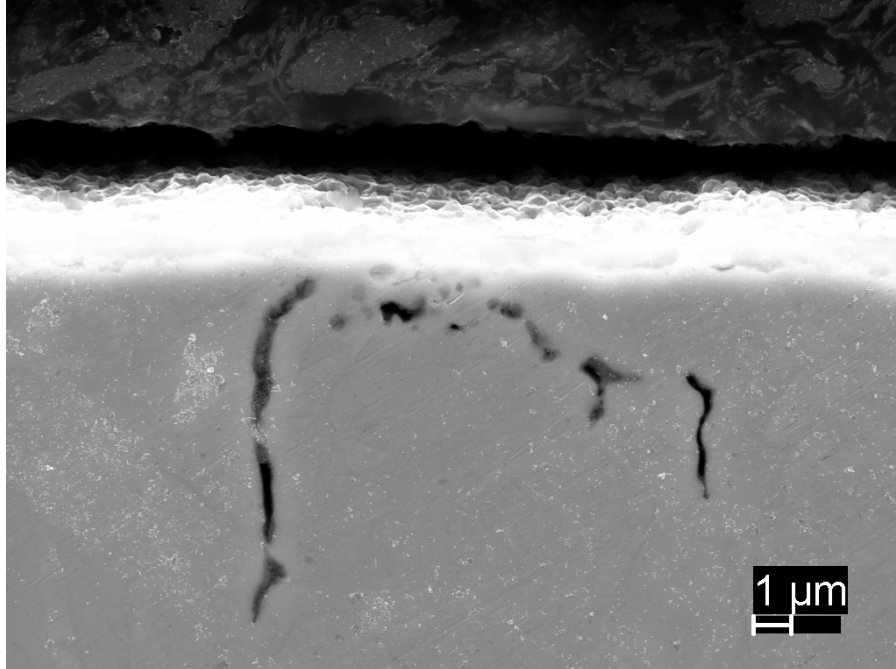
Figure 54. EDS Analysis of Sample 13 Cross-Sectional Surface Layer



This EDS analysis of the conductive material was conducted to determine the composition of the material in order to determine the origin of the contaminants observed in the surface layer.

Figure 55. EDS Analysis of Sample 13 Cross-Sectional Conductive Material

Samples 14–20 were also analyzed in a similar fashion and all samples were observed to have contaminants in the surface coating region. Most of these contaminants can be attributed to the preparation the samples underwent prior to characterization. It was later identified that the contamination occurred due to poor adhesion of the mounting material to the samples which resulted in a gap of approximately 1 μm, as illustrated by Figure 56. This led to the conclusion that the coating layer was greatly affected by sample preparation and the coating thicknesses obtained were not reliable.

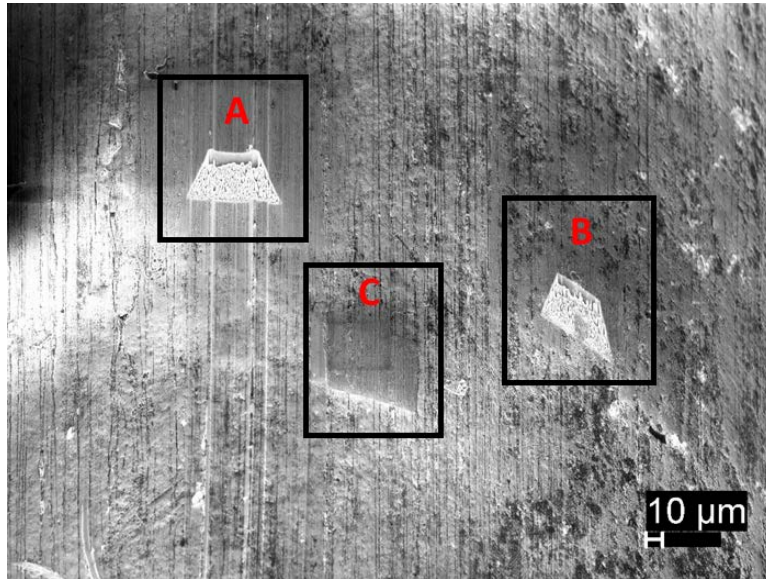


Inlens SEM microscopy revealed an gap between the sample and the conductive material. This poor adhesion led to the introduction of contaminants from preparing the samples and did not provide any clear indication of a thin chromium coating.

Figure 56. Inlens SEM Microscopy of Sample 14 Surface Layer

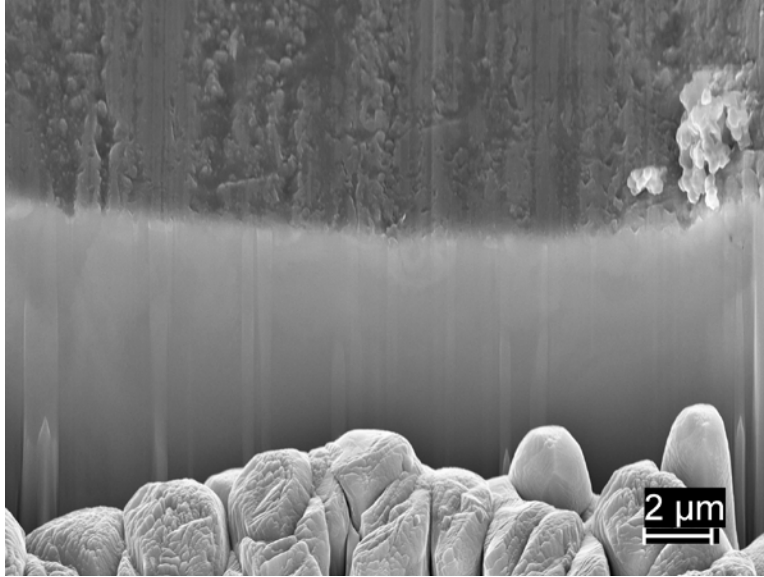
Upon identifying the shortcomings of obtaining thickness measurements from the mounted samples, the Focused Ion Beam (FIB) was used to mill trenches into the surface of a sample. This was necessary to find the interface between the iron and suspected coating, in order to obtain a thickness measurement. Sample 13 was chosen to be milled because the sample exhibited a shiny appearance after being coated. The FIB was used to mill two separate trenches in the surface. Then a portion of the surface was briefly milled to characterize the surface coating, as illustrated in Figure 57. First, the trench at Area “A” was milled. Upon inspection of the area, no clear interface between the iron and a suspected coating was visible, as illustrated in Figure 58. Then, an EDS area scan was conducted of the surface, as shown in Figure 59. This analysis determined that carbon, iron, and chromium elements were detected on the surface of the sample. Another EDS analysis was conducted on the exposed iron substrate and shows only iron is present with no other elements. This indicates that no alloying between the coating and substrate occurred, as illustrated in Figure 60. When comparing Figure 59 and Figure 60 there is an

obvious miss identification when the iron and oxygen peaks, as Fe-L1 should be much lower than the Fe-K α , as observed in Figure 60. This illustrates that perhaps the EDS analysis of the chemicals is not perfect, and perhaps the Fe-L1 peak in Figure 59, is really the oxygen K α peak, which would indicate the presence of both iron oxide and chromium oxide on the surface of Sample 13.



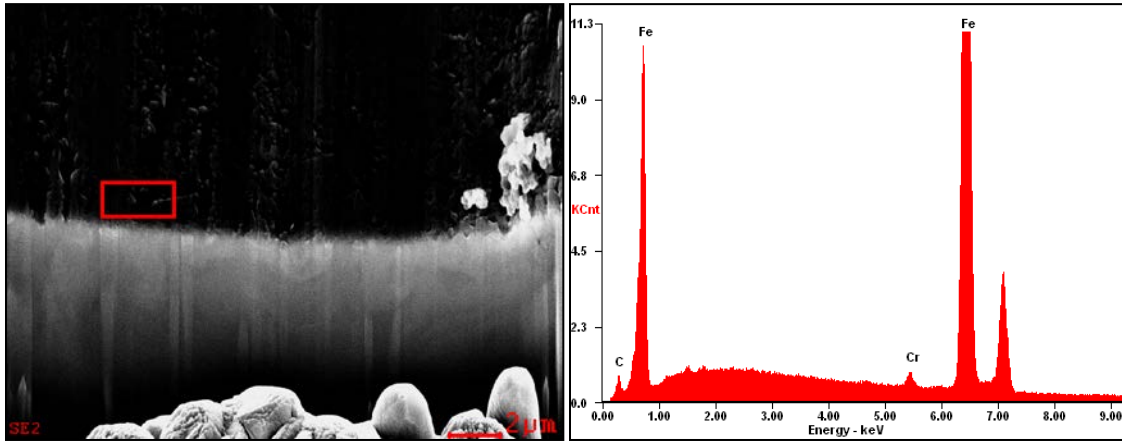
First, a FIB trench was milled into the surface of Sample 13 at Area “A.” Then, a second FIB trench was milled in to the surface of Sample 13 at Area “B.” Finally, the FIB was used to mill the surface of Sample 13 in order to determine if the amount of carbon on the surface could be reduced in Area “C.”

Figure 57. FIB Milled Surface of Sample 13



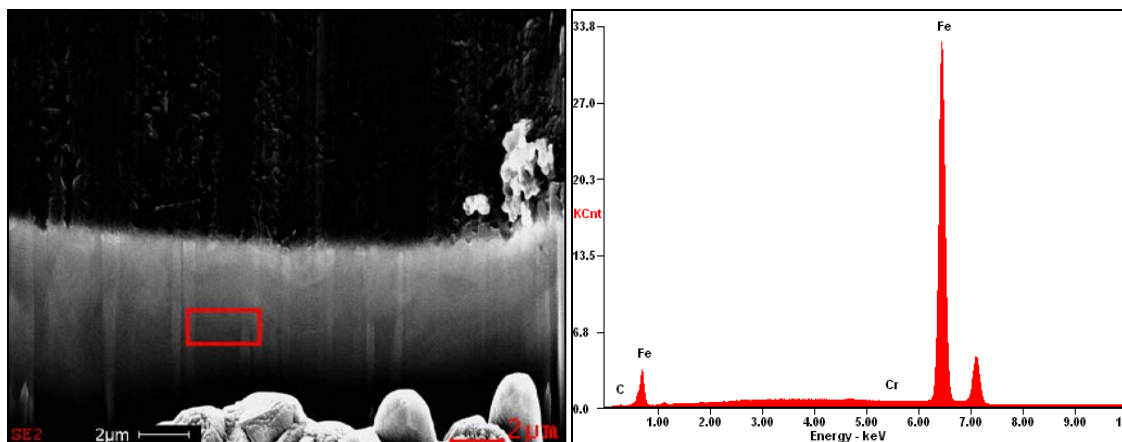
FIB milled trench at area “A” did not show any visible trace of a layer interface with the iron substrate.

Figure 58. FIB Milled Trench at Area “A” on Sample 13



EDS area scan of surface above FIB milled trench at area “A” on sample 13. This analysis shows the presence of carbon, iron, and chromium on the surface, but lacks the oxygen peak.

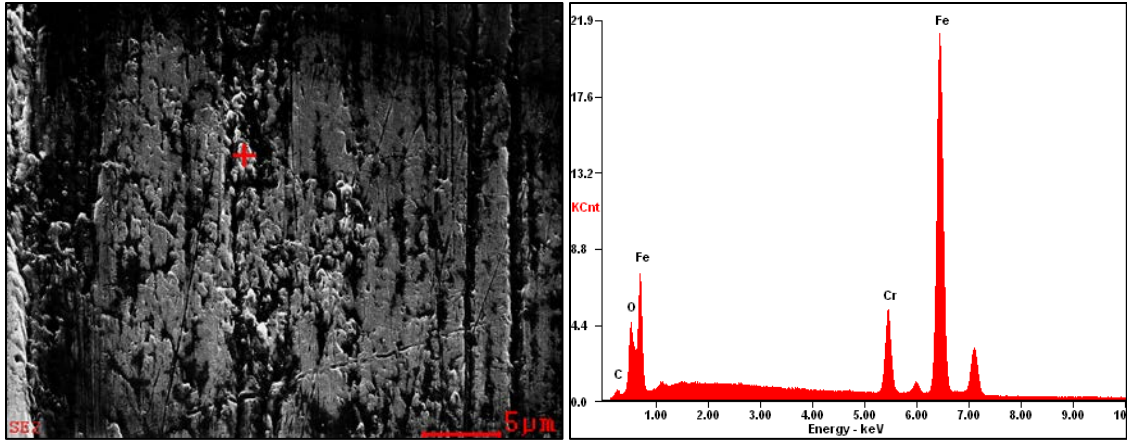
Figure 59. EDS Surface Analysis of Area “A” on Sample 13



This surface analysis indicates that only iron is present within the sample. This also shows that the coating did not alloy with the base material during the reductive heating process.

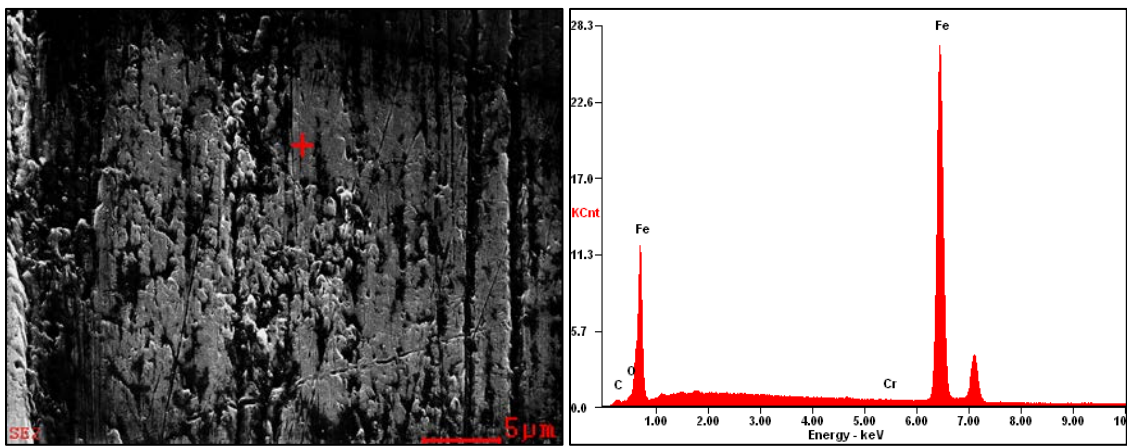
Figure 60. EDS Surface Analysis of FIB Trench at Area “A” on Sample 13

The FIB milled trench at Area “B” revealed the same information that was obtained from Area “A.” The last area analyzed on Sample 13 was Area “C,” in which the surface underwent a brief 30-second milling to learn more about the surface of the sample. The EDS point scan taken at Area “C” revealed a particle on the surface, which contained trace amounts of carbon, oxygen and chromium (Figure 61). When comparing this EDS analysis with that of Sample 10, the relative intensity of the oxygen peak has slightly increased compared to the chromium peak. This indicates that a small portion of the iron substrate had oxidized. Another point scan was conducted on what appeared to be the iron substrate revealed the material only contained iron, with no traces of other elements, as shown in Figure 62. This revelation meant that there was no film formed by the coating, but instead during the RES process the chromium (III) oxide particles were dispersed on the surface of the iron samples.



The EDS analysis shows the surface of sample 13 with a particle that has a relatively large amount of oxygen and chromium.

Figure 61. FIB Milled EDS Analysis of Chromium Rich Particle on the Surface of Sample 13

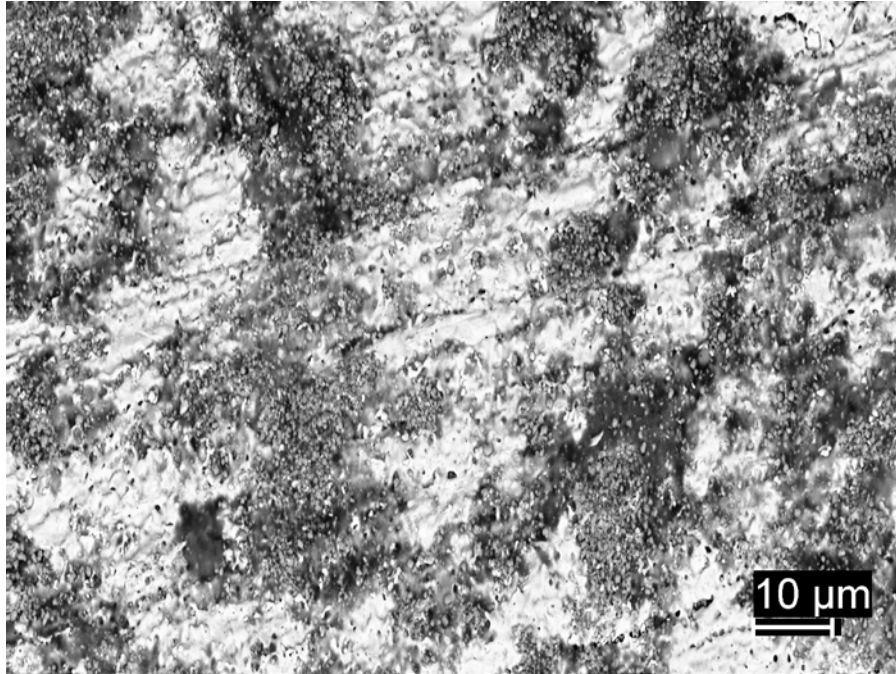


The EDS analysis of the iron surface confirmed that the coating was not continuous, but contained small particles randomly dispersed on the surface of the sample.

Figure 62. FIB Milled EDS Analysis of Iron Surface of Sample 13

After using the FIB to mill trenches, there was no indication of an interface between the iron and the surface coating and therefore no thickness measurements were obtained. Sample 18 was then characterized by mounting the sample directly to a specimen holder using carbon tape. Visual inspection showed a shiny chromium coating. Upon viewing the surface of Sample 18 with the backscattered detector in the SEM, it became clear the coating contained small particles attached to the surface of the iron

wire, as illustrated by Figure 63. As mentioned earlier [44], the backscatter image allows chemical elements with higher atomic average number to appear brighter and those with a lower average atomic number to appear darker. From this image, the iron substrate appears to be covered with an intermittent coating of particles with a lower atomic composition.



This image was taken with the use of the backscatter detector of Sample 18 at 1000X magnification. The brighter areas on the surface are atomically heavier elements such as iron, while the darker area indicates elements that are relatively lighter in atomic weight, such as chromium, oxides, and carbon.

Figure 63. SEM Backscattered Image of Coated Sample 18 Surface Layer

EDS analysis was used to characterize the surface of Sample 18. First, the small particles on the surface were analyzed to determine what elements were present, as illustrated by Figure 64. This EDS analysis determined that the dominant elements were oxygen, aluminum, and chromium. The relative intensity of the oxygen peak increased dramatically from the peak observed in Sample 10. This indicates that the aluminum identified is most likely aluminum oxide. Another EDS analysis was conducted on the exposed substrate to get a baseline, as shown in Figure 65. This EDS analysis also

indicates the relative intensity of oxygen has decreased, notably when there is no chromium peaks present. Also noted from these two EDS analyses is that the L1 peak of iron and the $K\alpha$ peak of oxygen are in such close proximity that either one will become dominant in the spectrum. This may indicate why the Fe-L1 peak is thought to have been miss identified by the EDS software, as the Fe-L1 peak should be lower than the Fe- $K\alpha$ peak. If the peak identified as Fe-L1 is actually oxygen, this EDS analysis indicates the presence of aluminum oxide and iron oxide. However, from these two EDS analyses, it becomes clear the particles on the surface of the sample contain both oxygen and chromium. Again, the relative intensity of oxygen to chromium (Figure 64) is higher than that of the previously analyzed Sample 10, which indicates additional oxygen and may be in the form of aluminum oxide.

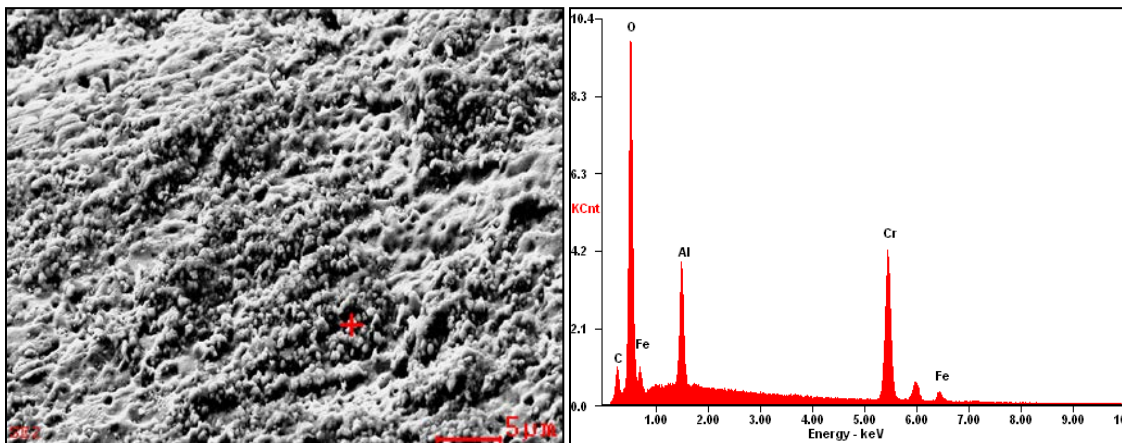


Figure 64. EDS Analysis of Sample 18 Surface Particles

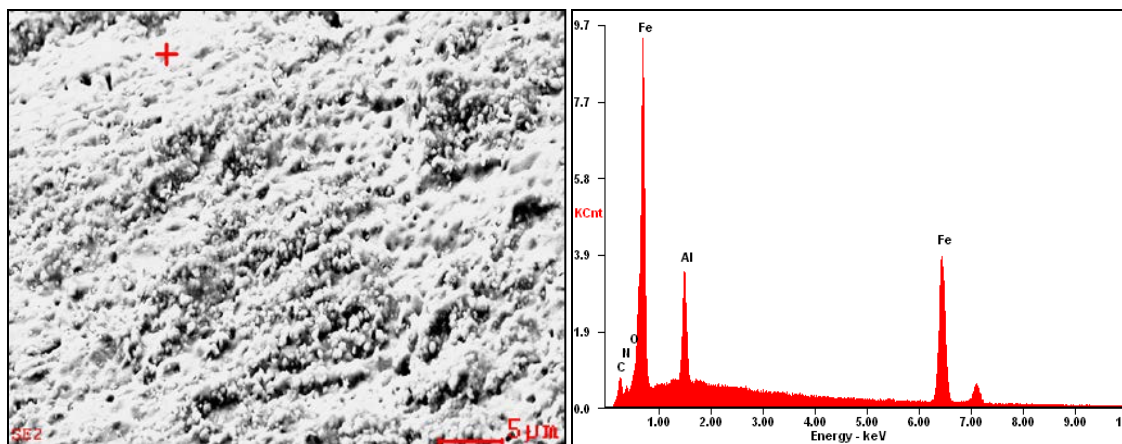
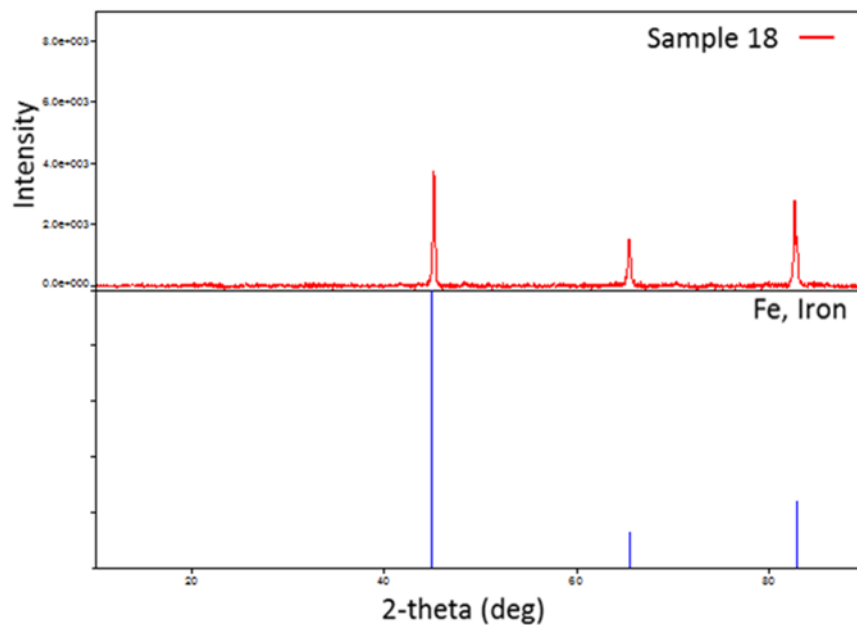


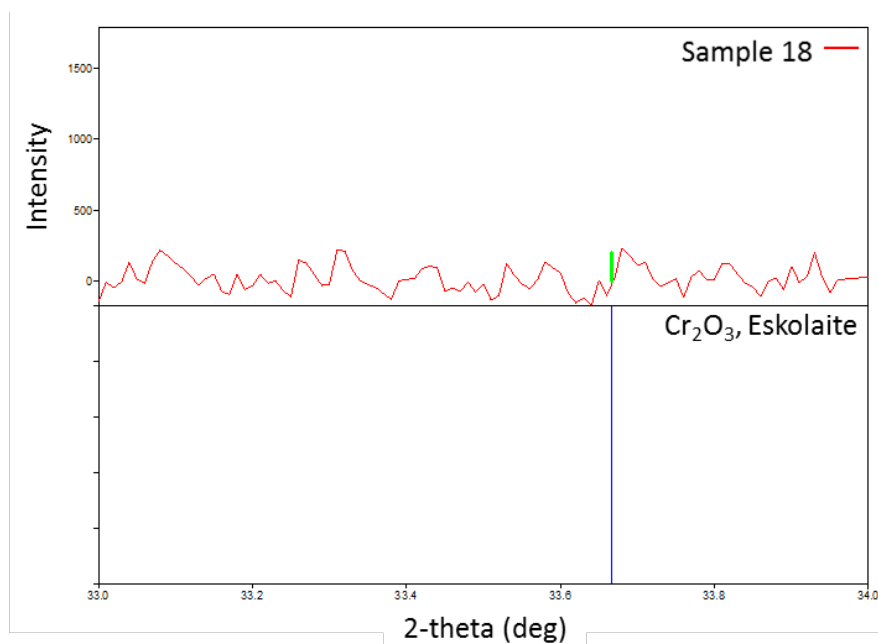
Figure 65. EDS Analysis of Sample 18 Substrate

Sample 18 was further analyzed using the XRD. This sample was cut into three lengths of approximately 1 cm and mounted side-by-side on a glass slide with carbon tape, in order to increase surface area. The XRD spectrum of this sample only revealed three predominant peaks, which were identified as iron (Figure 66). With the knowledge that the surface is coated with micron-size chromium-based particles, two more XRD spectrums were taken of Sample 18 to determine if the presence of chromium and chromium (III) oxide could be detected. The two most dominant peaks of chromium (III) oxide were attempted to be measured on Sample 18, as shown in Figure 67. This spectrum shows that chromium (III) oxide was not detected, as there is not peak with an intensity above which can be clearly identified. The analysis of the presence of chromium was very similar. Due to the dominant peak of chromium being in such close proximity of the iron peak, there was no chromium peak identified, as illustrated by Figure 68.



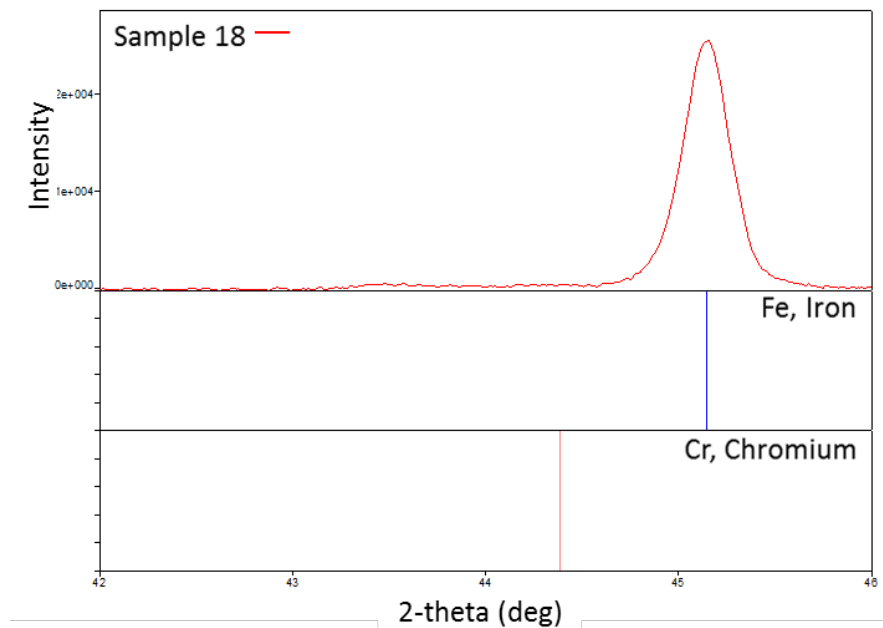
XRD analysis of Sample 18 confirms the presence of iron, but does indicate the presence of chromium or chromium (III) oxide.

Figure 66. X-Ray Diffraction Spectrum of Sample 18



Further analysis of Sample 18 shows that the chromium (III) oxide peaks that should be predominant, are not observed on the sample.

Figure 67. X-Ray Diffraction Spectrum of Sample 18 (Chromium (III) Oxide)



Further analysis of Sample 18 also revealed that chromium was not above a threshold where the machine detected its presence.

Figure 68. X-Ray Diffraction Spectrum of Sample 18 (Chromium)

From the analysis of these samples, it was determined that the samples mounted in the conductive material presented a few issues. First, the EDS analysis of these samples were inconclusive as a result of the poor adhesion of the mounting material to the sample. Due to the amount of contamination, the coating thickness measurements that were taken are highly unreliable as these measurements included the contaminants. From Sample 13 and the FIB milled areas, it was clear that a continuous coating did not form on the surface of the iron substrate. Instead, the surface of the iron sample was coated with randomly dispersed chromium and chromium oxide particles. The XRD analysis of Sample 18 does not show the presence of chromium-based particles on the surface of the iron wire. This is hypothesized to be due to the geometry of the sample and the particles did not form a thick coating on the surface. In an effort to study the potential for chromium-based coatings a concentrated effort was placed on reducing the chromium (III) oxide powder to chromium powder.

4. Chromium Powder Protocol

Eight chromium (III) oxide powder-based experiments were conducted in order to determine the best parameters that would result in chromium (Table 9). Initially the weight ratio of the urea was increased to ensure the oxide had enough material to reduce to a pure metal. The gas flow rate was decreased as this would permit the chemical to remain in the vicinity of the precursor powder and increase the likelihood of oxide reduction, as observed in [37]. Finally, four experiments were conducted using additional chemicals to increase the probability of reducing the oxide. Ratio A is a weight ratio of urea and iron to chromium (III) oxide of 2.4:1.1:1. Ratio B is a weight ratio of potassium carbonate and lignite to chromium (III) oxide of 5.5:0.2:1. Ratio C is a weight ratio of carbon to chromium (III) oxide of 5:1. Ratio D is a weight ratio of potassium carbonate and carbon to chromium (III) oxide of 10:5:1. After analyzing all eight samples in the XRD, it was qualitatively determined that none of the powders generated contained pure chromium.

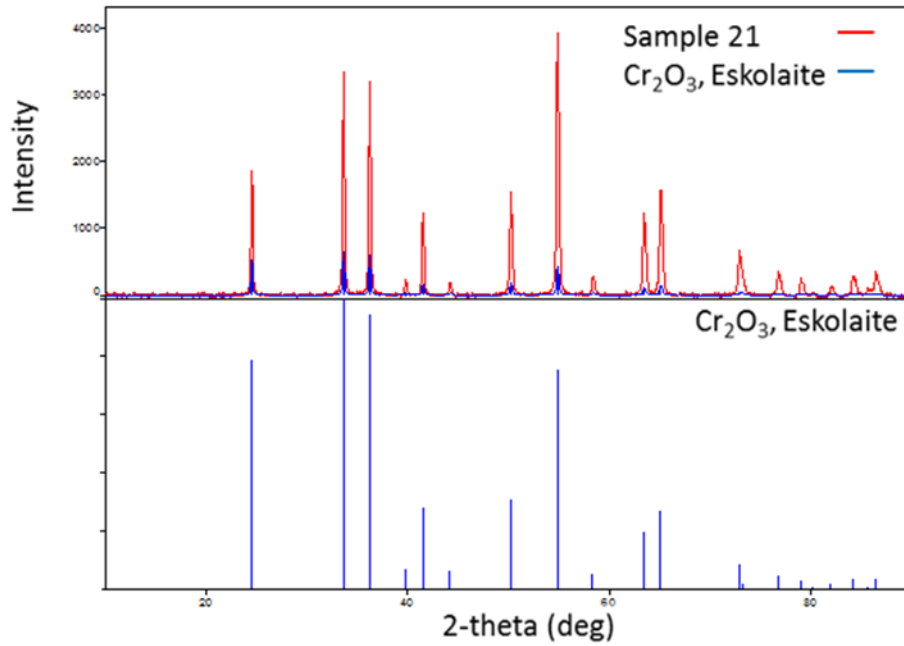
Table 9. Chromium Oxide Powder Experimental Parameters

Sample No.	Weight Ratio	Furnace Temperature	Nitrogen Flowrate
21	2.4:1	1000°C	25 SCCM
22	4:1	1000°C	14 SCCM
23	4:1	1100°C	14 SCCM
24	9.8:1	1000°C	14 SCCM
25	Ratio A	1000°C	25 SCCM
26	Ratio B	1000°C	25 SCCM
27	Ratio C	1000°C	8 SCCM
28	Ratio D	1000°C	8 SCCM

The urea to oxide weight ratio, temperature, and nitrogen flowrates were varied in the experiments in order to determine if the chromium (III) oxide would fully reduce. The weight ratios of Samples 21–24 were composed of urea and chromium (III) oxide.

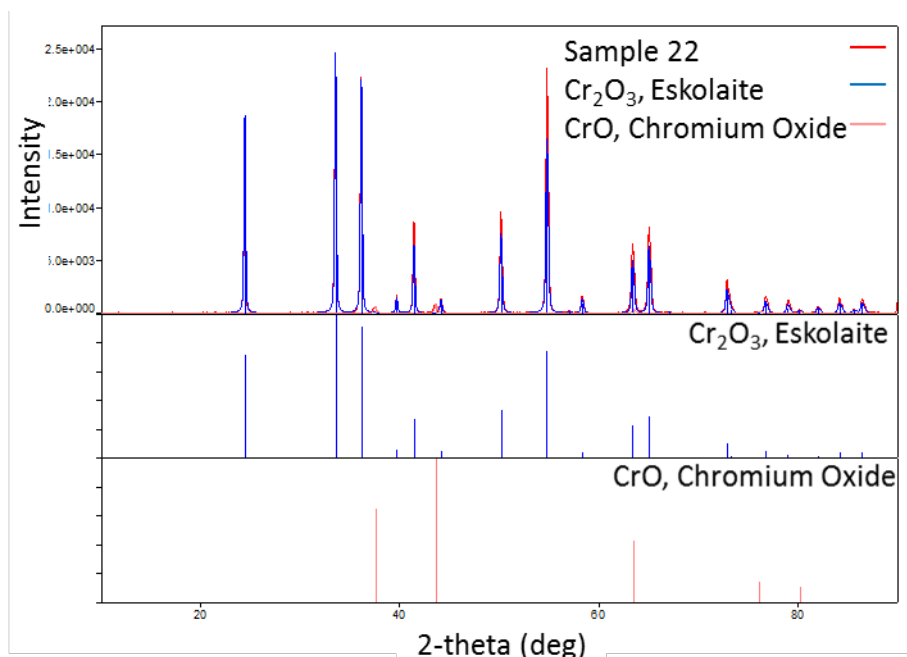
XRD analysis of Sample 21 spectrum clearly shows that the sample matches that of eskolaite phase of chromium (III) oxide, as shown by Figure 69. This illustrates that increasing the furnace temperature did not reduce the chromium (III) oxide. However, the XRD analysis of Sample 22 indicates slightly different results (Figure 70). The XRD

spectrum shows mostly the eskolaite phase and a small portion of a lower valent form of chromium, CrO. This shows that by increasing the weight ratio and decreasing the gas flowrate, chromium (III) oxide can reduce to another form of chromium oxide, but not fully reduce to chromium metal.



XRD analysis of Sample 21 shows the sample is the eskolaite phase of chromium (III) oxide.

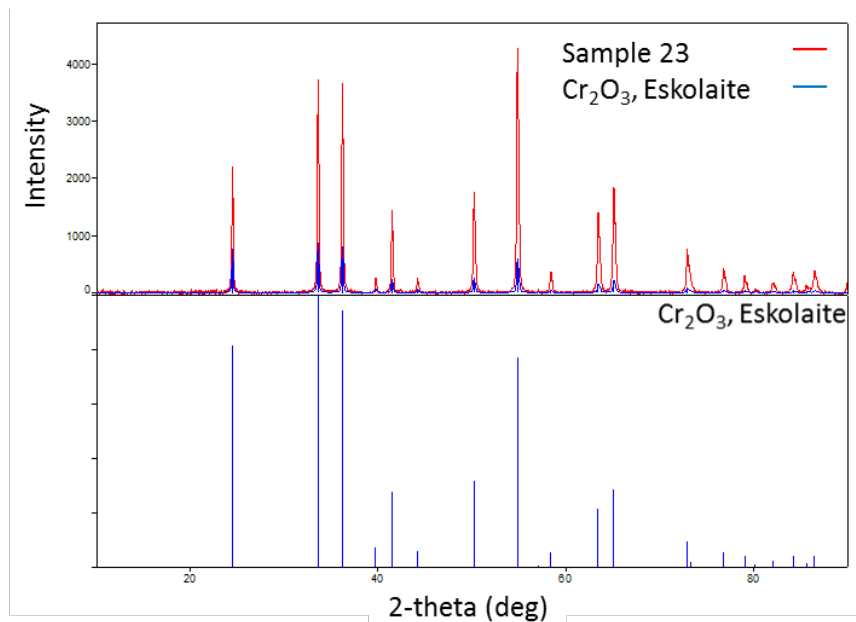
Figure 69. X-Ray Diffraction Spectrum of Sample 21



XRD analysis of Sample 22 indicates the presence of both the eskolaite phase of chromium (III) oxide and chromium oxide. The relative intensities of the two peaks observed in Sample 22 show the powder is mostly composed of chromium (III) oxide.

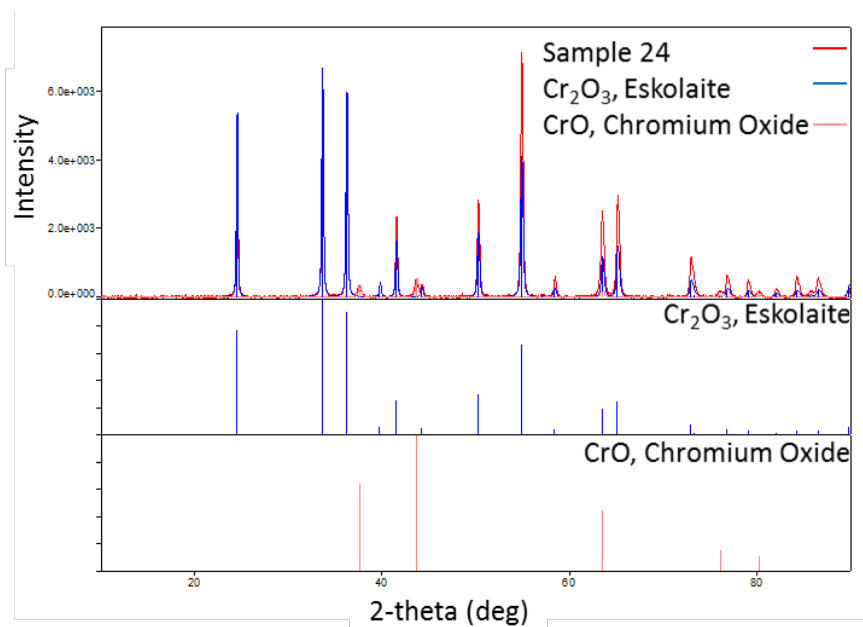
Figure 70. X-Ray Diffraction Spectrum of Sample 22

XRD analysis of Sample 23 shows results similar to Sample 21. The sample clearly has the crystal structure of the eskolaite phase of chromium (III) oxide (Figure 71). This shows that by increasing the urea weight ratio and temperature and decreasing the gas flowrate had no effect on the crystal structure of the chromium precursor. However, by further increasing the urea weight ratio with Sample 24, XRD analysis identified two crystal structures present similar to Sample 22, as shown in Figure 72. This presented some conflicting results, as Samples 22 and 23 were of the sample ratio but processed at two different temperatures. This would indicate that at lower temperature, it is possible to reduce the chromium (III) oxide to another form of chromium oxide, but not to pure chromium. However, increasing the urea weight ratio would not allow the chromium (III) oxide to reduce, but would remain as the same crystal structure.



XRD analysis of Sample 23 shows the sample is the eskolaite phase of chromium (III) oxide.

Figure 71. X-Ray Diffraction Spectrum of Sample 23

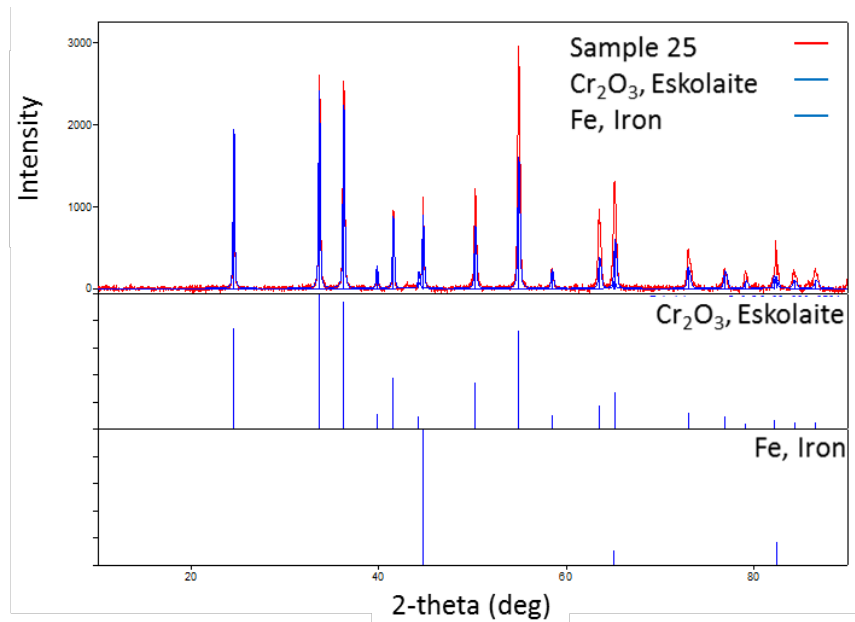


XRD analysis of Sample 24 indicates the presence of both the eskolaite phase of chromium (III) oxide and chromium oxide. The relative intensities of the two peaks observed in Sample 22 show the powder is mostly composed of chromium (III) oxide.

Figure 72. X-Ray Diffraction Spectrum of Sample 24

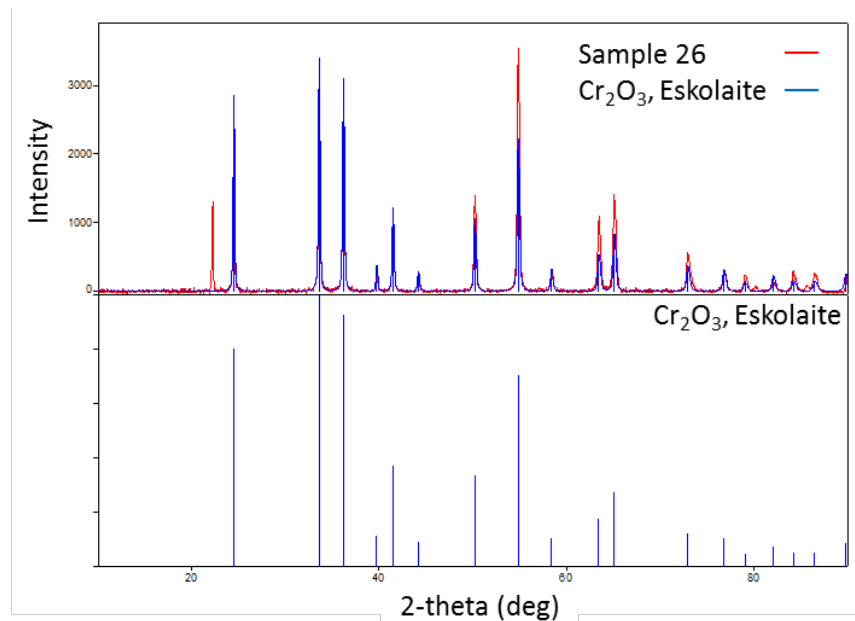
The remaining four samples were prepared with the use of different chemicals, as denoted by their respective ratios. The intent behind these experiments was to determine if other chemicals may assist in the reduction of oxide to metal would work for chromium (III) oxide. Sample 25 was prepared using iron mixed with the powder, because the iron would potentially oxidize and remove some of the oxygen molecules from the chromium particles. XRD analysis shows that the only two crystal structures in the powder are iron and chromium (III) oxide (Figure 73). This indicates that during the heat treatment in the furnace nothing chemically occurred with the chromium precursor. These results shed light to the possibility that during the chromium “RES Coating Protocol II” experiments, the precursor remained as chromium (III) oxide and did not create iron oxide on the surface of the wire. The XRD analysis of Sample 26, prepared with a different chemical ratio, remained as chromium (III) oxide (Figure 74). However, there was one characteristic peak that was not identified during the XRD analysis. This is thought to have been contamination during the removal of the chromium powder from the graphite foil.

Sample 27 was prepared using carbon and the precursor because it was thought that the oxygen molecules would bond to the carbon and create either carbon monoxide or carbon dioxide in the controlled environment. The results of the XRD analysis only identified crystal structure of chromium (III) oxide, as shown in Figure 75. However, this XRD spectrum also displays characteristics of an amorphous crystal structure, potentially carbon that was mixed during preparation. The XRD analysis of Sample 28 was very complicated due to decomposition of the potassium carbonate, as illustrated by Figure 76. However, when looking for two specific crystal structures such as chromium (III) oxide and chromium, it is very clear that some of the peaks coincide with chromium (III) oxide. However, there does not appear to be any peaks that coincide with pure chromium.



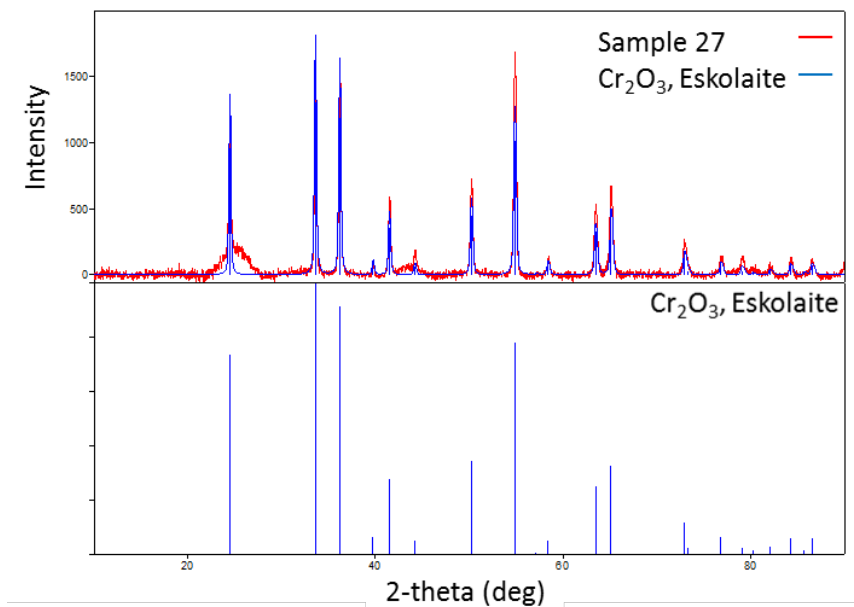
XRD analysis of Sample 25 shows the presence of the eskolaite phase of chromium (III) oxide and iron. The relative intensity of the iron peaks indicate the sample is composed mostly of chromium (III) oxide.

Figure 73. X-Ray Diffraction Spectrum of Sample 25



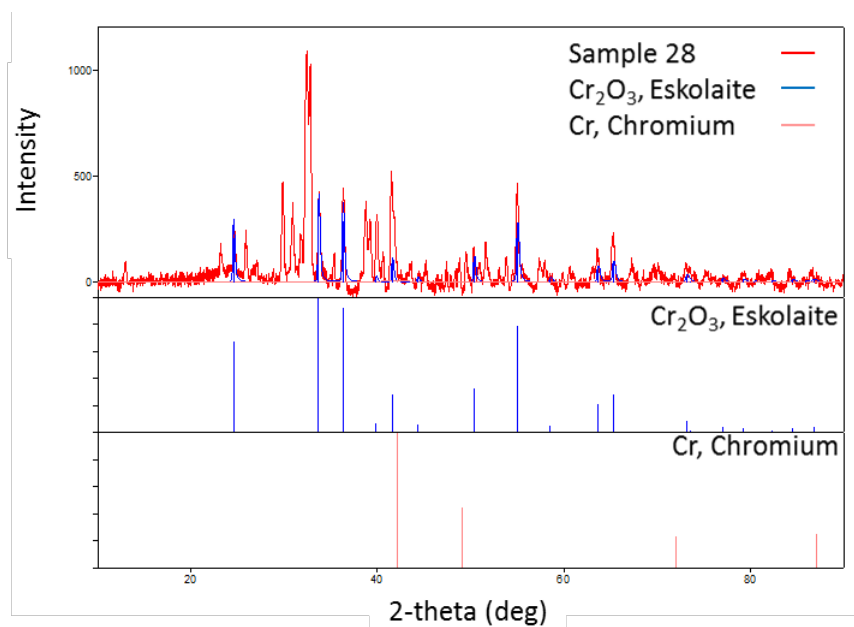
XRD analysis of Sample 26 shows the sample is the eskolaite phase of chromium (III) oxide.

Figure 74. X-Ray Diffraction Spectrum of Sample 26



XRD analysis of Sample 27 shows the sample is the eskolaite phase of chromium (III) oxide.

Figure 75. X-Ray Diffraction Spectrum of Sample 27



XRD analysis shows the complex nature of this sample. However, when comparing the characteristic x-ray peaks of chromium and chromium (III) oxide with those of Sample 28, the powder did not fully reduce to chromium metal particles.

Figure 76. X-Ray Diffraction Spectrum of Sample 28

To summarize the results of the eight chromium powder-based experiments, a semi-quantitative analysis was performed using the PDXL2 software and the XRD spectrums generated. The results are outlined in Table 10 and show the weight percent composition of chromium (III) oxide, chromium, and other materials. Notably, due to the complicated nature of Sample 28, it has been omitted from Table 10. The semi-quantitative analysis would have been inaccurate without identifying the materials that decomposed during the reductive heating process. Unfortunately, the results of the analysis performed on these samples did not provide any qualitative evidence that the chromium metal crystal structure was present in any of these samples.

Table 10. Quantitative Results of Chromium Based Powder Composition

Sample No.	Chromium (III) Oxide (Wt. %)	Chromium (Wt. %)	Other (Wt. %)
21	100%	0%	0%
22	98%	0%	2%
23	100%	0%	0%
24	96%	0%	4%
25	96%	0%	4%
26	100%	0%	0%
27	100%	0%	0%

All samples show a high weight percentage of chromium (III) oxide and other materials. The other materials found in Samples 22 and 24 are a reduced form of chromium oxide (CrO), which were found to be 2% and 4%, respectively. Sample 25 contained 4% of iron, as this sample was a mixture of iron and chromium (III) oxide.

C. RESULTS OF NICKEL BASED RES PROTOCOLS

To demonstrate some success using the RES method, nickel (II) oxide powder was reduced in powder-based experiments. Then, developing a coating RES protocol for the nickel (II) oxide, an iron foil was coated. The resultant coating was characterized as non-uniform nickel particles that did not form a smooth surface, which is desirable for most coating applications.

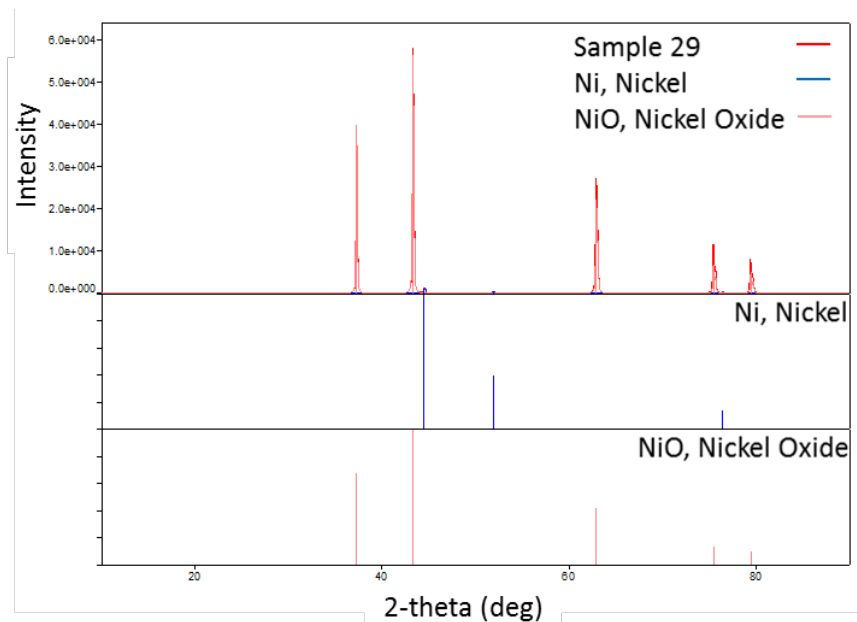
1. Nickel Powder Protocol

With the failure of the chromium-based coating protocols, it was decided to demonstrate that RES can be used to make some metal coatings. Nickel was selected for its relative ease of reduction and its common use as a metal coating for various household fixtures as well as an “adhesion coat” in chrome coatings. Initially, experiments were conducted with powders, in order to determine the parameters needed for a successful reduction of the metal oxide, as shown in Table 11. Samples 29 and 30 did not fully reduce, as the ratio of urea to nickel (II) oxide was very low. Sample 29 was analyzed using the XRD, illustrated in Figure 77, which resulted in identifying two separate crystal structures. The first crystal structure is Nickel (II) oxide and the second identified compound is nickel. From the relative intensity of the reduced nickel peaks in the spectrum to the nickel (II) oxide peaks, there is a trace amount of reduced nickel.

Table 11. Nickel Oxide Powder Experimental Parameters

Sample No.	Weight Ratio	Furnace Temperature	Nitrogen Flowrate
29	0.2:1	800°C	25 SCCM
30	0.1:1	800°C	25 SCCM
31	4:1	800°C	25 SCCM
32	3.2:1	800°C	25 SCCM
33	8.1:1	1000°C	14 SCCM
34	4.8:1	1100°C	8 SCCM

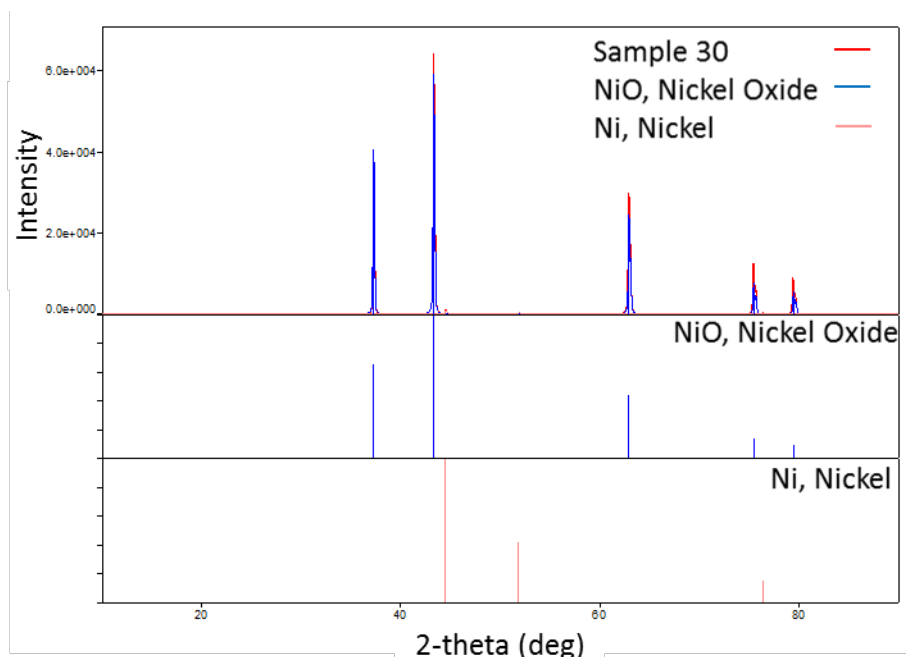
The urea to oxide ratio, temperature, and nitrogen gas flowrates were varied in the experiments in order to determine the best method to reduce the nickel oxide to nickel for a future coating application



XRD spectrum from sample 29 shows very small peaks of reduced nickel, with larger peaks from nickel (II) oxide powder. The relative intensity of the nickel peak suggests that a small amount of the oxide reduced to form nickel in the powder.

Figure 77. X-Ray Diffraction Spectrum of Sample 29

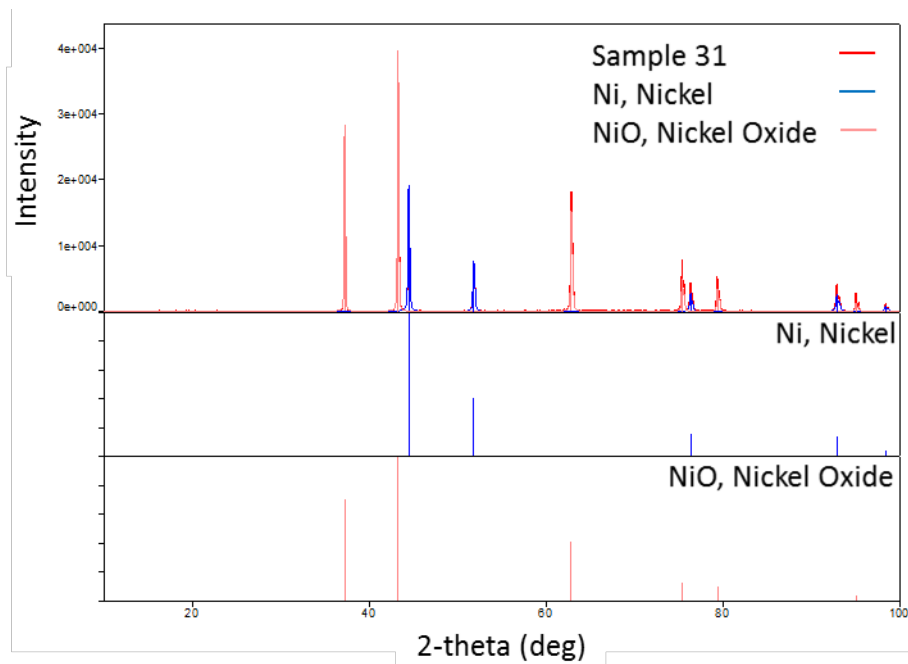
XRD analysis of Sample 30 indicated a small amount of reduced nickel among the powder, as shown in Figure 78. The PDXL2 software identified the first crystal structure as the bunsenite phase of nickel oxide and second crystal structure as pure nickel. Obviously, the relative intensity of the nickel is much smaller than the nickel oxide, which implies that the weight percent is low, in relation to the nickel oxide.



XRD spectrum from sample 30 shows very small peaks of reduced nickel with larger peaks from nickel (II) oxide powder. The relative intensity of the nickel peak suggests that a small amount of the oxide reduced to form nickel in the powder. This experiment was conducted with a smaller amount of urea, so the expected amount of reduced nickel in the powder should be less than sample 29.

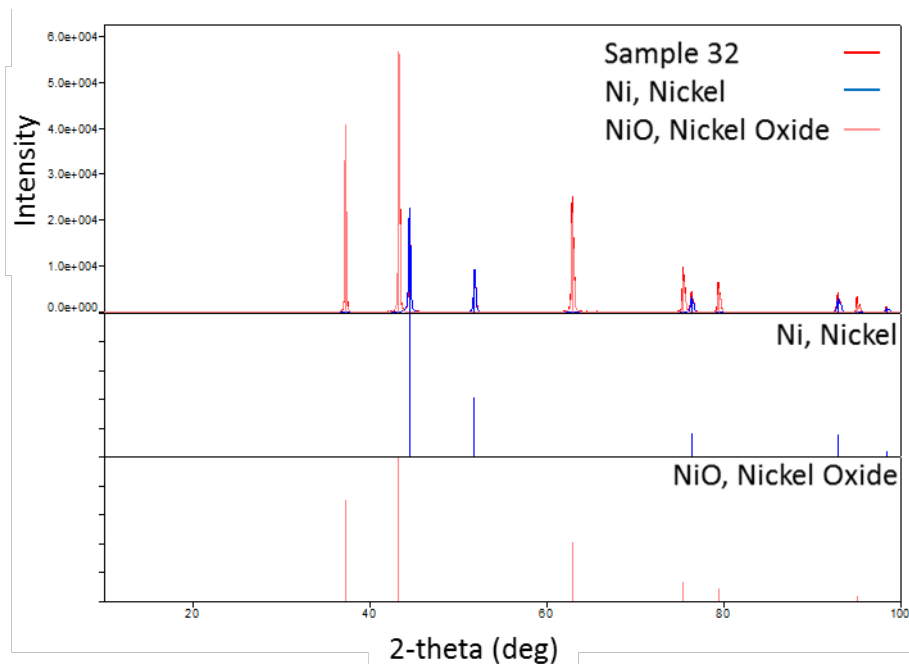
Figure 78. X-Ray Diffraction Spectrum of Sample 30

Samples 31 and 32 were prepared with an increased amount of urea in the powder, while keeping the furnace temperature and gas flowrate the same. These samples were analyzed using the XRD. From the spectrums, the PDXL2 software confirmed the crystal structures in each powder. The XRD spectrum of Sample 31 (Figure 79) shows a mixture of nickel oxide and nickel. XRD analysis of Sample 32 shows similar results that contain both nickel and nickel oxide, as illustrated in Figure 80.



XRD analysis shows that Sample 31 contains a mixture of both nickel and nickel (II) oxide.

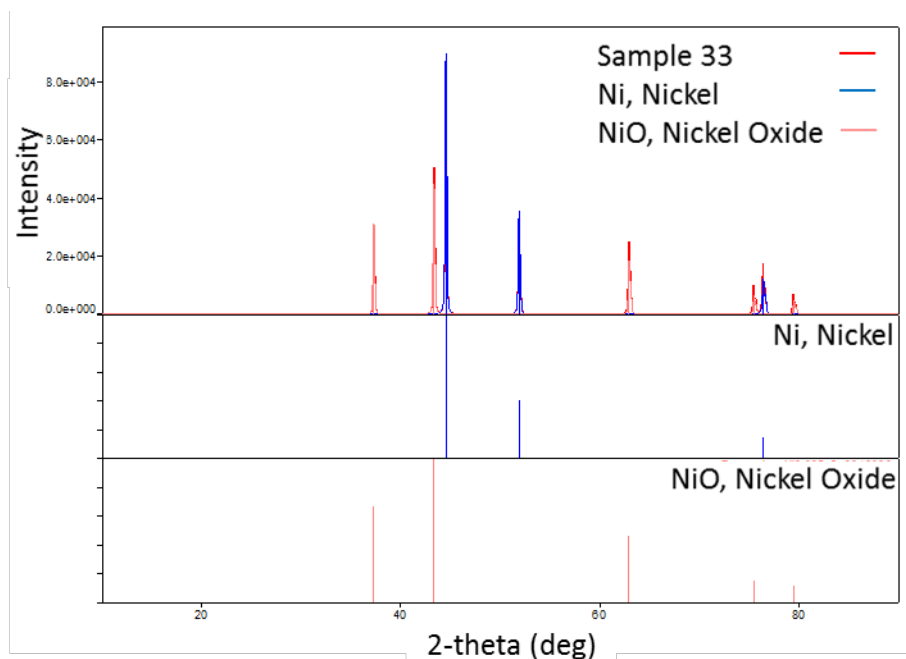
Figure 79. X-Ray Diffraction Spectrum of Sample 31



XRD analysis shows that Sample 32 contains a mixture of both nickel and nickel (II) oxide.

Figure 80. X-Ray Diffraction Spectrum of Sample 32

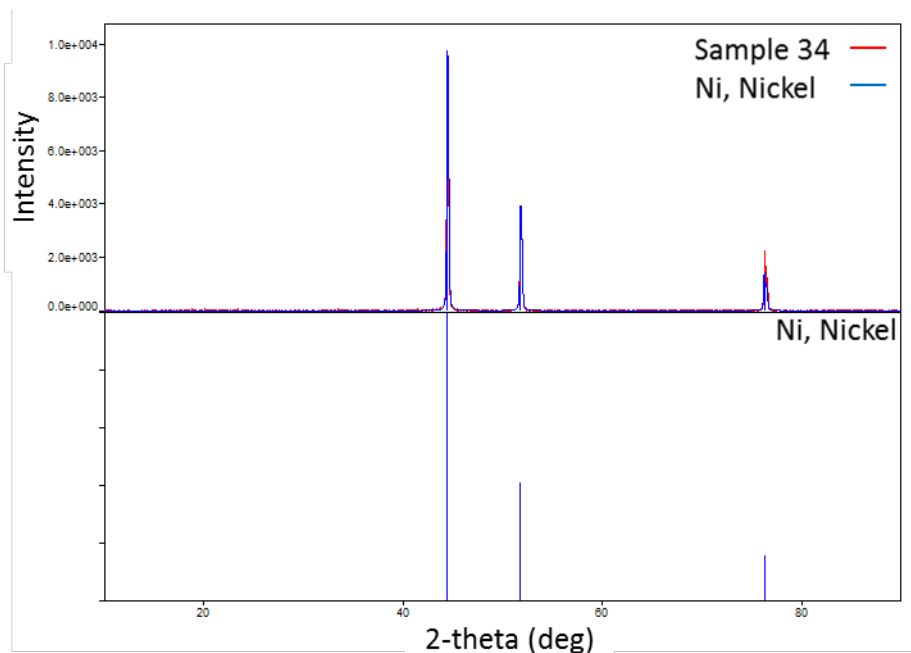
Sample 33 was prepared by increasing the amount of urea, increasing the furnace temperature, and decreasing the gas flowrate. This resulted in an XRD spectrum that contains two crystal structures, nickel and the bunsenite phase of nickel oxide, as shown in Figure 81. This spectrum shows a remarkable increase in the nickel, based upon the relative intensities of the nickel peaks versus those of the nickel oxide.



XRD analysis shows that Sample 33 contains a mixture of both nickel and nickel (II) oxide.

Figure 81. X-Ray Diffraction Spectrum of Sample 33

Sample 34 was prepared by increasing the furnace temperature and decreasing the gas flowrate. The ratio of urea to nickel oxide was reduced, which resulted in an XRD spectrum that only contained one crystal structure, as shown in Figure 82. The XRD analysis of this spectrum identified the crystal structure as nickel in Sample 34. This was the first successful reduction of a metal oxide to its metallic form. The ratio of urea to nickel oxide was then used to create a paste using the “RES Nickel Coating Protocol.”



XRD analysis of Sample 34 shows that powder contains only nickel.

Figure 82. X-Ray Diffraction Spectrum of Sample 34

Additional analysis was conducted on the nickel based powder samples. The PDXL2 software was used to provide some quantitative results of the composition of the crystal structures that were identified in these samples, as shown in Table 12. As previously stated, the small nickel peaks in Samples 29 and 30 resulted in a low composition of reduced nickel. Also of note, the ratios of Sample 31 and 34 were somewhat close and as the temperature was increased and the gas flowrate decreased, the nickel composition increased dramatically in sample 34.

Table 12. Quantitative Results of Nickel Based Powder Composition

Sample No.	Nickel (II) Oxide (Wt. %)	Nickel (Wt. %)
29	98	2
30	98	2
31	72	28
32	75	25
33	50	50
34	0	100

2. Nickel Coating Protocol

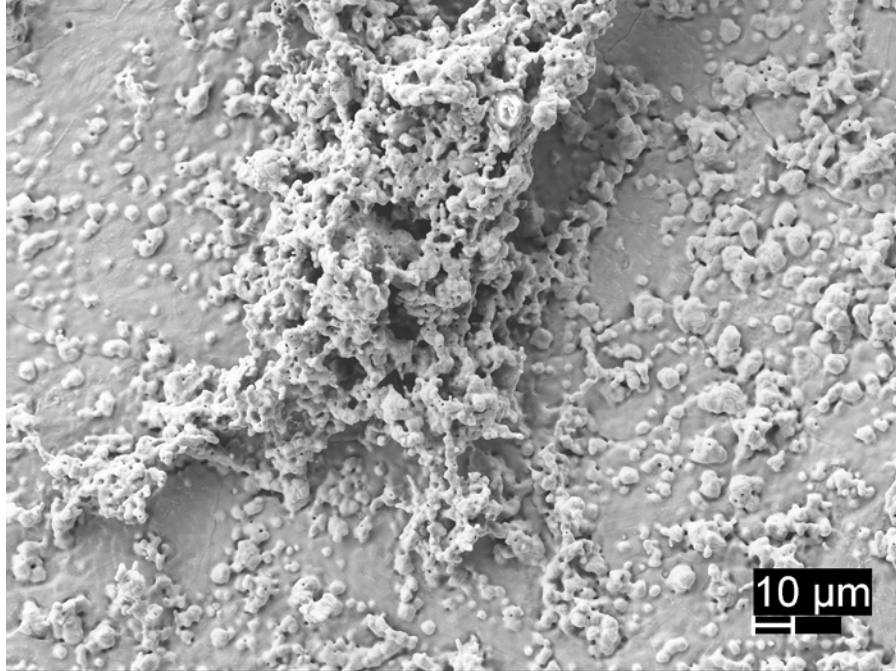
Following the success of reducing nickel (II) oxide to pure nickel, seen in Sample 34, it was decided to use the same experimental parameters for a nickel coating on an iron foil. The iron foil was observed to have a non-uniform coating with shiny areas that penetrate to the polished iron substrate, as shown in Figure 83.



Optical microscopy of sample 35 reveals areas that have been coated with the reduced nickel particles and areas that have not been coated.

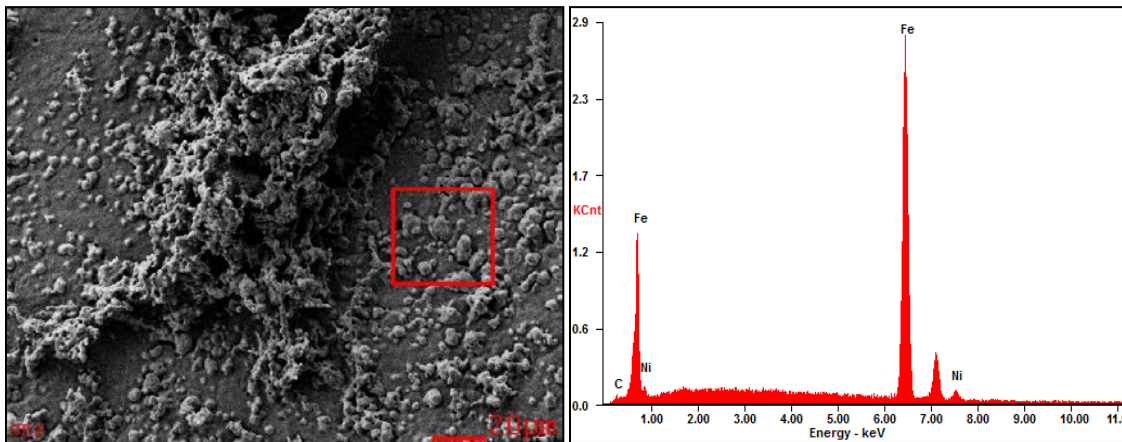
Figure 83. Optical Microscopy of Sample 35

Further analysis was conducted on Sample 35 using SEM. First, the surface morphology was observed. The first region shows small particles have deposited on to the surface of the iron, as illustrated in Figure 84. This shows there is some issues with achieving a uniform coating with a desired thickness. Next, an EDS analysis was conducted on the surface of Sample 35 that shows the particles that deposited on the iron substrate contain nickel, as shown in Figure 85.



This figure shows that the reduced particles did not achieve a uniform coating and deposited randomly on the surface of the iron foil.

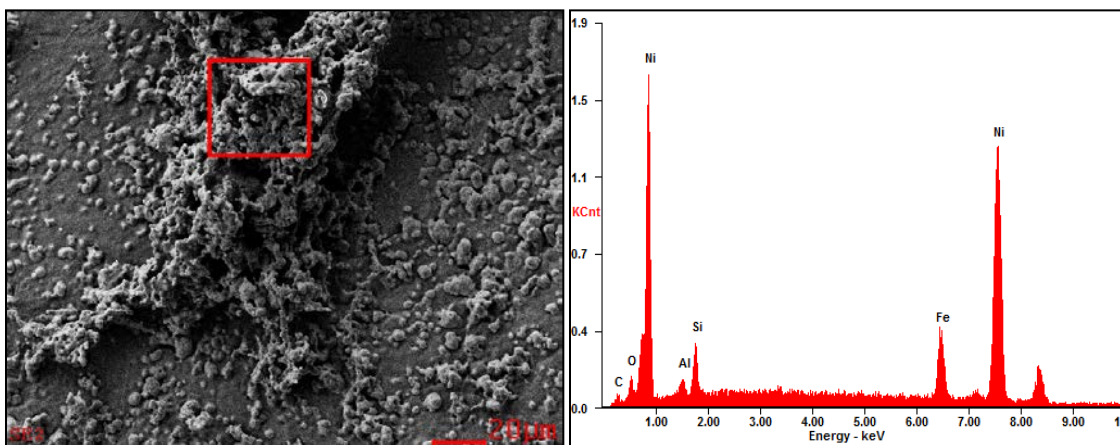
Figure 84. SEM Microscopy of Sample 35



EDS analysis of the foil shows that nickel is present, which would indicate the particles are reduced nickel particles and do not contain any oxides.

Figure 85. EDS Analysis of Surface on Sample 35

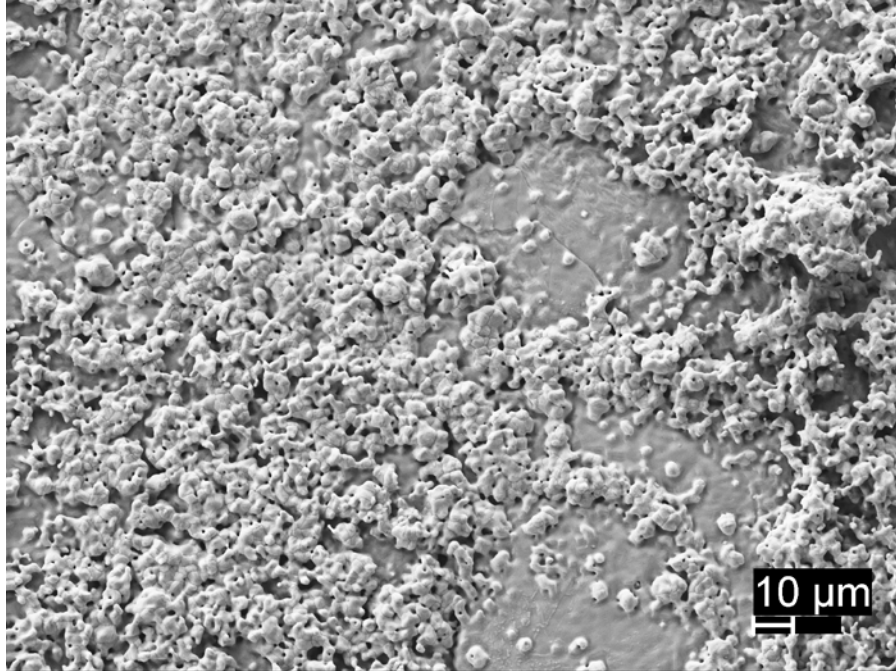
An EDS analysis was also conducted on the large agglomerated particle, as shown in Figure 86, which confirmed the particles contained large amounts of nickel, along with smaller amounts of carbon, oxygen, aluminum, silicon, and iron. Of the other elements that were found to be present, only iron can be explained because the substrate contains iron. The other elements present are contaminants of unknown origin. However, the presence of oxygen could be a component of silicon oxide or aluminum oxide, which are more likely a form of silica and alumina found on the surface.



EDS analysis of the agglomerated particle shows a large amount of nickel with small amounts of oxygen, aluminum, silicon, and iron.

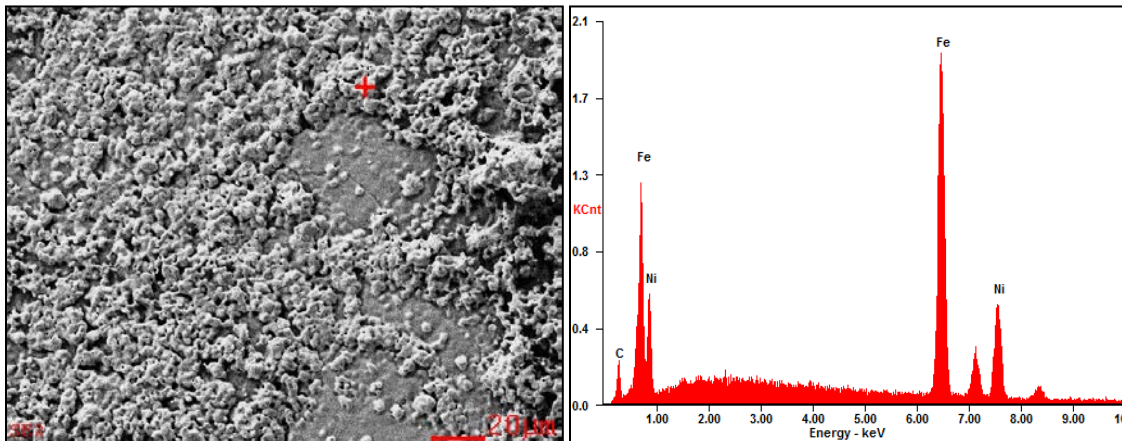
Figure 86. EDS Analysis of Agglomerated Particle on Sample 35

A second region on this sample was analyzed where the deposition of particles appears to be more uniformly dispersed on the surface, as shown in Figure 87. An EDS point analysis was conducted on the particles, which shows carbon, iron, and nickel (Figure 88). Conducting an EDS analysis of an area indicated a reduction in the relative amount of carbon on the surface where the nickel particles have been applied. It was also noted, in this EDS analysis, was the lack of contaminants, especially oxygen. This is consistent with the suggestion that nickel is not oxidized, and when an oxygen peak is observed, it is associated with the compounds of silicon and aluminum contaminants. Finally, an EDS area analysis was conducted on the surface of the iron foil, which confirmed the background spectrum to only contain iron, as shown in Figure 89.



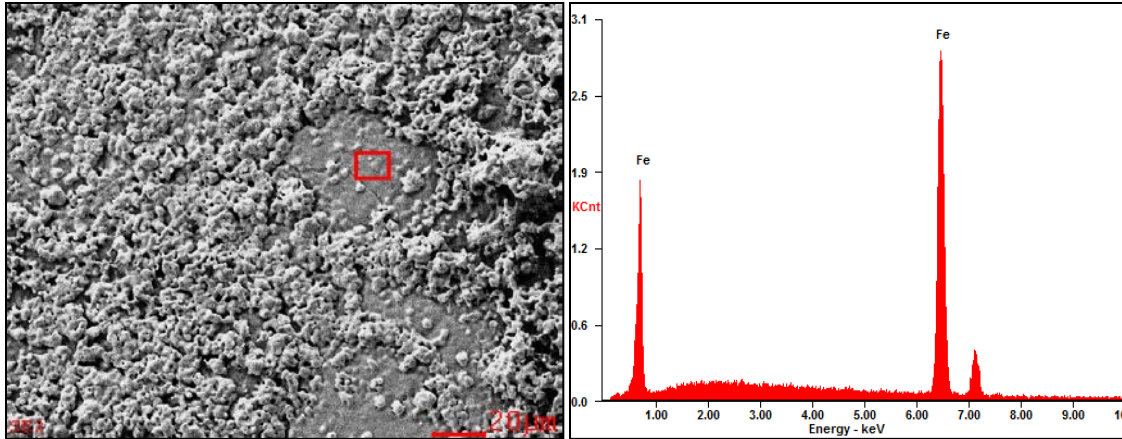
This figure shows a region in which the reduced particles appear to be of uniform height.

Figure 87. SEM Microscopy of Sample 35



This EDS point analysis shows reduced nickel particles on the surface of the iron foil.

Figure 88. EDS Point Analysis of Reduced Particles on Sample 35



This EDS analysis shows a region that appears to have a uniform surface composition of iron.

Figure 89. EDS Analysis of Iron Substrate on Sample 35

Sample 35 illustrates that the RES method is successful in reducing nickel oxide to nickel particles and can be used to coat the surface of an iron foil. This coating is by no means a smooth uniform coating that completely coats the surface of the substrate, which would be highly desirable for a protective coating against either wear or corrosion. The lack of a smooth coat may reflect the coarse, uneven application of the paste. It is quite possible the areas of the surface not coated by nickel were simply not properly coated initially. This suggests, as with many coating processes, that several layers must be created to form a fully coated substrate.

IV. DISCUSSION

This chapter provides a comparison between the preparation and RES method used in this study and methods used in industry to create metal coatings.

A. SURFACE PREPARATION

In this study, the iron substrates used were stored in laboratory environment where protective packaging was used to control the humidity and possible contamination. Prior to using a coating protocol, each sample was removed from the packaging and then cleaned with a metal polish. However, in industry, the metal substrates undergo a more rigorous cleaning process as the metal has been exposed to humidity and may have surface oxidation. Prior to the electroless plating the metal components must be cleaned and etched [19]. Mandrich [47] describes, the use of a hot alkaline cleaning solution to remove oil and scale prior to coatings for electroplating. The surface needs to be roughened for the thermal spray coating to properly adhere to the surface [27]. Sputtering, cold spray, and thermal evaporation techniques also require a clean surface that is free of oxides and greases, to prevent corrosion from occurring beneath the applied coating. Therefore, if the RES technique were used commercially, the impact of surface preparation on physical adherence would have to undergo further research.

B. DURATION OF COATING METHOD

The RES method used in this study took approximately one hour per coating application, which includes the flushing the atmosphere with an inert gas, heating, and cooling. Whereas, the electroplating and electroless plating require time in the solution in order to reach the desired thickness. Electroplating and electroless plating can achieve a deposition rate as high as 37.5 μm per hour (~ 10 nm/s) for chromium and 11.5 μm per hour (~ 3 nm/s) for nickel, respectively [19], [48]. Sputtering and thermal evaporation techniques have deposition rates of up to 2 nm/s and 10 nm/s respectively [30]. Cold and thermal spray techniques can generate thicker coating in a short period of time [26], [49].

C. TEMPERATURE DURING COATING

During this study it was found that the reduced nickel formed from nickel (II) oxide at 1100°C. This relatively high temperature was used for the nickel coating applied to Sample 35. However, the temperature of the plating baths used for electroplating and electroless plating range from 60–90°C [19], [48]. Sputtering can create thin films with either a high temperature vacuum or with a plasma [22]. As previously mentioned [24], the cold spray technique uses a temperature that ranges between 100–500°C. With thermal spraying the temperature used in the application is based on the melting temperature of the coating material. Similarly, the temperature used with thermal evaporation is based upon the vapor pressure of the material used for the coating application [30].

D. PRECURSORS USED FOR COATING

In this study the RES precursors were limited to chromium (III) oxide (Cr_2O_3) and nickel (II) oxide (NiO). As mentioned previously, the electroplating industry uses chromium (VI) trioxide (CrO_3) and sulfuric acid in the plating bath to create chrome coatings which have resulted in a higher risk of cancer [3]–[6], [10]. Electroless plating for nickel uses either nickel chloride or nickel sulfate [19]. The sputtering method uses a variety of target materials that can be used to create a thin film. Both the cold and thermal spray methods use powders to fuse the particles on the surface of the substrate. The thermal evaporation method uses specific metals as they have an appropriate vapor pressure that can be used to create thin films {E. Chen}.

E. GEOMETRY OF SUBSTRATE

In this study it was noted that the 1 mm iron wire had variability issues when the paste was applied, whereas the paste could be applied evenly to the iron foil. Both electroplating and electroless plating do not have issues with coating complex substrate geometries as they are submerged in the coating bath, however electroless plating will provide a more even coating [20]. Sputtering is better suited for flat geometries such as small electronic components and computer chips [22]–[23]. Thermal evaporation has poor uniformity when coating large flat objects and is better suited for smaller pieces [30].

Thermal and thus cold sprays are limited to their line-of-sight between either the arc gun or nozzle and the substrate, so these methods would be ideal for large components with a simple geometry [19], [40].

THIS PAGE INTENTIONALLY LEFT BLANK

V. CONCLUSIONS

This study illustrates some successes when using the Reduction Expansion Synthesis method to create a metal coating on another metal substrate. During the course of the analysis of the “Coating Protocol I” samples, it was determined that excessive carbon was present on the surface of the wire. In an effort to reduce the amount of carbon on the surface after processing, the “Coating Protocol II” was developed and implemented. The samples produced using “Coating Protocol II” showed some promise because the surface of the wire was visually shiny after the heat treatment. When these samples were placed in the conductive mounting material, it was observed that many contaminants were found in the surface layer from the process used to prepare the cross-sections for analysis. EDS analysis was able to detect chromium and oxygen in the surface layer, but did not provide definitive results as to whether or not the chromium had reduced or if it remained as chromium oxide. Even when the sample was milled with a Focused Ion Beam, a coating interface was not found. The EDS of this sample revealed the surface was only coated in particles, which lead to a brief study of the chromium powders. The XRD analysis of one of these wires illustrated that either due to the geometry of the wire or the dispersion of particles, the XRD was unable to detect the presence of chromium-based particles on the surface of the iron wire.

The chromium powder experiments demonstrated that when using very similar parameters of those used in the coating protocols, the powder produced following the heat treatment process resulted in a high weight percentage of chromium (III) oxide. These experiments illustrate that the coating applied to the iron wires is a very thin layer of dispersed chromium (III) oxide particles. With the lack of success with the chromium-based powders, nickel (II) oxide was used to determine if the RES coating process is totally unreliable or simply restricted to particular metals. In particular, experiments were designed to determine if nickel films can be produced using RES. Nickel was selected because two earlier published RES studies [35], [37], show nickel oxide particles can be reduced to nickel metal particles using RES. Hence, there is a basis for considering nickel a likely candidate for successful metal film formation using RES.

The results of the nickel powder experiments show that the oxide particles will reduce to create nickel particles at a very high temperature and low gas flowrate. The high temperature used would in effect cause the substrate to recrystallize, which would be detrimental to material characteristics such as strength and hardness.

When the “Nickel Coating Protocol” was used, it resulted in an obvious coating from visual observation with the optical microscope. However, upon using the high-resolution SEM, it was determined that the coating was not continuous, but comprised of regions well covered by nickel particles and ‘open regions’ in which the underlying iron surface is exposed. This feature alone is not highly desired for coating applications as it will not fully protect the substrate from corrosion.

Research should be continued in this field to improve the current methods used in industry to create protective coatings. This research should begin with a focus on reducing metal compounds that have a low Gibb’s free energy of formation, as these compounds may reduce at lower temperatures. Reducing a coating at a lower temperature will preserve the material characteristics of the coated component. It is also recommended to first conduct powder-based experiments with the use of different inert gases to conduct XRD analysis in order to determine the crystal structure of the powder. This will aid further analysis in the SEM, as the EDS will only determine what elements are present on a sample. The use of wires in this study illustrated that the paste applied and the surface tension of that paste greatly affect the resultant coating. In order to achieve a more uniform coating, thin metal foils should be used to ensure the coating is applied uniformly prior to the RES heat treatment. Once success is achieved with the pure metal foils, then other commonly used materials using in engineering applications should be tested to determine the composition of the coating. Once this is completed, then subsequent, testing can be conducted to determine how the coatings perform when placed into corrosive environments.

One very intriguing possibility arises from this work: the RES method may be a replacement for the metal particle/laser sintering process presently employed in 3D manufacturing of metal parts. In particular, the successful production of “irregular” nickel metal films using RES is suggestive. A clear nickel layer was created, however, it

was irregular in height and density. These irregularities may result from the imperfect method of precursor application. Assuming the irregularity does result from imperfect application leads to this postulate: Metal can be applied to a substrate in a designed pattern using (i) pastes composed of metal “precursor species” (e.g. NiO particles) and urea are applied in the desired pattern, (ii) metal is created in the applied locations simply by heating to a relatively low temperature of 1100°C in a furnace. The process is repeated to make a designed three-dimensional metal structure. The advantages include the removal of a high intensity laser from the production process. The promise of this technology is sufficiently exciting to merit additional study of RES metal deposition.

THIS PAGE INTENTIONALLY LEFT BLANK

LIST OF REFERENCES

- [1] C. Lee, K. Kim, and J. Lim, "Sputter-deposited Cr as an alternative to electroplated Cr," *Material Sci. Forum*, vol. 510–511, pp. 674–677, 2006.
- [2] I. Shuker and K. R. Newby, "Why functional trivalent chromium fails and hexavalent chromium is environmentally friendly," *Trans. of the Inst. of Metal Finishing*, vol. 83, no. 6, pp. 272–274, Dec. 2005.
- [3] R. A. Lane, C. Fink, C. Grethlein, and N. Rome, "Analysis of alternatives to hexavalent chromium: A program management guide to minimize the use of CrVI in military systems," *AMMTIAC-WSTIA*, vol. 1, no. 2, pp. 3–9, Sept. 2012.
- [4] C. Pellerin and S. M. Booker, "Reflections on hexavalent chromium: health hazards of an industrial heavyweight," *Environ. Health Perspect.*, vol. 108, no. 9, pp. A402–A407, Sept. 2000.
- [5] M. Costa, "Potential hazards of hexavalent chromate in our drinking water," *Toxicol. Appl. Pharmacol.*, vol. 188, no. 1, pp. 1–5, Apr. 2003.
- [6] P. Bright, P. S. Burge, S. P. O'Hickey, P. F. Gannon, A. S. Robertson, and A. Boran, "Occupational asthma due to chrome and nickel electroplating," *Thorax*, vol. 52, no. 1, pp. 28–32, Jan. 1997.
- [7] Department of Defense, Memorandum: "Minimizing the Use of Hexavalent Chromium (Cr⁺⁶)," Under Secretary of Defense (AT&L), Washington, DC, 2009.
- [8] H. H. Lou and Y. Huang, "Electroplating," in *Encyclopedia of Chemical Processing*, vol. 2, S. Lee, Eds, New York, NY: Taylor and Francis Group, 2006, pp. 839–848.
- [9] D. J. Jones, *Principles and Prevention of Corrosion*, 2nd ed. Upper Saddle River, NJ: Prentice Hall, 1996, pp. 477–512.
- [10] B. Sartwell. (2009, Jan. 13). Replacement of Hexavalent Chromium on DOD Weapons System. [Online]. Available: <http://www.denix.osd.mil/cmrrmp/ecmr/hexchrome/dodriskmanagement/>
- [11] K. Legg, M. Graham, P. Change, F. Rastagar, A. Gonzales, and B. Sartwell, "The replacement of electroplating," *Surface and Coating Technol.*, vol. 81, no. 1, pp. 99–105, May 1996.
- [12] Toxic and Hazardous Substances, 29 C.F.R. § 1910.1026 (2017).
- [13] Protection of Environment, 40 C.F.R. § 136 (2017).

- [14] M. Tomkiewicz, "Environmental Aspects of Electrodeposition," in *Modern Electroplating*, vol. 5, M. Schlesinger and M. Paunovic, Eds. Hoboken, NJ: John Wiley & Sons, Inc., 2010, pp. 555–571
- [15] S. Surviliene, O. Nivinskiene, A. Cesuniene, and A. Selskis, "Effect of Cr(III) solution chemistry on electrodeposition of chromium," *J. Appl. Electrochem.*, vol. 36, no. 6, pp. 649–654, Jun. 2006.
- [16] G. Saravanan and S. Mohan, "Pulsed electrodeposition of microcrystalline chromium from trivalent Cr-DMF bath," *J. Appl. Electrochem.*, vol. 39, no. 8, pp. 1393–1397, Aug. 2009.
- [17] L. Li, G. P. Swain, A. Howell, D. Woodbury, and G. M. Sawin, "The formation, structure, electrochemical properties and stability of trivalent chrome process (TCP) coatings on AA2024," *J. of the Electrochem. Soc.*, vol. 158, no. 9, pp. C274–C283, 2011.
- [18] O. Suarez, J. Olaya, and S. Rodil, "The effect of operating conditions during plating on the electrochemical behavior and morphology of trivalent solution-derived chromium coatings," *Revista Mexicana de Ingenieria Quimica*, vol. 12, no. 1, pp. 129–141, Apr. 2013.
- [19] M. Schlesinger, "Electroless deposition of nickel," in *Modern Electroplating*, vol. 5, M. Schlesinger and M. Paunovic, Eds. Hoboken, NJ: J. Wiley & Sons, Inc., 2010, pp. 447–458
- [20] R. Parkinson, "Properties and applications of electroless nickel," *Nickel Develop. Inst.*, 1997.
- [21] P. Benaben. (2011, Jan. 31). An overview of hard chromium plating using trivalent chromium solutions. [Online]. Available: <http://www.pfonline.com/articles/an-overview-of-hard-chromium-plating-using-trivalent-chromium-solutions>
- [22] Physical Vapor Deposition (PVD). [Online]. Available: <http://www.sigmaaldrich.com/materials-science/material-science-products.html?Page=108832720>. Accessed May 11, 2017.
- [23] U. Helmersson, M. Lattemann, J. Bohlmark, A. P. Ehiasarian,, and J. T. Gudmundsson, "Review ionized physical vapor deposition (IPVD): A review of technology and applications," *Thin Solid Films*, vol. 513, pp. 1–24, Aug. 2006.
- [24] U. S. Army. (n.d.) ARL center for cold spray- cold spray process. [Online]. Available: <https://www.arl.army.mil/www/default.cfm?page=370>. Accessed May 23, 2017.

- [25] F. M. White, *Fluid Mechanics*, 7th ed. New York, NY: McGraw Hill, 2011, pp. 637–641.
- [26] C. Reeve, (2001, Nov. 22). Thermal spray: better performance for less. *Machine Design* [Online]. Available: <http://machinedesign.com/archive/thermal-spray-better-performance-less>. Accessed May 23, 2017.
- [27] Metal coatings. (2002, Nov. 15) *Machine Design*. [Online]. Available: <http://machinedesign.com/basics-design/metal-coatings>. Accessed May 23, 2017.
- [28] D. Bolles, “HVOC thermal spraying: an alternative to hard chrome plating,” *Welding J.*, vol. 74, no. 10, pp. 31–34, Oct. 1995.
- [29] Advanced Coating. (n.d.). Thermal spraying techniques. [Online]. Available: <http://www.advanced-coating.com/english/spraying-arc.htm>. Accessed May 24, 2017.
- [30] E. Chen. (2004, Apr. 12). Thin Film Deposition. [Online]. Available: <http://www.mrsec.harvard.edu/education/ap298r2004/Erli%20chenFabrication%20II%20-%20Deposition-1.pdf>. Accessed May 23, 2017.
- [31] A. Baral and R. Engelken, “Chromium-based regulations and greening in metal finishing industries in the USA,” *Environ. Sci. & Policy*, vol. 5, no. 2, pp. 121–133, Apr. 2002.
- [32] D. M. Proctor, E.C. Shay,, and P. K. Scott, “Health-based soil action levels for trivalent and hexavalent chromium: A comparison of state and federal standards,” *J. of Soil Contamination*, vol. 6, no. 6, pp. 595–648, 1997.
- [33] EPA. (2016, Sep.) Chromium compounds hazard summary. [Online]. Available: <https://www.epa.gov/sites/production/files/2016-09/documents/chromium-compounds.pdf>.
- [34] EPA. (n.d.). IRIS advanced search. [Online]. Available: <https://cfpub.epa.gov/ncea/iris/search/index.cfm>. Accessed May 23, 2017.
- [35] H. Zea, C. C. Luhrs, and J. Phillips, “Reductive/expansion synthesis of zero valent submicron and nanometal particles,” *J. Mater. Res.*, vol. 26, no. 5, pp. 672–681, Mar. 2011.
- [36] M. Koebel and M. Elsener, “Determination of urea and its thermal decomposition products by high-performance liquid chromatography,” *J. of Chromatography*, vol. 689, no. 1, pp. 164–169, Jan. 1995.
- [37] C. Luhrs, M. Kane, Z. Leseman, and J. Phillips, “Novel process for solid state reduction of metal oxides and hydroxides,” *Metallurgical and Mater. Trans.*, vol. 44, no. 1, pp. 115–122, Feb. 2013.

- [38] L. E. Eiselstein, D. M. Proctor, and T. C. Flowers, "Trivalent and hexavalent chromium issues in medical implants," *Mater. Sci. Forum*, vol. 539–543, pp. 698–703, 2007.
- [39] G. Almaguer-Busso, G. Velasco-Martinez, G. Carreno-Aguilera, S. Guiterrez-Granados, E. Torres-Reyes, and A. Alatorre-Ordaz, "A comparative study of global hexavalent chromium removal by chemical and electrochemical processes," *Electrochem. Commun.*, vol. 11, no. 6, pp. 1097–1100, Jun. 2009.
- [40] K. A. Greenaway, "A novel nonelectrolytic process for chromium and nickel coating," M.S thesis, Dept. Mech. And Aero. Eng., Naval Postgraduate School., Monterey, CA, 2015.
- [41] P. Wynn, "Managing the transition to hexavalent chromium free anti-corrosion coatings," *Trans. of the Inst. of Metal Finishing*, vol. 84, no. 6, pp. 280–285, Nov. 2006.
- [42] M. L. Klingenberg, E. W. Brooman, and T. A. Naguy, "Nano-particle composition plating as an alternative to hard chromium and nickel coatings," *Plating and Surface Finishing*, vol. 92, no. 4, pp. 42–48, Apr. 2005.
- [43] S. I. Sandler, *Chemical and Engineering Thermodynamics*, New York: J. Wiley & Sons, 1989, pp. 601–603.
- [44] Y. Leng, *Materials Characterization Introduction to Microscopic and Spectroscopic Methods*, 1st ed. Hoboken, NJ: Wiley., 2008, pp. 123–133.
- [45] EDAX interactive slide rule by atomic number. (n.d.). EDAX. [Online]. Available: <http://www.edax.com/EDAX/Interactive-Slide-Rule-Atomic-Number.aspx> Accessed Apr. 27, 2017.
- [46] D. R. Anderson, D. J. Sweeney, and T. A. Williams, *Essentials of Modern Business Statistics with Microsoft Office Excel*, 6th ed. Boston: Cengage Learning, 2013, pp. 125–130.
- [47] N. Mandich. (n.d.). Surface preparation of metal prior to plating. [Online]. Available: <http://www.nmfrc.org/pdf/sf2002/sf02s02.pdf>. Accessed May 23, 2017.
- [48] N. Mandich and D. Snyder, "Electrodeposition of chromium," in *Modern Electroplating*, vol. 5, M. Schlesinger and M. Paunovic, Eds. Hoboken, NJ: J. Wiley & Sons, Inc., 2010, pp. 205–241.
- [49] A. Moridi, S. Hassani-Gangaraj, M. Guagliano and M. Dao, "Cold spray coating: review of material systems and future perspectives," *Surface Eng.*, vol. 30, no. 6, pp. 369–395, Jun. 2014.

INITIAL DISTRIBUTION LIST

1. Defense Technical Information Center
Ft. Belvoir, Virginia
2. Dudley Knox Library
Naval Postgraduate School
Monterey, California